

Copyright  
by  
Andrew Francis Parisi  
2018

**The Thesis Committee for Andrew Parisi  
Certifies that this is the approved version of the following thesis:**

**Geochronological Constraints on two Proposed Ordovician Meteorite  
Event Impact Structures in North America**

**APPROVED BY  
SUPERVISING COMMITTEE:**

**Supervisor:**

---

Elizabeth Catlos

---

Mark Cloos

---

Sean Gulick

**Geochronological Constraints on two Proposed Ordovician Meteorite  
Event Impact Structures in North America**

**by**

**Andrew Francis Parisi**

**Thesis**

Presented to the Faculty of the Graduate School of

The University of Texas at Austin

in Partial Fulfillment

of the Requirements

for the Degree of

**Master of Science in Geological Sciences**

**The University of Texas at Austin**

**August 2018**

## **Dedication**

*ἐξίσταται γὰρ πάντ' ἀπ' ἀλλήλων δίχα*

*“For all things change, making way for each other”*

## **Acknowledgments**

I would briefly like to thank everyone who assisted with this project. This work was the result of a collaborative effort between many parties who were able to help me through problems I wouldn't have been able to solve myself. First, my advisor Dr. Liz Catlos, who was able to guide this project from initial idea to completed work. Second, the other members of my thesis committee, Drs. Mark Cloos and Sean Gulick, who also provided help and guidance. Others who helped in various ways include Dr. Michael Brookfield, Jaspal Singh, James Mahner, Tom Etzel, Emily Pease, Will Pollard, and the Stockli research group. I'd like to thank the staff at the UT-Austin Thermochronology Lab, the Oregon State University Argon Geochronology Lab and the Heidelberg Ion Probe laboratory at the Heidelberg University for their assistance in performing the various analysis. Lastly, a big thanks to the Oklahoma Geologic Survey and the Ontario Ministry of Natural Resources for allowing me the permission to collect samples.

## **Abstract**

### **Geochronological Constraints on two Proposed Ordovician Meteorite Event Impact Structures in North America**

Andrew Francis Parisi M.S.Geo.Sci.

The University of Texas at Austin, 2018

Supervisor: Elizabeth Catlos

Following the breakup of the L-Chondrite Parent Body in the Mid-Ordovician, the Earth experienced a drastic increase in the number of meteorite impacts. This event, the Ordovician Meteorite Event (OME), has been confirmed from impact structures or meteoritic debris in Sweden, Russia and China. Yet despite the long lasting and global nature of this event, only two OME impact structures have been identified outside of Sweden, with no OME evidence having been found in the Western Hemisphere.

In North America, there is a series of impact structures which are speculated to have formed during the OME. All of these structures have been tentatively dated to the mid-Ordovician, but absolute formation dates have not yet been obtained. The ages of these structures have been constrained based on stratigraphic and biostratigraphic evidence, but radiometric ages have proven difficult to determine.

This project attempts to determine the formation age and likely origin of two of those Impact Structures. The Ames Astrobleme (OK, USA) and Slate Islands Archipelago (ON, Canada) were chosen due to previous work and the ease of accessing impact generated material. For this project, shock metamorphosed minerals from impactites was dated via thermochronological techniques. Samples of impactite and shocked target rock were collected from each of the impact structures. K-feldspar ( $^{40}\text{Ar}/^{39}\text{Ar}$ ) and zircon (U/Pb) were dated from the impacted rocks. The hypothesis was

that these minerals would be ‘reset’ from the heat and/or pressure generated by the impact, and could have the potential to provide the age of formation of the crater. This is similar to the way traditional metamorphic events are dated using these minerals, although the events in question occur over vastly different time scales.

The analysis determined significant events in the thermal histories of the two impact structures. At the Ames Astrobleme, initial cooling of the basement granodiorite was confirmed to be  $1428 \pm 31$  Ma with a significant thermal episode at  $372 \pm 42$  Ma. At the Slate Islands, initial cooling of the basement syenite was confirmed to be  $2706 \pm 20$  Ma with significant thermal episodes at  $614 \pm 27$  Ma,  $481 \pm 13$  Ma, and  $331 \pm 9$  Ma. In both cases, the data does not conclusively confirm an OME related origin for the impact structures. Of all the zircons analyzed, only three from the Slate Islands have concordant dates which match the time frame of the OME. Even more puzzling, most of the young dates cannot be explained by nearby tectonic events. It is likely that these discrepancies are due to a combination of factors, including a lack of understanding of the regional geologic history, an incorrect determination of stratigraphic constraints on the timing of impact structure formation, and the difficulties of using shock metamorphosed minerals when dating impact structures.

## Table of Contents

|  |           |
|--|-----------|
| List of Tables .....   | xi        |
| List of Figures .....  | xiii      |
| <b>I: PROJECT OUTLINE: .....</b>   | <b>1</b>  |
| 1.1 Introduction:.....   | 1         |
| 1.2 Problem Statement .....  | 6         |
| 1.3 Methods of Analysis .....  | 7         |
| 1.4 Organization of the Thesis .....   | 8         |
| <b>II: GEOLOGIC SETTING: THE ORDOVICIAN METEORITE EVENT (OME), AMES<br/>ASTROBLEME AND THE SLATE ISLANDS ARCHIPELAGO .....</b> | <b>10</b> |
| 2.1 Overview .....   | 10        |
| 2.2 Terrestrial evidence for OME .....   | 10        |
| 2.3 The L-Chondrite Parent Body: Observation and Interpretation .....  | 14        |
| 2.4 Ames Astrobleme.....   | 19        |
| 2.5 The Slate Islands Archipelago .....  | 25        |
| <b>III: METHODS CHAPTER .....</b>  | <b>30</b> |
| 3.1 Overview.....  | 30        |
| 3.2 Sample Collection.....   | 30        |
| 3.2.1 Ames Astrobleme Sample Collection.....   | 30        |
| 3.2.2 Slate Islands (Patterson Island) Sample Collection .....   | 35        |
| 3.3 Mineral Separation.....  | 39        |
| 3.4 Geochronology.....   | 41        |
| 3.4.1 Zircon U-Pb dating via Laser Ablation-Inductively Coupled Plasma-Mass<br>Spectrometry (LA-ICP-MS) .....                  | 41        |
| 3.4.2 U-Pb Geochronology via Secondary Ion Mass Spectrometry (SIMS)  | 43        |

|   |           |
|---|-----------|
| 3.4.3 $^{40}\text{Ar}/^{39}\text{Ar}$ Geochronology via step heating..... | 44        |
| <b>IV: RESULTS.....</b>   | <b>45</b> |
| 4.1 Overview.....   | 45        |
| 4.2 Petrographic Analysis: Mineralogy and Impact Generated Textures.....  | 45        |
| 4.2.1 Ames Astrobleme.....  | 45        |
| 4.2.2 Slate Islands.....  | 50        |
| 4.3 U-Pb Zircon Geochronology.....  | 54        |
| 4.3.1 Ames Astrobleme.....  | 54        |
| 4.3.2 Slate Islands.....  | 61        |
| 4.4 $^{40}\text{Ar}/^{39}\text{Ar}$ Geochronology via step heating.....   | 70        |
| 4.4.1 Ames Astrobleme.....  | 70        |
| 4.4.2 Slate Islands Archipelago.....                                      | 72        |
| 4.5 Summary.....  | 75        |
| <b>V: DISCUSSION AND INTERPRETATION.....</b>                              | <b>76</b> |
| 5.1 Overview.....   | 76        |
| 5.2 Ames Astrobleme Discussion.....                                       | 76        |
| 5.2.1 Age Population Identification.....                                  | 76        |
| 5.2.2 Geologic Significance of Age Populations.....                       | 77        |
| 5.3 Slate Islands Archipelago.....  | 82        |
| 5.3.1 Age Population Identification.....                                  | 82        |
| 5.3.2 Geologic Significance of Age Populations.....                       | 83        |

|  |            |
|--|------------|
| 5.4 A Non-Tectonic Explanation for the Geologic Disparities.....   | 86         |
| 5.5 Summary and Future Work.....   | 88         |
| <b>VI: APPENDICES .....</b>  | <b>91</b>  |
| 6.1 Hand samples from Ames Astrobleme .....  | 91         |
| 6.2 CL Images of Analyzed Zircons .....  | 93         |
| 6.2.1 CL images of zircons from Ames Astrobleme CL images of zircons from<br>Ames Astrobleme.....                    | 93         |
| 6.2.2 CL images of zircons from the Slate Islands Archipelago .....  | 95         |
| 6.3 Data from U-Pb analysis of zircons from Ames Astrobleme .....  | 100        |
| 6.4 Data from U-Pb analysis of zircons from Slate Islands Archipelago .....  | 105        |
| 6.5 Data from $^{40}\text{Ar}/^{39}\text{Ar}$ analysis via step heating performed at Oregon State<br>University..... | 112        |
| 6.6 Data from step heating analysis of samples from Slate Islands.....   | 120        |
| <b>VII: REFERENCES .....</b>   | <b>122</b> |

## List of Tables

|  |     |
|--|-----|
| Table 1.1. Proposed OME-related impact structures in North America.....  | 4   |
| Table 2.1: Proposed age constraints for Slate Islands.....   | 29  |
| Table 3.1. Ames Astrobleme sample information .....  | 32  |
| Table 3.2. Slate Islands sample information.....   | 36  |
| Table 4.1: Ames Astrobleme U-Pb zircon geochronology analysis by LA-ICP-MS<br>(University of Texas at Austin). All uncertainties are reported at the 2-<br>sigma level. See Appendix 6.3 for complete details..... | 56  |
| Table 4.2: Ames Astrobleme U-Pb zircon geochronology analysis by SIMS<br>(Heidelberg University). All uncertainties are reported at the 1-sigma<br>level. See Appendix 6.3 for complete details. ....              | 57  |
| Table 4.3: Slate Islands U-Pb zircon geochronology analysis by LA-ICP-MS<br>(University of Texas at Austin). All uncertainties are reported at the 2-<br>sigma level. See Appendix 6.4 for complete details.....   | 63  |
| Table 4.4: Slate Islands Archipelago U-Pb zircon geochronology analysis by SIMS<br>(Heidelberg University). All uncertainties are reported at the 1-sigma<br>level. See Appendix 6.4 for complete details. ....    | 64  |
| Table 4.5: Summary of results from step heating experiments. ....  | 74  |
| Table 6.1 Ages of Zircon analysis corresponding with Figure 6.2.....   | 93  |
| Table 6.2 Data from U-Pb analysis via LA-ICP-MS performed at the University of<br>Texas at Austin .....  | 100 |
| Table 6.3 Data from U-Pb analysis via SIMS performed at the Heidelberg University<br>.....   | 102 |

|  |     |
|--|-----|
| Table 6.4 Data from U-Pb analysis via LA-ICP-MS performed at the University of Texas at Austin ..... | 105 |
| Table 6.5 Data from U-Pb analysis via SIMS performed at the Heidelberg University .....              | 107 |
| Table 6.6: Data from step heating analysis of Sample S4 9022' from the Ames Astrobleme.....          | 112 |
| Table 6.7: Data from step heating analysis of Sample S5 9026' from the Ames Astrobleme.....          | 114 |
| Table 6.8: Data from step heating analysis of Sample S6 9027' from the Ames Astrobleme.....          | 115 |
| Table 6.9: Data from step heating analysis of Sample S7 9031' from the Ames Astrobleme.....          | 117 |
| Table 6.10: Data from step heating analysis of Sample S9 9034' from the Ames Astrobleme.....         | 119 |
| Table 6.11: Data from step heating analysis of Sample S2 (metasyenite) from the Slate Islands. ....  | 120 |

## List of Figures

- Figure 1.1: Locations of confirmed OME deposits, impact structures or dispersed extraterrestrial chromite (Eastern Hemisphere). Data compiled by Schmitz (2013).....3
- Figure 1.2. Map of impact structures in North America which have been proposed to have formed during the OME. Crosses denote impact structures considered under this study.....5
- Figure 2.1: Fossil meteorite (Österplana 035) and Orthoceras in limestone plate. Plate has been cut parallel to bedding plane. Picture taken by B. Schmitz, modified from Schmitz et al., (2001).....12
- Figure 2.2: Comparison of relative probability of  $^{40}\text{Ar}/^{39}\text{Ar}$  ages determined from L (top) and H (bottom) chondrites. Figures show a bimodal age distribution for L chondrites, with a unique increase at ~470 Ma when compared with H chondrites. Figures modified from Swindle et al., 2013.....18
- Figure 2.3: Location of Ames, Oklahoma in relation to generalized geologic provinces. Ames Astrobleme is buried, with its center roughly beneath the town of Ames. Impact structure approximately 16 km in diameter. Base map modified from Johnson (2008).....21

Figure 2.4: Stratigraphic chart showing geologic formations from Southern Oklahoma (Arbuckle Mountains) contrasted with simplified petrologic log of the Nicor Chestnut 18-4 Core. Lithology identification modified from Fischer (1997). Blue formations indicate possible age range of crater shale conodonts based on Repetski (1997). Red formations indicate Arbuckle dolostones and likely age range for impact. Stratigraphic information from the International Commission on Stratigraphy. Note that the Series and Stages in this portion of North America are ill defined, and are not included here. ....24

Figure 2.5: Location of Slate Islands Archipelago within Lake Superior. ....27

Figure 2.6: Contact between older Archean felsics (right) and younger Keweenawan mafics (left). Outcrop approximately 85 meters wide, located on southwestern shore of Patterson island. ....28

Figure 2.7: Nine to twelve-meter-tall shatter cones on Slate Islands. Outcrop is located between sample E1 and E2 (see Fig. 3.3). See Hollings et al., 2006 for exact location.....28

Figure 3.1: Map, photographs, and overview of the Nicor Chestnut 18-4 Core drill core from the Ames Astrobleme. Core is approximately three inches in diameter. White circles represent locations of collected sample plugs. Inset map shows the location of boreholes which penetrate the Arbuckle Group, including the Nicor Chestnut 18-4 Core, with bold circles indicating inferred outer and inner crater rim (modified from Koeberl et al., 2001). See Table 3.1 for sample information.....33

Figure 3.2: Polished slab taken from Nicor Chestnut 18-4 core representative of suevite texture. Sample S7 9031' removed from adjacent portion of core. ....34

Figure 3.3: Sample location map for rocks collected within the Slate Islands. Inset shows location of Slate Islands within Lake Superior. Large white box indicates location of Fig. 3.4. Bold colors indicate location of previously mapped outcrops, transparent colors indicate inferred geologic boundaries. Note thick vegetation cover preventing travel to interior of island. See Table 3.2. for sample data. Geologic map modified and simplified from Sage (1991). ....37

Figure 3.4: Sample locations and bedrock geology on east coast of Patterson Island. Note thick vegetation cover preventing travel to interior of island. See Fig. 3.3 for location of this region within the context of the Slate Islands. ....38

Figure 3.5: Suevite outcrop G1. Note flow banding within and recessed nature of suevite. Also note felsic brecciated clasts within suevite. ....39

Figure 4.1: Ames Astrobleme hand samples showing apparently competent granodiorite clasts. A: Sample S6 9027' B: Sample S7 9031'. Compare with Fig. 4.2. ....47

Figure 4.2: Photomosaics of thin sections from the Nicor Chestnut 18-4 core. A: Sample S4 9022' (Plane polarized light). B: Sample S4 9022' (Cross polarized light). C: Sample S6B 9027' (Plane polarized light). D: Sample S6B 9027' (Cross polarized light). E: Sample S7 9031' (Plane polarized light). F: Sample S7 9031' (Cross polarized light). ....48

Figure 4.3. Thin section S6B (9027') with key features highlighted. 4.3A: Overview (Cross polarized light). 4.3B: melt injection texture (Cross polarized light). 4.3C: Curvilinear fractures within dolomite (Cross polarized light). 4.3D: Melt texture around shocked dolomite clast. (Cross polarized light). 4.3E: Mosaic texture within quartz crystal (Plane polarized light). 4.3F: Inclusions within quartz along crystallographic axis (Cross polarized light). .....49

Figure 4.4. Hand sample of syenite. Sample S1 showing syenite appearance. ....51

Figure 4.5. Hand sample of suevite with examples of clast lithology labeled. See Section 2.4 for likely identities of the clasts. ....52

Figure 4.6 Thin section of syenite sample S1. Texture is characteristic of an alkali porphyry rather than a 'true' syenite. Compare with figure 4.3A. Left: plane polarized light. Right: cross polarized light. ....53

Figure 4.7 Thin section of suevite sample G1 showing the texture characteristic of a polymict lithic breccia. Note brecciated texture of sample. Felsic clasts are either syenite or rhyolite, mafic clasts are either gabbro or basalt. Left: plane polarized light. Right: cross polarized light. ....54

Figure 4.8 Concordia plot of data from all analyzed zircons from Ames Astrobleme. Red ellipses indicate zircons analyzed via SIMS, blue ellipses indicate zircons analyzed via LA-ICP-MS. Blue error ellipses are  $2\sigma$ , red error ellipses are  $1\sigma$ . Inset highlights cluster of ages at lower intercept....58

Figure 4.9 Ames Astrobleme U-Pb simplified zircon age distribution plot. Red data points indicate zircons analyzed via SIMS, blue data points indicate zircons analyzed via LA-ICP-MS. Dashed lines indicated values of upper and lower discordia line intercepts as seen in Fig. 4.8. Figure shows only best ages from analyses, see Appendix 6.3 for full data.59

Figure 4.10: Images of select zircons from Ames Astrobleme showing locations where age measurements were taken. Crosses indicate location of measurement via Laser Ablation-ICP-MS, circled areas indicate location of measurement via SIMS. A: Zircon AAOK\_7 CL image. B: Zircon AAOK\_8 CL image. C: Zircon AAOK\_9 and AAOK\_10 CL image. Numbered spots are the following ages: \*1: 363.7±10.5 Ma, \*2: 355.8±14.1 Ma, \*3: 341.3±9.7 Ma, \*4: 364.8±4.7 Ma, \*5: 369.3±8.3 Ma, \*6: 1379±17 Ma, \*7: 1414±22 Ma, \*8: 1407±30 Ma, \*9: 1396±24 Ma, \*10: 1335±23 Ma, \*11: 1294±25 Ma, \*12: 1324±25 Ma.....60

Figure 4.11 Concordia plot of data collected from zircons from Slate Islands. Red ellipses indicate zircons analyzed via SIMS, blue ellipses indicate zircons analyzed via LA-ICP-MS. Blue error ellipses are 2σ, red error ellipses are 1σ. ....66

Figure 4.12 Concordia plot of data collected from zircons from Slate Islands highlighting Phanerozoic ages. Red ellipses indicate zircons analyzed via SIMS, blue ellipses indicate zircons analyzed via LA-ICP-MS. Blue error ellipses are 2σ, red error ellipses are 1σ.....67

Figure 4.13 Age distribution plot of data collected from zircons from the Slate Islands. Red data points indicate zircons analyzed via SIMS, blue data points indicate zircons analyzed via LA-ICP-MS. Dashed lines indicated values of upper and lower discordia line intercepts as seen in Fig. 4.11. Figure shows only best ages from analyses, see Appendix 6.4 for full data.....68

Figure 4.14: Images of select zircons from the Slate Islands. Circled areas indicate location of measurement via SIMS. A: Zircon SION\_G2\_20 CL image. B: Zircon SION\_G1\_7 image. C: Zircon SION\_G2\_26 CL image. D: Zircon SION\_G2\_21 CL image. E: Zircon SION\_G1\_5 CL image. F: Zircon SION\_G2\_5 CL image.....69

Figure 4.15:  $^{40}\text{Ar}/^{39}\text{Ar}$  analysis of Ames Astrobleme S1 9014.9'. A: Age spectrum following step heating experiment. B: Inverse isochron plot .....71

Figure 4.16:  $^{40}\text{Ar}/^{39}\text{Ar}$  analysis of Ames Astrobleme S4 9020'. A: Age spectrum following step heating experiment. B: inverse isochron plot. ....71

Figure 4.17:  $^{40}\text{Ar}/^{39}\text{Ar}$  analysis of Ames Astrobleme S6 9027'. A: Age spectrum following step heating experiment. B: Inverse isochron plot .....71

Figure 4.18:  $^{40}\text{Ar}/^{39}\text{Ar}$  analysis of Ames Astrobleme S7 9031'. A: Age spectrum following step heating experiment. B: Inverse isochron plot .....72

Figure 4.19:  $^{40}\text{Ar}/^{39}\text{Ar}$  analysis of Ames Astrobleme S9 9034'. A: Age spectrum following step heating experiment. B: Inverse isochron plot .....72

Figure 4.20:  $^{40}\text{Ar}/^{39}\text{Ar}$  analysis of Slate Islands syenite S2. A: Age spectrum following step heating experiment. B: Inverse isochron plot .....73

Figure 5.1 Ames Astrobleme U-Pb zircon age distribution plot with  $^{40}\text{Ar}/^{39}\text{Ar}$  step heating age ranges. The distinct age populations, upper and lower discordia intercepts, and the range of the OME have been highlighted. ....81

Figure 5.2 Slate Islands Archipelago U-Pb zircon age distribution plot. The distinct age populations (including subdivisions of population 3), upper and lower discordia intercepts, and the range of the OME have highlighted. ....83

Figure 6.1: Images of hand samples collected from Ames Astrobleme Nicor Chestnut Core.....91

Figure 6.2: CL images of zircons analyzed from Ames Astrobleme.....94

Figure 6.3: CL images of zircons analyzed from the Slate Islands. ....95

Figure 6.4: Age distribution plot of all measurements from Ames Astrobleme zircons. Red data points indicate zircons analyzed via SIMS, blue data points indicate zircons analyzed via LA-ICP-MS. Error bars designate  $2\sigma$ .104

Figure 6.5 Age distribution plot of all measurements from Slate Islands zircons. Red data points indicate zircons analyzed via SIMS, blue data points indicate zircons analyzed via LA-ICP-MS. Error bars designate  $2\sigma$ .....111

# **I: PROJECT OUTLINE:**

## **1.1 Introduction:**

The Ordovician Meteor Event (OME) refers to the period of time (470-450 Ma) during which the Earth experienced a drastic increase in the number of meteorite impacts and amount of related extraterrestrial material (Schmitz et al., 2001). This was not a single impact, such as the asteroid which created the picturesque Barringer crater in Arizona (Barringer 1905, 1915, 1924), or the Chicxulub crater in Yucatan that caused the extinction of the dinosaurs (Alvarez et al., 1980). Rather, the event saw the tonnage of extraterrestrial material being delivered to the Earth increase by an order of magnitude for a period of approximately 30 million years (Schmitz et al., 2001). The peak of this event is hypothesized to be ca.  $467.3 \pm 1.6$  Ma based on  $^{40}\text{Ar}/^{39}\text{Ar}$  age distribution of multiple L-chondrites associated with the event (Korochantseva et al., 2007). Previous studies have confirmed the global nature of the event (Fig. 1.1), with impacts structures or debris being discovered in Sweden (Thorslund and Wickman, 1981; Schmitz, 2013), and China (Heck et al., 2010). Material from the same parent body as the OME meteorites, but not from Ordovician bedrock has been identified in Texas (Kunz et al., 1997; Korochantseva, 2007), Oman (Korochantseva, 2007), Australia (Turner, 1969; Bogard et al., 1976), Canada (Turner 1969; Turner et al., 1966), Uganda (Kunz et al., 1997; Korochantseva et al., 2007), and Brazil (Kunz et al., 1997; Korochantseva et al., 2007). The spatial and temporal scale of the event suggests that it should have left the face of the Earth marked by an abundance of craters.

A series of impact structures in North America have been speculated to be candidates for formation during the OME (Table 1.1, Fig. 1.2). All of these structures have been tentatively dated to the mid-Ordovician, based on stratigraphic and biostratigraphic evidence, but accurate radiometric ages have proven difficult to determine. These structures have also not been connected to known OME material through chemical signatures, in the way that Eurasian OME events have been connected on the basis of titanium and vanadium concentrations in identified chromite grains (Schmitz and Häggström, 2006). Accurately determining the formation age of these impact structures is the first step to identifying a conclusive OME connection.

Quantifying the extent of the OME is important to understanding the influence the event may have played in related geologic events, specifically the evolution of modern life. It is hypothesized that the OME may have led to the Ordovician Biodiversification Event, a rapid diversification of the Paleozoic fauna that occurred during the mid-Ordovician (Harper, 2006, Servais et al., 2010). It has been suggested that the large number of impacts would have excavated huge amounts of material from the interior of the continents, moving nutrients to the oceans (Parnell, 2008). This nutrient increase could have provided the impetus for the evolution of new species, or made more niche space available into which new species could adapt (Schmitz et al., 2008). Conversely, the numerous impacts could have put stress on the environment, leading to the extinction of some species while making room for those with better adaptations. These hypotheses cannot be adequately tested until the full extent of the OME is better understood.

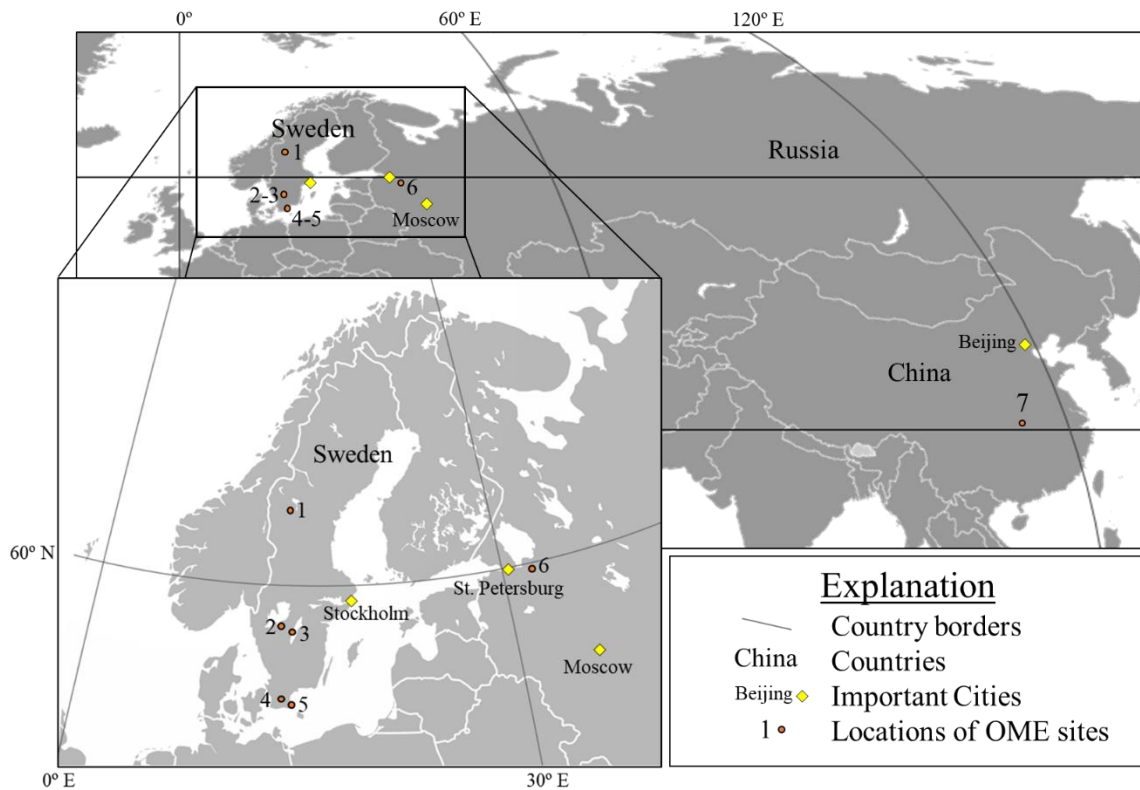


Figure 1.1: Locations of confirmed OME deposits, impact structures or dispersed extraterrestrial chromite (Eastern Hemisphere). Data compiled by Schmitz (2013).

1. Brunflo quarry, Sweden (Thorslund and Wickman, 1981)
2. Thorsberg quarry, Kinnekulle, Sweden (Nyström et al., 1988), and Hällekis quarry, Kinnekulle, Sweden (Schmitz and Häggström, 2006)
3. Gullhögen quarry, Sweden (Tassinari et al., 2004)
4. Fågelsång section, Sweden (Häggström and Schmitz, 2007)
5. Komstad quarry, Sweden (Häggström and Schmitz, 2007)
6. Lynna River, St. Petersburg Russia (Lindskog et al., 2012)
7. Puxi river, Hubei district, China (Cronholm and Schmitz, 2010)

Table 1.1. Proposed OME-related impact structures in North America

| Site name <sup>a</sup>    | Location (lat/lon)                                     | Speculated age (Ma, method)                         | Current condition    | Reference <sup>b</sup> |
|---------------------------|--|---|----------------------|------------------------|
| USA Locations             |  |   |                      |                        |
| Ames Astrobleme           | Oklahoma, USA<br>(N 36° 15', W 98° 12')                | 470 +/- 30 Ma<br>(Biostratigraphy)                  | Deeply Buried        | JC 1997                |
| Decorah Crater            | Iowa, USA  | <505 Ma<br>(Stratigraphy)                           | Buried               | Heck et al., 2004      |
| Rock Elm                  | Wisconsin, USA<br>(N 44° 43', W 92° 14')               | <505 Ma   | Buried, near surface | Peters et al., 2002    |
| Grover Bluff              | Wisconsin, USA<br>(N 43° 58', W 89° 32')               | <500 Ma<br>(Stratigraphy)                           | Exposed, quarried    | Renard, 2011           |
| Brussels Hill             | Wisconsin, USA   | Mid-Ordovician<br>(Stratigraphy)                    | Buried               | ZB 2015                |
| Calvin Crater             | Michigan, USA  | Ordovician<br>(Stratigraphy)                        | Exposed, flooded     | Milstein, 1994         |
| Newporte Crater           | North Dakota, USA<br>(N 48° 58', W 101° 58')           | <500 Ma<br>(Stratigraphy)                           | Buried               | Renard, 2011           |
| Canada Locations          |  |   |                      |                        |
| Slate Islands Archipelago | Ontario, Canada<br>(N 48° 40', W 87° 00')              | 800-300 Ma<br>(Stratigraphy)                        | Central peak exposed | DS 1997                |
| Lac Couture               | Quebec, Canada<br>(N 60° 8', W 75° 20')                | 430±25 Ma<br>( <sup>40</sup> Ar/ <sup>39</sup> Ar)  | Exposed, flooded     | Bottomley et al., 1990 |
| Lac Clearwater (East)     | Quebec, Canada<br>(N 56° 5', W 74° 7')                 | 460-470 Ma<br>( <sup>40</sup> Ar/ <sup>39</sup> Ar) | Exposed, flooded     | Bottomley et al., 1990 |
| Pilot Crater              | Northwest Territory, Canada<br>(N 60° 17', W 111° 01') | 445±2 Ma<br>( <sup>40</sup> Ar/ <sup>39</sup> Ar)   | Exposed, flooded     | Bottomley et al., 1990 |

a. See Figure 1.2 for locations.

b. Abbreviations (JC1997= Johnson and Campbell, 1997; DS1997= Dressler and Sharpton, 1997; DH1991= Dietz and McHone, 1991; ZB2015 =Zawacki and Bjornerud, 2015)

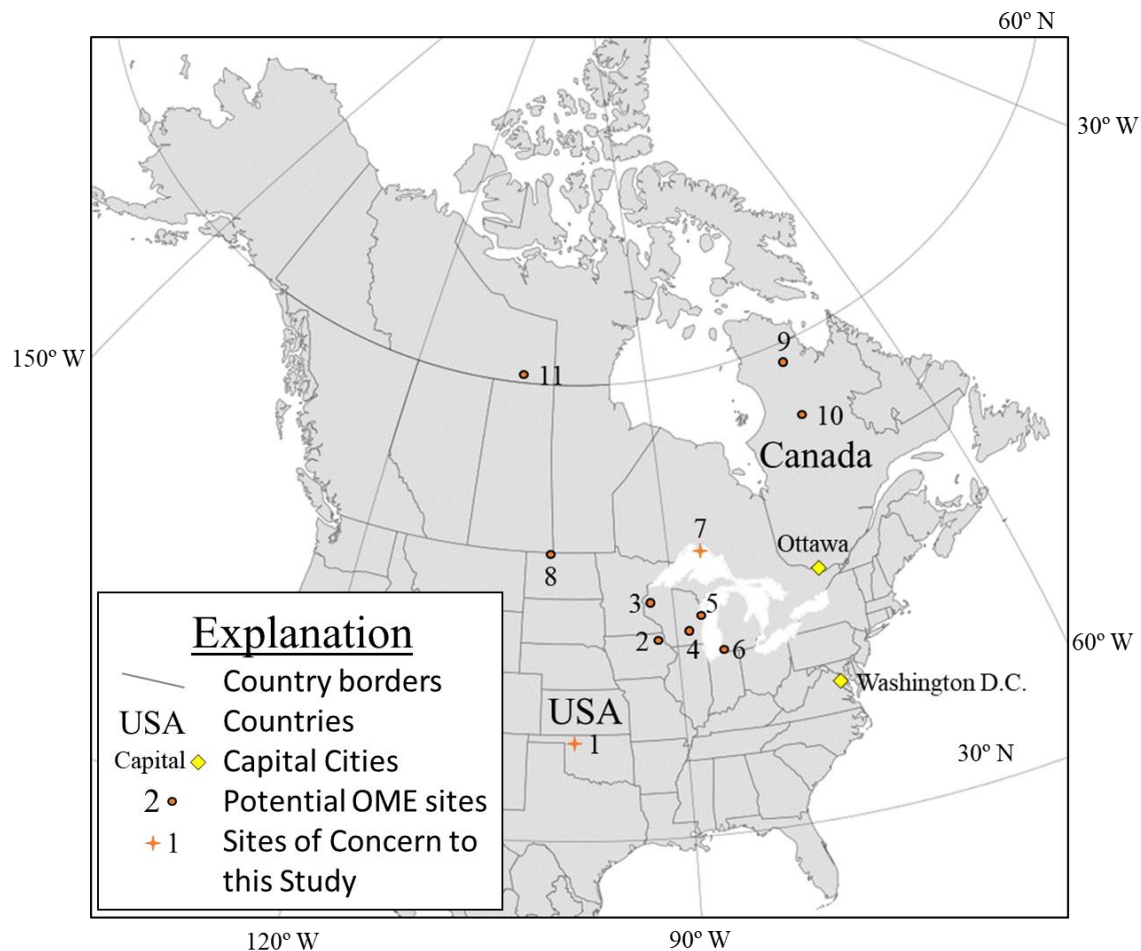


Figure 1.2. Map of impact structures in North America which have been proposed to have formed during the OME. Crosses denote impact structures considered under this study.

1. Ames Astrobleme, Oklahoma, USA (Johnson and Campbell, 1997)
2. Decorah Crater, Iowa, USA (Kass et al., 2013)
3. Rock Elm, Wisconsin, USA (Peters et al., 2002)
4. Grover Bluff, Wisconsin, USA (Renard, 2011)
5. Brussels Hill, Wisconsin, USA (Zawacki and Bjornerud, 2015)
6. Calvin disturbance, Michigan, USA (Milstein, 1994)
7. Slate Islands Archipelago (Dressler and Sharpton, 1997)
8. Newporte, North Dakota, USA (Renard, 2011)
9. Lac Couture (Bottomley et al., 1990)
10. Lac Clearwater (East) (Bottomley et al., 1990)
11. Pilot Crater (Bottomley et al., 1990)

## 1.2 Problem Statement

**The goal of this thesis is to determine the formation age of two proposed OME impact structures: the Ames Astrobleme in Oklahoma, USA and the Slate Islands Archipelago in Ontario, Canada (Table 1.1; Fig. 1.2).** These two structures were chosen due to previous research establishing the impact origin and ease of access to sampling material. Impact-shocked rocks from the Slate Islands are exposed on the archipelago with a total surface area of 40<sup>2</sup> km (Sage, 1991; Hollings et al., 2006), whereas drill core from the Ames Astrobleme were extracted in the 1990s as part of oil exploration projects (Carpenter and Carleson, 1997; Evans, 1997).

Both of these impact structures have proven difficult to date. Dating the Ames Astrobleme is limited by the amount of material available (Fischer, 1997), the poor quality of recovered index fossils (Repetski, 1997), and later probable thermal overprinting (Koerbels et al., 2001). Attempts have been made to date the glass formed during the impact, but were unsuccessful (Koerbels et al., 1997, 2001). Dating of the Slate Islands is limited by the remoteness of the archipelago and the complicated structural geology (Dressler and Sharpton, 1997). Formation ages suggested for the impact structures range from 282 Ma to <800 Ma (Table 2.1).

In this thesis, additional dating techniques will be used in an attempt to determine the age of the two impact structures. Rather than melt glass formed in the impact, this project will utilize pre-existing minerals (zircon and feldspars) involved in the formation of the impact structure. These minerals should have experienced conditions which could

‘reset’ their internal isotopic systematics, allowing daughter products from radiogenic decay to leave their crystals structures, thus providing the minimum age of the crater.

### **1.3 Methods of Analysis**

This project re-examined geologic evidence and used two techniques to determine the formation date for the Ames Astrobleme and the Slate Islands Archipelago. The emphasis of this project was on age information hosted by zircon ( $\text{ZrSiO}_4$ ) and K-feldspar ( $\text{KAlSi}_3\text{O}_8$ ) separated from rocks affected by the crater forming impact. For both structures, the target basement rock includes felsic, pre-Cambrian intrusive igneous assemblages. During crater formation, clasts from the target rock were ejected and subsequently deposited in the newly formed crater in the form of ejecta debris or washback deposits (Glass and Simonson, 2012). These clasts, called ejecta debris, settled into the crater surrounded by heated glass particles, which had melted during the meteorite impact. The residual heat in the crater would have raised the temperature of the clast above the closure temperature for the respective minerals. It is speculated that the internal chronometers were reset during shock metamorphism of target minerals. If those internal chronometers are reset, then the age analysis will reveal the age of the impact itself. Samples of impactite (impact debris) and target rocks were collected from each field site and the appropriate minerals were separated. K-feldspar grains were analyzed using the  $^{40}\text{Ar}/^{39}\text{Ar}$  laser step-heating at the Oregon State University Argon Geochronology Lab. Zircon grains were analyzed using the U-Pb technique via Laser Ablation-Inductively Coupled Plasma-Mass Spectrometry (LA-ICP-MS) at the

University of Texas at Austin and via Secondary Ion Mass Spectrometry at Heidelberg University. These techniques are widely known and applied and will be further explained in Chapter 3.

## **1.4 Organization of the Thesis**

The dissertation is organized into five chapters and four appendices. The work presented here is part of collaborative efforts and will be included in several future conference abstracts and two papers for publication.

Chapter 2 presents the relevant background material for the project. It introduces the OME, the evidence for the OME, and discusses the hypothesized causes and effects. It also introduces the field areas included in this study. Both the Ames Astrobleme and Slate Islands are discussed in terms of regional geology, previous research performed, development of the scientific understanding of the structures, and best efforts to date their formation.

Chapter 3 describes the methods used, in regard to the collection (field work), sample preparation, and the analytical techniques. It describes where individual samples were collected in regards to the geologic context of the two sites. It also describes the particular parameters used in analysis of the samples.

Chapter 4 presents the results of the analyses. This includes petrologic descriptions of the hand samples and thin sections, U-Pb isotopic data obtained from analysis of zircons, and argon data obtained from the analysis of K-feldspar.

Chapter 5 presents an interpretation of the data, and important trends are identified and discussed. The results are considered within the context of the OME and the broader research questions.

## **II: GEOLOGIC SETTING: THE ORDOVICIAN METEORITE EVENT (OME), AMES ASTROBLEME AND THE SLATE ISLANDS ARCHIPELAGO**

### **2.1 Overview**

This chapter summarizes the evidence for the Ordovician Meteorite Event (OME), including the proposed cause. A summary of research related to the OME is provided. It then discusses the two field areas that are the focus of this proposal: the Ames Astobleme in Oklahoma and Slate Islands in Ontario Canada. This chapter also includes a discussion of previous research and geologic interpretations which lead to our understanding of the two areas. A geologic summary for each field area is also provided.

### **2.2 Terrestrial evidence for OME**

The first indication of a mid-Ordovician extra-terrestrial anomaly came in 1952, when a section of limestone containing an unusual clast was extracted from the Brunflo Quarry in central Sweden (Fig. 1.1) (see Thorslund and Wickman, 1981; Thorslund et al., 1984; Nystrom and Wickman, 1991). The polished section was presented at Uppsala University, who initially identified the clast as the altered remains of a terrestrial ultramafic rock. It was not until 1979 that the clast was identified as extraterrestrial in origin. This clast, the fossil Brunflo meteorite, was the first in a multitude of mid-Ordovician extra-terrestrial objects soon to be found in the area.

Key work to identify the OME record was conducted at Thorsberg Quarry in southern Sweden. The Thorsburg quarry extracts Orthoceratitic limestone which formed

on the Baltoscandian shield during the late early to mid-Ordovician (Jaanusson, 1972, 1973) (Fig. 2.1). At the time, southern Sweden was part of the Baltica paleocontinent (Cocks and Torsvick, 2005), covered by an epicontinental sea 100-300 meters deep (Chen and Lindström, 1991, Schmitz et al., 1996). Previous researchers interpreted this limestone as accumulating slowly, only a few millimeters per kyr (Jaanusson, 1972, 1973). Sedimentation occurred in intermittent bursts, leading to the development of thin (2-20 cm) beds separated by hard-ground surfaces (Lindström, 1962, 1979). The chance discovery of a fossil meteorite in the quarry dump pile inspired a systematic survey of the quarry beginning in 1992 (Schmitz et al., 2001). Limestone from the quarry was being quarried for decoration purposes, and the workers would donate to researchers any meteorite containing slabs. By 1996, with 13 fossil meteorites found, it was apparent this quarry contained more meteorites than was to be expected given modern background meteor flux (Schmitz et al., 1996, 1997, 2001).

By 2012, 100 fossil meteorites (1-21 cm in diameter) had been discovered at Thorsberg quarry (Schmitz et al., 2013). The objects were determined to be extraterrestrial based on oxygen isotope ratios and inclusion chemistry, both of which indicate that the objects were all from L Chondrite type meteorites. The fossil meteorites are concentrated in a 4.7 m interval beginning at the base of the *Lenodus Variabilis* conodont zone; this corresponds with the Darriwillian stratigraphic section (467.3 Ma to 458.4 Ma). The fossil meteorites are further concentrated onto several hardground surfaces within the section. The discrete layering of the fossil meteorites, combined with the consistently varying cosmic ray exposure ages indicates, multiple meteorite falls are

preserved (Schmitz et al., 2001). Across the area of the quarry floor, the number of grains of chromite per kilogram of rock, and thus the amount of meteorites which fell on the seafloor in the mid-Ordovician was at least 1-2 orders of magnitude higher than present day (Halliday et al., 1989, Huss, 1991, Bevan et al., 1998, Bland, 2001). Yet the question remained: could the fossil meteorite accumulation be due to local factors, such as a local concentration of material eroded from elsewhere. Fortunately, the systematic survey of Thorsberg quarry allowed comparisons with corresponding stratigraphic sections in other locations.

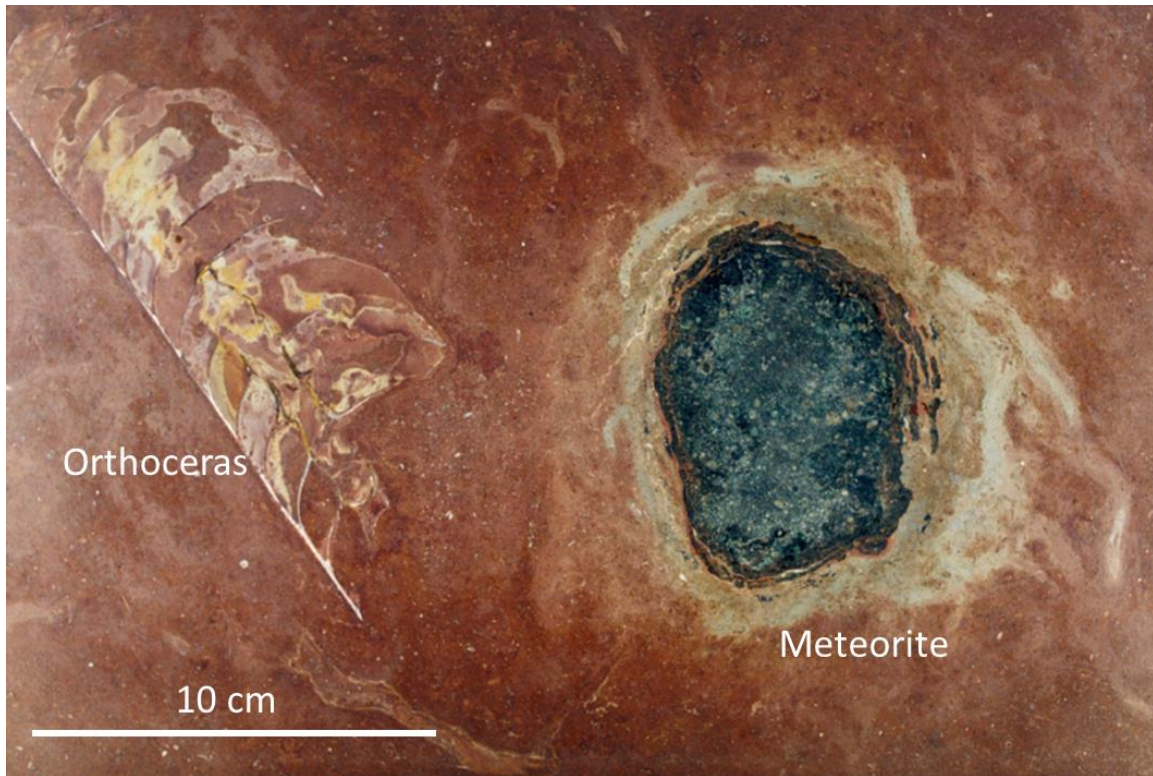


Figure 2.1: Fossil meteorite (Österplana 035) and Orthoceras in limestone plate. Plate has been cut parallel to bedding plane. Picture taken by B. Schmitz, modified from Schmitz et al., (2001).

The sharp increase in extraterrestrial material is seen in quarries all across southern Sweden (Fig. 1.1). A large meteorite was removed from Gullhögen quarry 35 km to the southeast of Thorsberg (Tassinari et al., 2004). The block containing the meteorite was discovered purely by accident, having fallen off a truck transporting slabs of limestone. Analysis of the fossils in the rock revealed it belonged to the same conodont interval as the meteorite bearing layers at Thorsberg. A survey of the Hällekis quarry 45 km to the northwest of Thorsberg showed similarly elevated amounts of meteorite material (Schmitz and Häggstrom, 2006). The rock above the base of the *L. Variabilis* zone is enriched by 2+ orders of magnitude compared with samples taken immediately below the base of the zone. The Fågelsång-Komstads quarries 350 km south of Thorsberg also contain this interval enriched in fossil meteorites. Rocks in the enrichment interval contain 2-6 grains of extraterrestrial chromite per 1 kg compared with 1 grain of extraterrestrial chromite per 62.5 kg of rock from layers above the enrichment area (Häggstrom and Schmitz, 2006). Increases in extraterrestrial material are also found in samples from just above the base of the *L. Variabilis* zone in the Siljjan and Öland areas of Sweden (Schmitz et al., 2003). It is clear that evidence for the OME is present in southern Sweden.

Similar patterns have been found outside of Sweden (Fig. 1.1). At the Lyma River near St. Petersburg, extraterrestrial chromite counts changed from 1 grain per 19 kg of rock below the *L. Variabilis* zone to 5-10 grains per 1 kg of limestone above the base of the zone. At a section of the Puxi river in Hubei, China, extraterrestrial chromite counts changed from 1 grain per 110 kg of rock below the *L. Variabilis* zone to 0.6-4 grains per

1 kg of limestone above the base of the zone (Chronholm and Schmitz, 2010). The OME appears to represent a global event.

One might ask why the vast majority of the samples have been found in or near Sweden. Why has no one definitively identified OME material outside of the Baltic, with the exception of the one section in China? Ordovician age carbonates were deposited in many other areas around the world. The explanation is simply that very few researchers are looking. Most of the OME related studies have been performed by or with Dr. Birger Schmitz of Lund University. Researchers working in Ordovician age carbonates may be either unfamiliar with the OME, may not be looking for the fossil meteorites, or else are misidentifying them, or all three. Researchers are already looking for OME evidence outside of Eurasia (Schmitz et al., 2016). As the OME becomes better known, and as more researchers become trained to look for fossil meteorites, more evidence will be uncovered.

### **2.3 The L-Chondrite Parent Body: Observation and Interpretation**

The leading hypothesis for the cause of the OME is the catastrophic break-up of an asteroid referred to as the L-chondrite Parent Body. The break-up of this asteroid is suggested to have occurred  $470\pm 6$  Ma (Korochantseva, 2007). There are several lines of evidence which support this hypothesis which are presented here.

Almost all of the OME related material recovered is classified as L-chondritic (Schmitz et al., 2016). L-chondrites are broadly defined as having lower total iron content

than H-chondrites, but lower fayalite/forsterite content than LL-chondrites. L-chondrites are the second most common type of meteorite, representing 35% of catalogued meteorites (Sean and Dodd, 1988, Kiel, 1994). The OME related material matched the chemical composition of L-chondrite meteorites in terms of trace element chemistry (Schmitz et al., 2013),  $\delta^{17}\text{O}/\delta^{18}\text{O}$  (Heck et al., 2010), fayalite/forsterite values of olivine inclusions (Alwmark and Schmitz, 2009), and size of recovered chondrules (Bridges et al., 2007).

Studies of L-chondrite meteorites from museum collections showed that most have been highly shocked. Stöfler et al., (1991) determined 54% of studied L-chondrites were shocked at conditions  $\geq 15$  GPa, whereas Rubin (1994) determined 40% show similar shocked textures and conditions. Studies of L-chondrite meteorites also reveal low levels of gasses derived from solar wind, such as  $^{21}\text{Ne}$ . About 3% of L-chondrites contain significant levels of solar wind particles, whereas ~15% of H chondrites contain such levels (Crabb and Schultz, 1981). This indicates most of the L-chondrites were exhumed from the parent body from beneath the penetration depth of the solar wind. Lastly, metallographic cooling rates calculated from L-chondrites indicate it was part of a parent body that was at least 50 km across (Taylor et al., 1987; Wood, 1979, Haack et al., 1996). The event which removed the L-chondrites from the parent body must have been violent enough to remove material from at least 25 km below the parent body surface.

K/Ar retention ages have been determined from relict L-Chondrite grains, indicating the time of the parent body break up. Korochantseva et al., (2007) determined the age of this breakup to be  $470 \pm 6$  Ma based on  $^{40}\text{Ar}/^{39}\text{Ar}$  dating of the Ghubara

regolith. This age supersedes other previously determined ages (e.g. Turner 1969; Bogard et al., 1976, 1995; Bogard and Hirsch 1980; McConville et al., 1988).  $^{40}\text{Ar}/^{39}\text{Ar}$  Ages determined from L-Chondrite grains indicate the breakup of a single parent body at ~470 Ma, as opposed to multiple parent body breakups <1.0 Ga indicated for H-Chondrite grains (Swindle et al., 2014) (Fig. 2.2). The age of the parent body breakup is coincidentally close to the beginning of the OME, especially considering the short travel time experienced by OME meteorites. (see Heck et al., 2004)

Studies have also determined OME related material travel time based on solar wind particles (Heck et al., 2004, 2008). Solar wind particles would be absorbed by L-chondrite meteors when exposed to the sun while traveling toward Earth after the parent body disruption. Thus, the presence and amount of solar wind particles imbedded in a meteorite act as a proxy for extraterrestrial travel time. The researchers analyzed levels of  $^3\text{H}$  and  $^{21}\text{N}$  in chromite grains from Thorsberg and Gullhögen quarry. Based on low levels of  $^3\text{H}$  and  $^{21}\text{N}$  in the grains, OME related material appeared to reach the Earth within 100 to 200 kyr after the disruption of its parent body (Heck et al., 2004, 2008).

All of this evidence suggests a unique origin for L-chondrites and the OME. The current hypothesis is that there was an L-chondrite parent body orbiting in the asteroid belt, with a diameter of  $\geq 60\text{km}$ . The parent body suffered a catastrophic disruption circa  $470\pm 6\text{ Ma}$  (Korochantseva, 2007), probably due to a collision with another asteroid. Remnant particles from this parent body were then transferred to a mass resonant orbit, which launched the particles toward the Earth. Material began crossing the Earth's orbit

as soon as 100 ky after origination and continued for between 10 and 30 million years. It is this sudden increase in meteorite activity that is recorded as the OME.

Some researchers have attempted to identify the remains of the L-chondrite parent body within the asteroid belt. Two major candidates have been proposed. First, 433 Eros has been identified as an L-Chondrite meteor by the Near-Earth Asteroid Rendezvous (NEAR) mission (Peplowski et al., 2015). The Flora family of asteroids is also thought to be an L-chondrite type asteroid based on reflectivity spectra (Vernazza et al., 2008).

Nesvorný et al., (2002) attempted to calculate the dispersal patterns of the members of the Flora family and concluded that it may have formed via a disruption event approximately 500 Ma. Vokrouhlicky and Farinella (2000) likewise conclude that material ejected from the position of the Flora family could reach the Earth within the period suggested by previously mentioned cosmic ray exposure ages. No substantial evidence exists to link an extant asteroid or asteroid family to the OME.

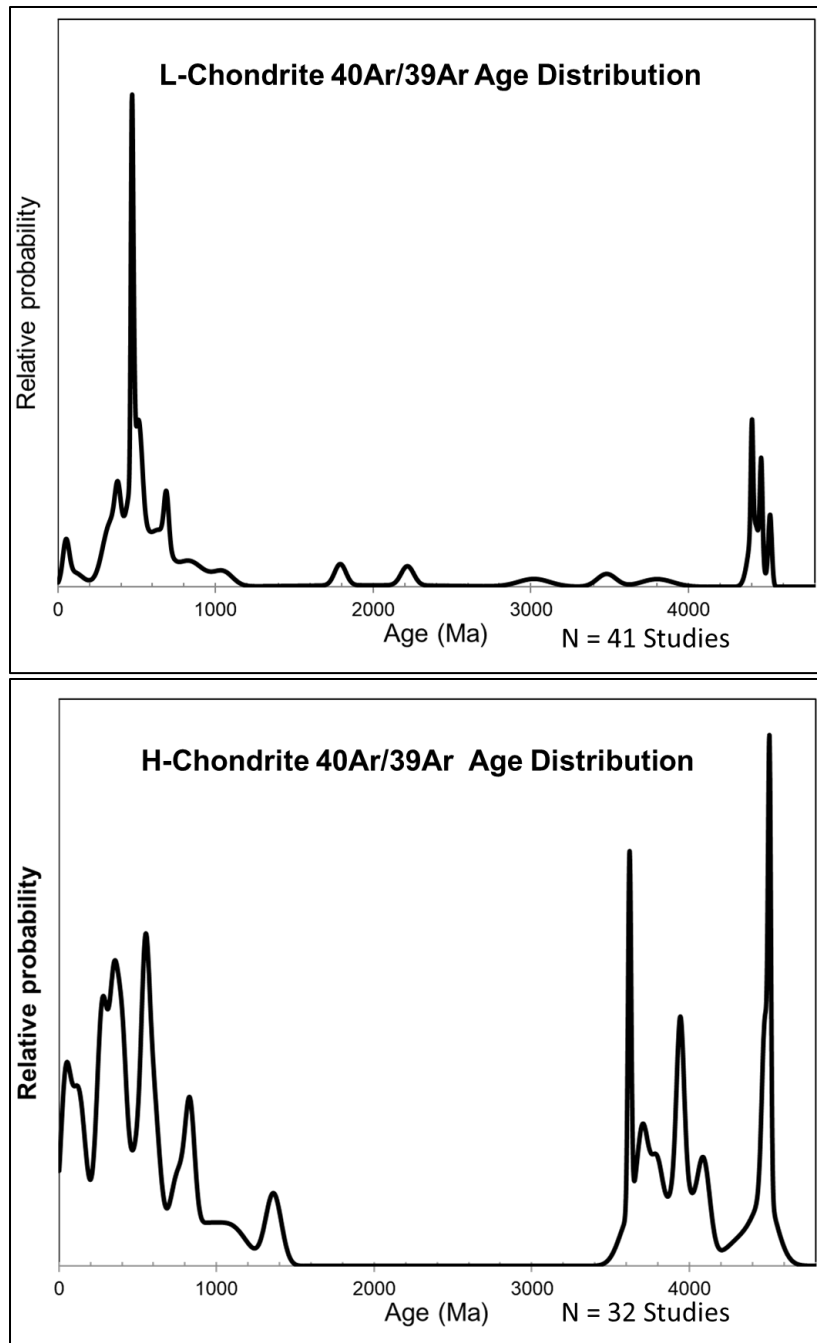


Figure 2.2: Comparison of relative probability of  $^{40}\text{Ar}/^{39}\text{Ar}$  ages determined from L (top) and H (bottom) chondrites. Figures show a bimodal age distribution for L chondrites, with a unique increase at ~470 Ma when compared with H chondrites. Figures modified from Swindle et al., 2013.

## 2.4 Ames Astrobleme

The Ames astrobleme is a complex impact structure centered on the town of Ames, Northwest Oklahoma (Fig. 2.3) (Carpenter and Carlson, 1992, 1997). The structure was initially identified via exploratory oil drilling by the D.&J Oil Company in 1990, when it was noticed that Hunton group (mainly limestone) was unusually low and thick in that area. It was further drilled to the crater floor where it was discovered not only brecciated target rocks, but also oil.

Initially called only the “Ames Hole”, various methods of its formation were proposed over the years. Local geologists referred to part of the structure as the “Hunton Graben” (Roberts and Sandridge, 1992), but the feature has no relationship to major named faults in Oklahoma. Other geologists preferred the suitably vague term “cryptoexplosion” and interpreted the feature as an unknown form of volcanic eruption. For example, Coughlon and Denney (1993, 1997) argued the feature was formed similarly to a kimberlite, one which took advantage of the relict zones of crustal weakness formed during the Keweenawan Rift. However, the authors never prove the rift system actually extended into Oklahoma, nor explain how those faults could remain active after ~600 million years. They also admit the crater is filled with felsic material, but a kimberlite type explosion would produce ultramafic material. They dismiss the Planar Deformation Features (PDFs), parallel planes of glassy material within sialic minerals, conclusively showing an impact origin. They also admit they have been unable to reproduce these features in a lab using non-impact conditions. Bridges (1997), in what he termed a ‘bold new proposal’ suggested formation via caldera collapse, with

brecciated granitic material being transported into the depression via a high-pressure slurry, which in turn vitrified some of the material, and also that the features typically associated with shock metamorphism were formed during the Pre-Cambrian via faulting.

A number of features are consistent with the “Ames Hole” to be an ancient asteroid crater (see review in Johnson and Campbell, 1997). The structure has the morphological and geophysical characteristics of other complex impact structures such as the Red Wing Creek Structure (Brenan et al., 1975; Koeberl and Reimold, 1995; Koeberl et al, 1996), Avak Structure (Kirschner et al, 1992), and the Manson Structure (Koeberl and Anderson, 1996). PDFs were identified in thin sections made from the brecciated target rock. The presence of shocked quartz and feldspar mineral grains conclusively identify the feature as formed by a hypervelocity impact (Carpenter and Carlson, 1992; 1997; Ambers et al, 1997; Fischer, 1997; Huffman, 1997, Koeberl et al, 1997).



Figure 2.3: Location of Ames, Oklahoma in relation to generalized geologic provinces. Ames Astrobleme is buried, with its center roughly beneath the town of Ames. Impact structure approximately 16 km in diameter. Base map modified from Johnson (2008).

The formation of the Ames Astrobleme is often described thus (summarized from Carpenter and Carlson, 1992, 1997): at approximately the time of the end of deposition of the Arbuckle Dolostone, a bolide impacted the surface at what is now Ames, Oklahoma. This impact induced shock metamorphism and melting in the target bedrock and fractured and excavated target bedrock to a depth of ~600 m. Following this excavation phase, crater modification began. The crater floor initially filled with a mixture of melted particles and shock metamorphosed lithic clasts of the target rock composition, primarily granodiorite and dolostone. All of the literature on the Ames Astrobleme refers to this material as either impact ‘breccia’ or ‘melt breccia’. This material is more properly a

polymict impact breccia with a melt glass matrix, or 'suevite'. This thesis will refer to this material as suevite following the recommendation of the IUGS Subcommission on Systematics of Metamorphic Rocks (Stöffler and Grieve, 2007). Moving stratigraphically upward, the suevite grades into an increasingly fine grained diamictite, interpreted as the impact ejecta which fell back into the crater. Concurrently with impactite deposition, the rims of the crater collapsed inward and the central portion rebounded, forming the interior peak ring. In the immediate aftermath of the crater formation, the exposed crater rims were partially eroded, with material 'washing' back into the crater and covering the various polymict breccias. This marked the end of deposition of the impact related lithologies.

The crater was then overlain with a unit called by Fischer (1997) the 'crater shale' of mid-Ordovician age. Many follow the lead of Carpenter and Carlson (1992) who define this shale as the Oil Creek Formation. However, Repetski (1997) suggests that based on graptolite analysis this crater shale belongs to the McLish Formation. This provides a minimum age of formation at approximately 453 Ma. As an explanation for the missing units between the Arbuckle dolomite and McLish Shale, Repetski suggests the crater rim stood above the surrounding sea, isolating the crater until flooded by sea level rise during the Tippecanoe sequence. A comparison of the interpretation of the crater lithologies in relation to regional stratigraphy is presented in Fig. 2.4. The crater was then buried by successive sedimentary units until the Upper Permian (Johnson and Smith, 1997), all of which show structural modification due to settling of the crater rocks.

There have been two attempts to determine the absolute date of formation of the impact structure. Koeberl et al., (1997) performed an  $^{40}\text{Ar}/^{39}\text{Ar}$  incremental release analysis of whole rock impact melt samples taken from the suevite portion of the drill core (9026'-9027') but obtained an age of  $285\pm 24$  Ma. Koeberl et al., (2001) performed  $^{40}\text{Ar}/^{39}\text{Ar}$  analyses with LA-MS on samples from a different set of drill core, but again obtained a wide range of ages centered around  $\sim 300$  Ma. Both of these studies contradict the 450-470 Ma age determined from biostratigraphic constraints. The authors concluded that the Ames Astrobleme was reheated in the late Pennsylvanian-Permian, during an event possibly related to the Nemaha uplift. The goal of this thesis is to provide new evidence which illuminates the cause of these discrepancies.

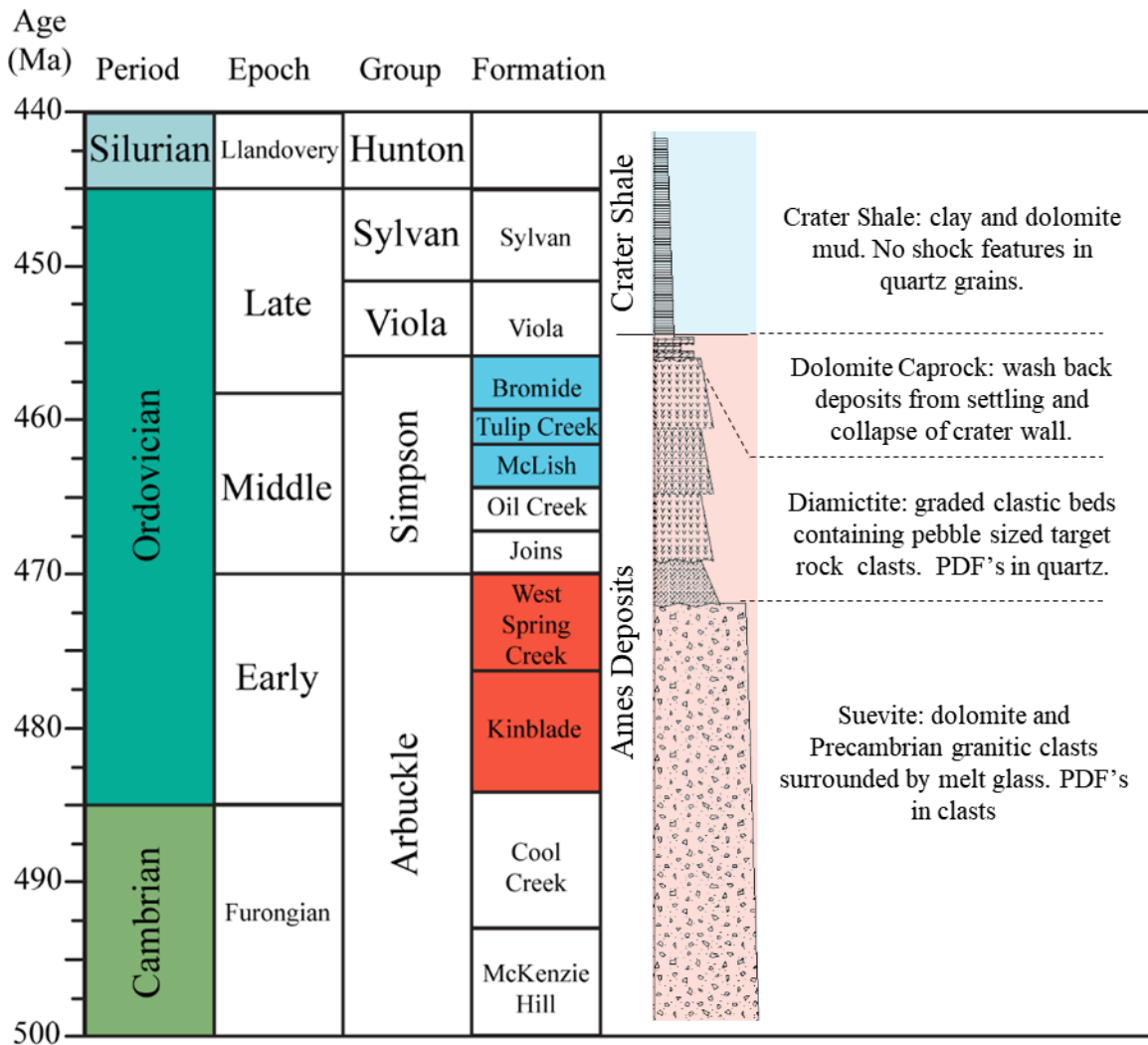


Figure 2.4: Stratigraphic chart showing geologic formations from Southern Oklahoma (Arbuckle Mountains) contrasted with simplified petrologic log of the Nicor Chestnut 18-4 Core. Lithology identification modified from Fischer (1997). Blue formations indicate possible age range of crater shale conodonts based on Repetski (1997). Red formations indicate Arbuckle dolostones and likely age range for impact. Stratigraphic information from the International Commission on Stratigraphy. Note that the Series and Stages in this portion of North America are ill defined, and are not included here.

## 2.5 The Slate Islands Archipelago

The Slate Islands impact structure is an archipelago of 17 islands situated 10 km southwest of Terrace Bay in Ontario, Canada (Fig. 2.5). The roughly circular archipelago is 7 km wide with 40 km<sup>2</sup> of surface area. There are two main islands (named Patterson and Mortimer), five minor islands, and 10 islets which comprise the archipelago.

Patterson Island is the largest and most geologically complex. The islands are interpreted as the eroded remnants of the central uplift peak of an ancient asteroid crater (Halls, 1975, 1976; Robertson and Grieve, 1976; Halls and Grieve, 1976; Halls and Stesky, 1978; Dressler et al., 1995, 1998, 1999) and have been mapped several times over the last 100 years (Coleman, 1901; Parsons, 1918; Sage, 1975, 1991).

The bedrock on the islands consist of three major units of pre-Cambrian age (see Fig. 3.3, Fig. 2.6). The majority of the bedrock consists of Archean greenschist facies metavolcanics equivalent to the Schreiber-Hemlo greenstone belt in the Wawa/Abatibi subprovince (Sage, 1991). The initial composition of the Slate Islands metavolcanics ranges from felsic pyroclastic flows to tholeiitic basalt. Considering the similarities to the Wawa/Abatibi greenstone belt, this unit was likely part of the subduction zone/island arc collision during the Algoman/Kenoran orogeny. Other Archean units include isolated portions of metasedimentary rocks interpreted as a turbidite sequence (Sage, 1991).

The other two pre-Cambrian units outcrop only in the southwest corner of Patterson Island. The second oldest unit is the Paleoproterozoic Animikie Group, representing the banded iron formation of the Gunflint Formation (Sage, 1991). The youngest of the pre-Cambrian units is the Osler Group, representing the basalts and

gabbros of the Keweenaw rift (Fig. 2.6). The islands are also cut by numerous diabase dikes, which have been related to the timing of Keweenaw rift (L. Heaman, University of Alberta 1994, personal communication referenced in Dressler et al., 1999). However, many of these dikes are younger than this (Sage, 1991), and the origin of the dikes remains contentious.

The most notable event affecting the area in the Phanerozoic was the impact of an asteroid. Bathymetry surveys show a submerged trough and ring structure 30-32 km in diameter, interpreted as the surrounding crater floor and rim (Halls and Grieve, 1976; Dressler et al., 1995; Mariano and Hinze, 1994). From this, it can be calculated that the impacting asteroid was ~1.5 km in diameter (Sharpton, 1997). Numerous shatter cones on the island are the most prominent feature which indicate the structures' origin as an ancient asteroid crater (Fig. 2.7). The islands themselves are what remains from the central uplift peak of that crater. Glacial erosion exposed the central uplift impact structure (Sage, 1991) which, being erosional resistant compared to other crater fill, remained to form the islands themselves.

Similar to the Ames Astrobleme, however, alternative modes of formation for the Slate Islands have been suggested. Sage (1991, 1999) described the islands as being formed by a 'cryptoexplosion' facilitated by explosive events astride two intersecting fault zones. In this interpretation, the suevites on the islands are lamprophyrite and were emplaced into dikes from a deep (>35km) volatile rich magma chamber. However, this interpretation fails to explain the presence of PDFs or numerous shatter cones. Also, no evidence for the deep, volatile rich magmas have been reported. The timing of this

'lamprophyrite' emplacement is also contentious and has been used to argue both for and against the impact origin based on the interpretation of individual researchers.

Since 2 Ma, several episodes of glaciation covered the area (Sage, 1991). In historical times, the islands were exploited for timber and gold; traces of this activity can still be seen on the islands. The archipelago is now a provincial park and receives visitors only as campers and the occasional scientist.



Figure 2.5: Location of Slate Islands Archipelago within Lake Superior.



Figure 2.6: Contact between older Archean felsics (right) and younger Keweenaw mafics (left). Outcrop approximately 85 meters wide, located on southwestern shore of Patterson island.



Figure 2.7: Nine to twelve-meter-tall shatter cones on Slate Islands. Outcrop is located between sample E1 and E2 (see Fig. 3.3). See Hollings et al., 2006 for exact location.

Table 2.1: Proposed age constraints for Slate Islands.

| Observation   | Age Constraint    | Comment   | Reference* |
|---|-------------------|---|------------|
| Brecciated Keweenaw<br>Mafics   | <1.1 Ga           | Constraint on oldest possible age   | 1,2        |
| Shock-deformed and<br>brecciated lamprophyre  |                   |   |            |
| K-Ar (antigorite and<br>phlogopite)   | <282 to<br>310 Ma | Dating of intrusive dikes which<br>post-date impact   | 3          |
| U-Pb (perovskite)   | <1.1 Ga           | More reliable for date of impact  | 4          |
| Brecciated sandstone of the<br>Jacobsville Formation  | <800 Ma           | Jacobsville is 1.1 Ga, but clasts<br>may be interflow sandstones<br>from within Osler-like volcanic<br>flows. | 5          |
| Apparent absence of<br>Ordovician/Devonian rock<br>fragments in impact breccia                      | >350 Ma           | Hudson Bay Lowlands and<br>Michigan basins were almost<br>certainly connected during<br>Ordovician/Devonian   | 6,7        |
| Similarity of Slate Islands<br>erosion level with that of<br>357 Ma Charlevoix impact<br>structure. | <350 Ma           | Erosion levels are variable in<br>various parts of the Canadian<br>Shield                                     | 8          |

\*1= Halls and Grieve, 1975; 2= Dressler and Sharpton, 1997; 3= Sage, 1991; 4= L. Heaman, U of Alberta; 5= Card et al., 1994; 6= Norris and Sanford, 1968; 7= Sharpton et al., 1996; 8= Grieve et al., 1995.

## **III: METHODS CHAPTER**

### **3.1 Overview**

This project focuses on deciphering the age of impact structures in two field areas: Ames Astrobleme in Oklahoma and the Slate Islands Archipelago (specifically Patterson Island) in Canada. This chapter documents the sample collection locations and methods, and the various analytical techniques used. It presents the unique challenges and solutions that were required for each field area. It also provides a brief overview of the theoretical background of the analytical techniques, as well as the specifications used for each technique.

### **3.2 Sample Collection**

#### **3.2.1 AMES ASTROBLEME SAMPLE COLLECTION**

Ames Astrobleme in central Oklahoma is buried under 2.5-2.7 km of overburden (Fischer, 1997) (Fig. 3.1). The Nicor Chestnut 18-4 well was drilled in the depressed central ring of the crater. Fifteen meters of core representing the unique stratigraphy of the impact structure from the crater well was first described by Fischer (1997) and is stored in the Oklahoma Petroleum Information Center in Norman, Oklahoma. Available core ranged in depth from 8990' (2740.2 m) to 9037' (2754.5 m), and access was provided by the Oklahoma Geologic Survey (OGS). The OGS Core Repository was visited on January 10, 2017, where the total core was made available for petrographic

observations. The core was photographed and analyzed to compare with the interpretation of Fischer (1997). See the geologic background section for detailed core interpretation.

Nine sample sites from the impact melt rock unit of the Nicor Chestnut 18-4 Core drill core were selected and photographed (Fig. 3.1; Table 3.1). Sites were selected on the core based on the location of visible granodiorite clasts to maximize mineral recovery (Fig. 3.2). Cylindrical samples (plugs) were taken from the section (see Fig. 4.1). These samples are one inch in diameter and vary in length depending on the initial location within the core. These were selected to ensure a representative suite of textures present in the lower portion of the core. Competent granodiorite clasts, melt rock and the melt rock/clast interface were represented. Samples were photographed and cleaned with an abrasive pad to remove markings and oxidation. Thin sections were then made from the plugs for petrographic analysis.

Table 3.1. Ames Astrobleme sample information  
 Location: Section 18, Township 21N, Range 9W  
 (Latitude: 36.292107, Longitude, -98.19898)

| Sample Number    | Elevation (feet) | Weight (g) | Comments <sup>a</sup>               |
|------------------|------------------|------------|-------------------------------------|
| 1 <sup>b</sup>   | 9014.90          | 39.6       | Mix of melt glass and igneous clast |
| 2 <sup>b</sup>   | 9017.00          | 25.9       | Mix of melt glass and igneous clast |
| 3 <sup>b</sup>   | 9018.25          | 36.1       | Melt glass prominent                |
| 4 <sup>b,c</sup> | 9022.00          | 42.8       | Mix of melt glass and igneous clast |
| 5 <sup>b,c</sup> | 9026.00          | 31.1       | Mix of melt glass and igneous clast |
| 6 <sup>b,c</sup> | 9027.00          | 35.2       | Mix of melt glass and igneous clast |
| 7 <sup>b,c</sup> | 9031.00          | 26.8       | No melt glass in sample             |
| 8 <sup>b</sup>   | 9033.00          | 47.9       | Mix of melt glass and igneous clast |
| 9 <sup>b,c</sup> | 9037.00          | 26.3       | Mix of melt glass and igneous clast |

a. All samples were taken from the impact melt rock unit of the core. All samples were 1-inch round plugs of granodiorite and contain quartz, feldspar, melt glass, and accessory minerals.

b. Zircons from these 9 samples dated using LA-ICP-MS and SIMS.

c. K-feldspar from these 5 samples dating using <sup>40</sup>Ar/<sup>39</sup>Ar geochronology.

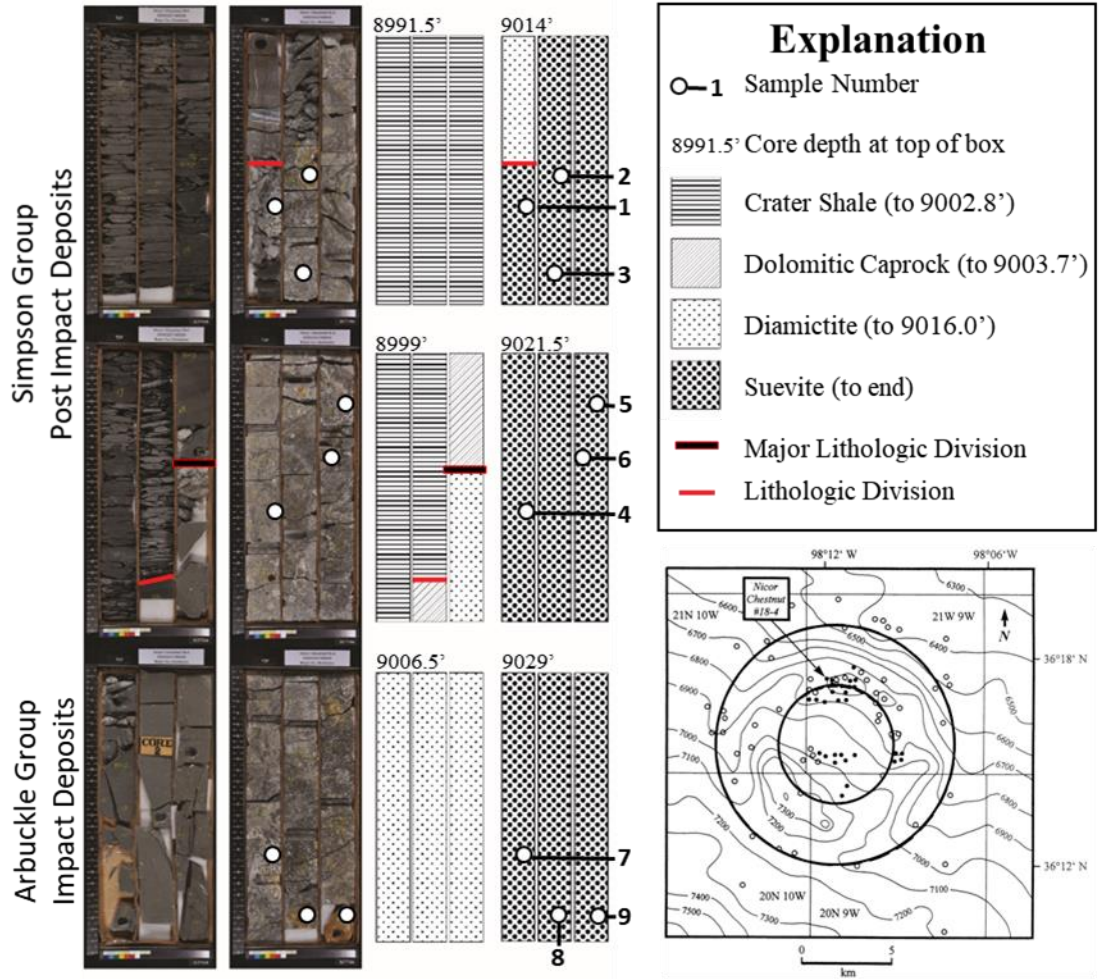


Figure 3.1: Map, photographs, and overview of the Nicor Chestnut 18-4 Core drill core from the Ames Astrobleme. Core is approximately three inches in diameter. White circles represent locations of collected sample plugs. Inset map shows the location of boreholes which penetrate the Arbuckle Group, including the Nicor Chestnut 18-4 Core, with bold circles indicating inferred outer and inner crater rim (modified from Koeberl et al., 2001). See Table 3.1 for sample information.



Figure 3.2: Polished slab taken from Nicor Chestnut 18-4 core representative of suevite texture. Sample S7 9031' removed from adjacent portion of core.

### **3.2.2 SLATE ISLANDS (PATTERSON ISLAND) SAMPLE COLLECTION**

Samples from the Slate Islands were collected during a trip to the islands in July 2017 (Figs. 3.3, 3.4). The islands were accessed via charter boat, and a camp site was established on the northernmost point of Patterson Island. Rock outcrops along the shore were accessed via kayak. An attempt was made to walk to outcrops in the center of the island; but this was prevented by the lack of trails through the underbrush. Sample sites were identified based on previous geologic surveys and maps (Sage, 1991). Fifteen total samples were collected from the island bedrock, of which four were used for the current analysis. The other samples are being reserved for future projects. Representative samples of five major groups on the island were collected with an emphasis on sampling suevite (a breccia made from target rock clasts and solidified melt particles) (Fig. 3.5). Suevite samples were difficult to collect due to the melt glass which comprise the rock matrix. The suevite was easily altered and erosionally weak compared to surrounding lithologies. Samples used for analysis were collected from exposed seaside cliffs and outcrops. Samples were described and labeled and transported to the University of Texas at Austin.

Table 3.2. Slate Islands sample information

| Sample Name      | Latitude | Longitude | Lithology <sup>a</sup>        |
|------------------|----------|-----------|-------------------------------|
| McColl Island    |          |           |                               |
| D1               | 48.6690  | -87.0142  | Diabase                       |
| Patterson Island |          |           |                               |
| E1               | 48.6690  | -86.9872  | Rhyolite <sup>a</sup>         |
| E2               | 48.6705  | -86.9905  | Rhyolite <sup>a</sup>         |
| E3               | 48.6706  | -86.9913  | Rhyolite <sup>a</sup>         |
| R1               | 48.6624  | -87.0158  | Rhyolite <sup>a</sup>         |
| R2               | 48.6616  | -87.0167  | Rhyolite <sup>a</sup>         |
| R3               | 48.6567  | -87.0214  | Rhyolite <sup>a</sup>         |
| H1               | 48.6583  | -87.0240  | Gabbro <sup>a</sup>           |
| H2               | 48.6617  | -87.0218  | Gabbro <sup>a</sup>           |
| C1               | 48.6554  | -87.0537  | Metaconglomerate <sup>a</sup> |
| C2               | 48.6540  | -87.0549  | Metaconglomerate <sup>a</sup> |
| G1               | 48.6600  | -86.9576  | Suevite <sup>b</sup>          |
| G2               | 48.6624  | -86.9577  | Suevite <sup>b</sup>          |
| S1               | 48.6569  | -86.9575  | Syenite <sup>a b</sup>        |
| S2               | 48.6534  | -86.9563  | Syenite <sup>a b c</sup>      |

a: All Pre-Cambrian lithologies have undergone low-grade metamorphism. Sample labels were determined based on lithology and/or proximity to nearby landmarks. (e.g.,

D1=Diabase #1, R1=Rhyolite #1, G1=Gabbro #1 S1=Suevite #1)

b: Zircons from these samples dated using Laser Ablation-ICP-MS and/or SIMS.

c: K-feldspar from these samples dating using  $^{40}\text{Ar}/^{39}\text{Ar}$  geochronology.

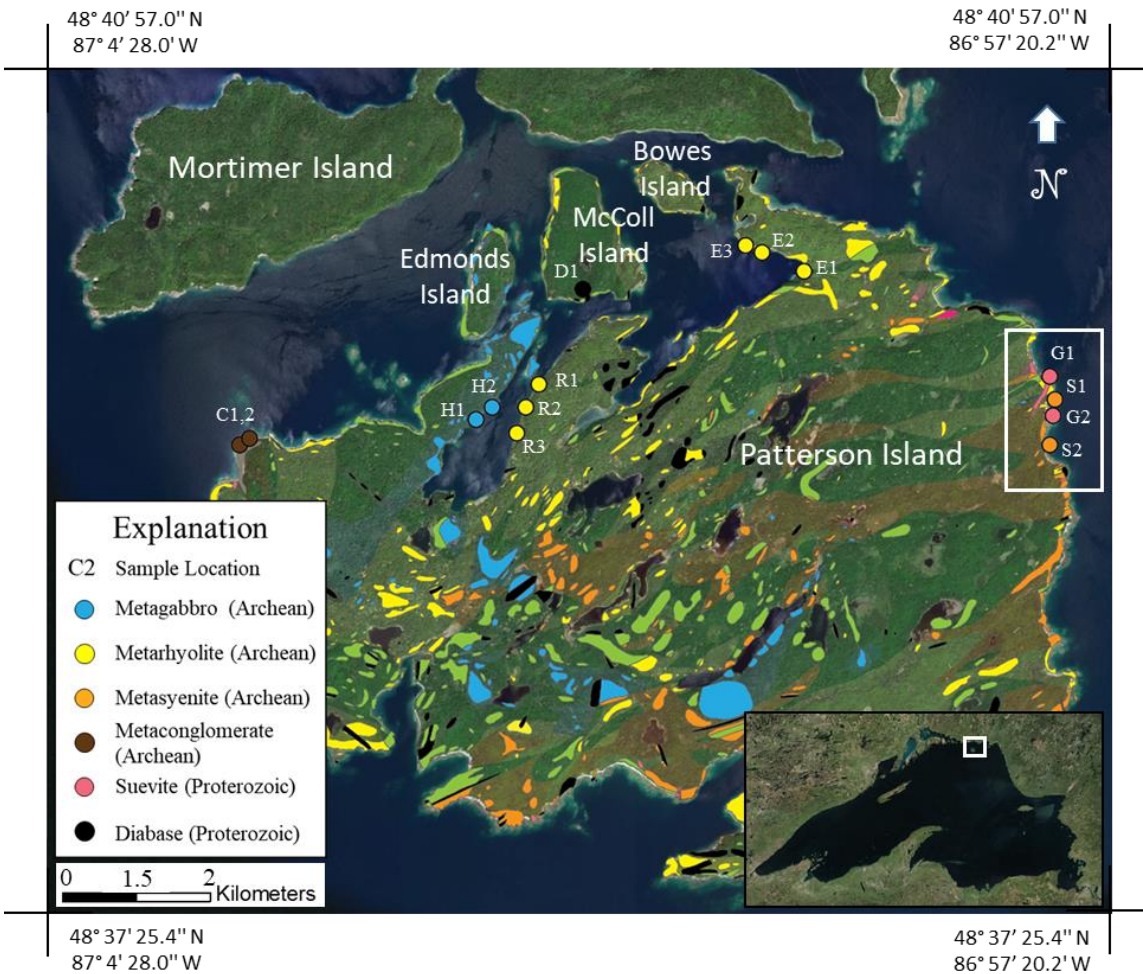


Figure 3.3: Sample location map for rocks collected within the Slate Islands. Inset shows location of Slate Islands within Lake Superior. Large white box indicates location of Fig. 3.4. Bold colors indicate location of previously mapped outcrops, transparent colors indicate inferred geologic boundaries. Note thick vegetation cover preventing travel to interior of island. See Table 3.2. for sample data. Geologic map modified and simplified from Sage (1991).

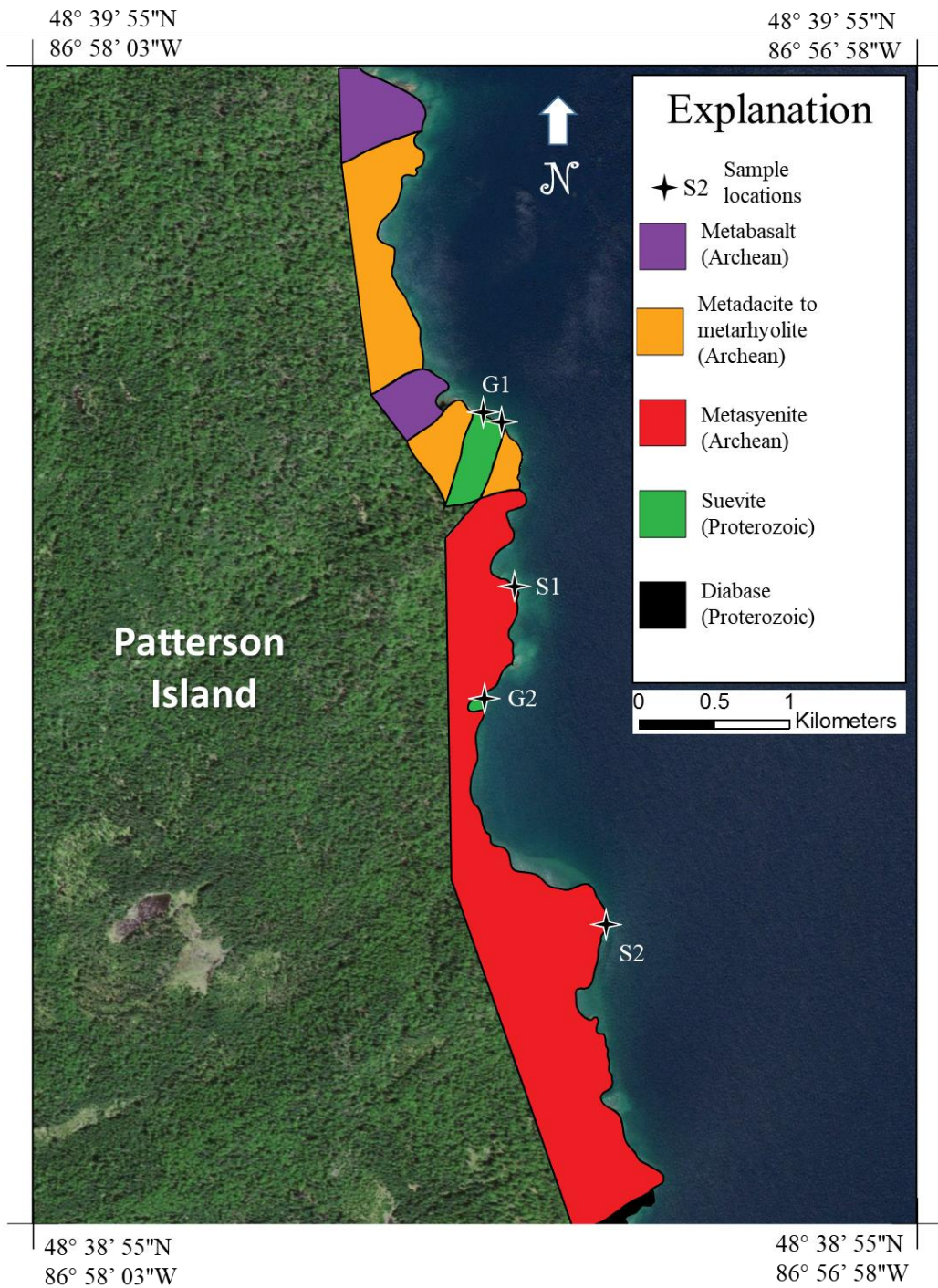


Figure 3.4: Sample locations and bedrock geology on east coast of Patterson Island. Note thick vegetation cover preventing travel to interior of island. See Fig. 3.3 for location of this region within the context of the Slate Islands.



Figure 3.5: Suevite outcrop G1. Note flow banding within and recessed nature of suevite. Also note felsic brecciated clasts within suevite.

### 3.3 Mineral Separation

Upon return to the University of Texas at Austin, all samples were cleaned, weighed, and photographed (see Appendix 6.1). Portions of samples were removed as 1cm x 2.5cm billets from which thin sections were made. All thin sections were photographed in plain-polarized and cross-polarized light [see Ch. 4 (Results) for thin section images].

All remaining samples were processed to extract zircons and K-feldspar using standard mineral separation techniques (e.g., Strong and Driscoll, 2016). The process was modified due to the small size of the samples and need to extract as many radiogenic minerals as possible from each rock, and is briefly described herein. Samples were first

crushed using a Marcy jaw crusher, and then pulverized using a Bico vertical disk mill. After being pulverized, samples were sieved to separate into fractions bigger and smaller than 0.149 mm (100 mesh); coarse material was re-pulverized until all sample was smaller than 1 mm. A portion of this coarse material was reserved for the collection of K-feldspar. The remainder continued with the rest of the zircon separation procedure.

Heavy minerals were then isolated from the light minerals. Heavy minerals were first winnowed using a Wilfley water table. The Wilfley table is a slightly sloped surface with rows of parallel ridges onto which the sample material is slowly poured. A motor shakes the table side to side while water washes the sample toward collecting cups on the opposite side. Minerals of relatively low density are pushed over the ridges, while heavy minerals are carried along the ridges to appropriately placed collection cups. The table was rinsed clean before and after every use. Once separated, heavy and light minerals are placed in labeled containers and set out to dry. The more voluminous light material was left to dry on an open-air shelf, while heavy minerals were placed in a drying oven at 100°C overnight.

Heavy minerals were further isolated using the heavy liquid (bromoform) separation technique. Separating equipment was set up under a fume hood according to standard procedures. Small portions of the sample to be separated were placed in a separatory funnel with enough bromoform to cover the sample. The sample was allowed to sit while heavy minerals (including zircon) sank to the bottom of the funnel. A stopcock on the bottom of the funnel was then opened and quickly closed, allowing the heavy minerals to drop on to a funnel lined with filter paper below. The process is

repeated for the light minerals with clean filter paper. Samples were then washed with acetone to remove bromoform and left in the fume hood to dry.

Samples were then processed to remove magnetic minerals. A hand magnet was passed over the sample to remove the strongest magnetic minerals. The remaining sample was passed through a Franz Isodynamic Magnetic separator in multiple runs of increasing magnetic strength to isolate zircon and other non-magnetic minerals. Lastly, zircon crystals were picked from the non-magnetic portion by hand, and stored in a clean, labeled container.

Six samples were subjected to mineral separation for feldspar, which was performed by the Oregon State University. Previously crushed material was sieved, and the 120-180  $\mu\text{m}$  size fraction was cleaned with 1% HCl and deionized water prior to packing in aluminum capsules for irradiation. The additional steps needed to prepare the feldspar crystals will be explained in section 3.4.3.

## **3.4 Geochronology**

### **3.4.1 ZIRCON U-Pb DATING VIA LASER ABLATION-INDUCTIVELY COUPLED PLASMA-MASS SPECTROMETRY (LA-ICP-MS)**

Ten whole zircon grains from Ames Astrobleme (Table 3.1) and nineteen whole zircon grains from the Slate Islands (Table 3.2) were available after the first round of mineral separation. These were dated using an Element2 High Resolution (HR)-ICP-MS with an Excimer (192 nm) laser ablation system instrumentation in the Geo-

Thermochronometry lab at the University of Texas at Austin (see Chapter 4 for full discussion of analytical results). Size of the grains ranges from 10-15 $\mu\text{m}$  to ~100 $\mu\text{m}$  in length. In this method, an ablated dry aerosol is introduced into the HR-ICP-MS using ultra-high purity He carrier gas for  $^{238}\text{U}$ ,  $^{232}\text{Th}$ ,  $^{206}\text{Pb}$ , and  $^{208}\text{Pb}$  isotopic measurements using ion-counting. Each analysis consisted of a 2-pulse cleaning ablation, a background measurement taken with the laser off, a 30-sec measurement with the laser firing, and a 30-sec cleaning cycle. The laser spot size used was 30 $\mu\text{m}$ . Selected grains that were of larger size were dated with additional spots during the analytical session. Common Pb was corrected using the measured  $^{204}\text{Pb}$  (Hg-corrected) and assuming initial composition reported by Stacey and Kramers (1975). Elemental and isotopic fractionation of Pb/U and Pb isotopes, respectively, was corrected by interspersed analysis of primary and secondary zircon standards with a known age (GJ1, Jackson et al., 2004, Plešovice, Sláma et al., 2008, and Pak1, internal age standard). The common unknown to standard measurement ratio was typically 4:1. Uncertainty resulting from calibration correction is <10% for both  $^{206}\text{Pb}/^{207}\text{Pb}$  and  $^{206}\text{Pb}/^{238}\text{U}$ .

After ablation, five grains from Ames Astrobleme and two grains from Slate Islands samples S2 were selected for additional dating using SIMS at Heidelberg University. These grains were large and competent enough to survive both the ablation and remounting procedures. These individual grains were removed from the LA-ICP-MS mount, and mounted in epoxy, and sectioned. In addition to these zircons, eight zircons from Ames Astrobleme and forty zircons from Slate Islands were also dated. These additional grains had been recovered in a second round of mineral separation. All grains

were imaged in cathodoluminescence (CL) at the University of Texas at Austin to identify the lased and/or ion beam spots.

### **3.4.2 U-Pb GEOCHRONOLOGY VIA SECONDARY ION MASS SPECTROMETRY (SIMS)**

Overall, ten zircon grains from Ames Astrobleme and 42 zircon grains from the Slate Islands were dated using the Cameca IMS 1280-HR at the Heidelberg University, Germany. These included the previously mentioned grains which had been dated via LA-ICP-MS, as well as additional zircons obtained during a second round of mineral separation. All zircons were mounted in epoxy resin with a set of age standards (AS3,  $1099.1 \pm 0.5$  Ma, Schmitz et al., 2003) and polished lightly to expose their cross-sectional areas. Prior to dating by SIMS, grains were imaged in CL to ascertain ideal locations for spot analysis (see Results chapter).

During SIMS analyses, a focused oxygen primary beam ( $\sim 50 \mu\text{m}$ ) sputtered following species over 10 cycles per spot:  $^{94}\text{Zr}^{16}\text{O}$ ,  $^{204}\text{Pb}$ ,  $^{206}\text{Pb}$ ,  $^{207}\text{Pb}$ ,  $^{208}\text{Pb}$ ,  $^{232}\text{Th}$ ,  $^{238}\text{U}$ , and  $^{238}\text{U}^{16}\text{O}$ . Forty-one spots were placed on standard AS3, which created a calibration curve in  $\text{UO}_2^+/\text{U}^+$  vs.  $\text{Pb}/\text{U}$ , Relative Sensitivity Factor with a slope of 0.903551 and intercept of  $0.134581 \pm 0.0329$ . The calibration reproduced the standard age to  $1095 \pm 36$  Ma. Most zircon grains were imaged after dating using CL and backscattered-electron images.

### 3.4.3 $^{40}\text{Ar}/^{39}\text{Ar}$ GEOCHRONOLOGY VIA STEP HEATING

Five samples of granodiorite from the Ames Astrobleme and one sample of metasyenite from the Slate Islands were subjected to  $^{40}\text{Ar}/^{39}\text{Ar}$  whole-rock dating at the Oregon State University Geochronology Laboratory. The samples were loaded in evacuated quartz tubes, alternating with packages of FCT-3 biotite monitor standard (28.04 Ma; Renne et al., 1998) and irradiated at the Oregon State University Geochronology Laboratory in one batch for approximately 6 hours. Pure  $\text{CaF}_2$  and  $\text{K}_2\text{SO}_4$  salts were also irradiated with the samples to estimate the Ar produced by nuclear reactions on Ca and K isotopes. The following correction factors are used for correcting the reactor produced interfering Ar isotopes:  $(^{36}\text{Ar}/^{37}\text{Ar})_{\text{Ca}} = 0.002227$ ,  $(^{39}\text{Ar}/^{37}\text{Ar})_{\text{Ca}} = 0.034342$  and  $(^{40}\text{Ar}/^{39}\text{Ar})_{\text{K}} = 0.0381106$ . The relative variation in the neutron fluence within the capsule was monitored by pure Ni wire that was also irradiated with the samples. Argon gas was extracted via step heating in a furnace, utilizing a laser which had its power output calibrated to certain temperatures. Analysis began at 0.3% to 1.0% of maximum output and was increased in steps ranging from 0.2% to 1.0%. The amount of increase per step (and thus, the number of total steps used) varied based on the needs of individual samples. For example, increases in power output per step would be reduced when large releases of argon gas were anticipated. The analysis was concluded when the sample began to release negligible amounts of argon, typically between 13% and 20% of total output. The gas released at each step was cleaned using Ti-Zr getters and analyzed for Ar isotope ratios in the Mass Analyzer Products (MAP) Model 215-50 single collector mass spectrometer (ThermoFisher).

## **IV: RESULTS**

### **4.1 Overview**

This chapter presents the petrographic analysis of the samples that were collected from the Ames Astrobleme (all samples) and Slate Islands, Canada (Samples G1, G2, S1, S2). Next, ages from the LA-ICP-MS and SIMS dating of zircon (U-Pb) and the  $^{40}\text{Ar}/^{39}\text{Ar}$  analysis of feldspars are reported and trends in the data are identified. The data are also compiled in graphical form. The data and its geologic context will be discussed in chapter 5.

### **4.2 Petrographic Analysis: Mineralogy and Impact Generated Textures**

#### **4.2.1 AMES ASTROBLEME**

All samples from the Ames Astrobleme core were collected from the suevite portion (>9016', see Table 3.1); as such, they exhibit similar petrographic characteristics. All samples contain varying percentages of melt glass, granodiorite clasts, and dolomite clasts (Figs. 4.1-4.3). The varying ratios of glass to clasts are due to the heterogeneous nature of the sampled material. Whereas hand samples appear to show competent mineral grains in granodiorite clasts (Figs. 3.2, 4.1), thin section analysis shows many individual mineral grains have been reduced to diaplectic glass. Glass of feldspar composition is maskelynite. Fig. 4.3 shows thin sections from several samples showing textures present in the suevite. Figs. 4.3A and 4.3B shows the interface between granodiorite clast (top half) and diamictite (bottom half); note the presence of veins and fractures permeating the

granodiorite clast and smaller dolomite clasts within the melt glass. Figs. 4.3C and D show a sample dominated by impact melt glass (now devitrified). Figs. 4.3E and F show a thin section dominated entirely by granodiorite clast; note the highly fractured textures within certain quartz and feldspar grains.

All thin sections show distinct shock textures and planar deformation features (Fig. 4.3). The suevite matrix is comprised of spherical and fibrous glass particles which has the appearance of having flowed around the lithic clasts while cooling (Fig. 4.3B). The mineral maskelynite is also present. Maskelynite is a glass with the composition of plagioclase. The identity of the mineral as maskelynite was confirmed via BSD analysis at the University of Texas at Austin. Mineral crystals throughout the breccia are significantly fractured along crystallographic axes (Figs. 4.3C, D, F). PDFs are also present, including mosaic textures and inclusions formed along crystallographic axes (Fig. 4.3E).

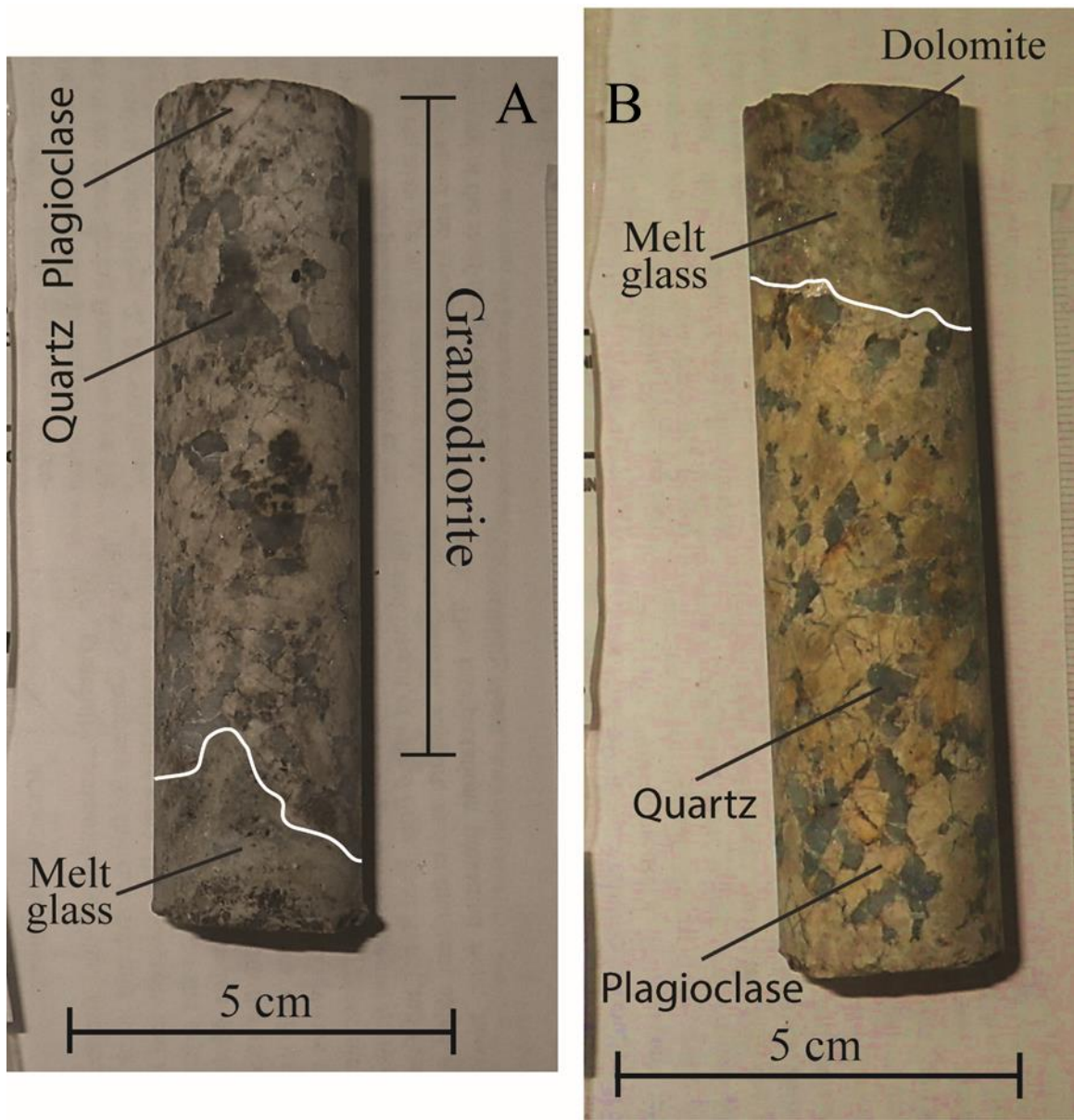


Figure 4.1: Ames Astrobleme hand samples showing apparently competent granodiorite clasts. A: Sample S6 9027' B: Sample S7 9031'. Compare with Fig. 4.2.

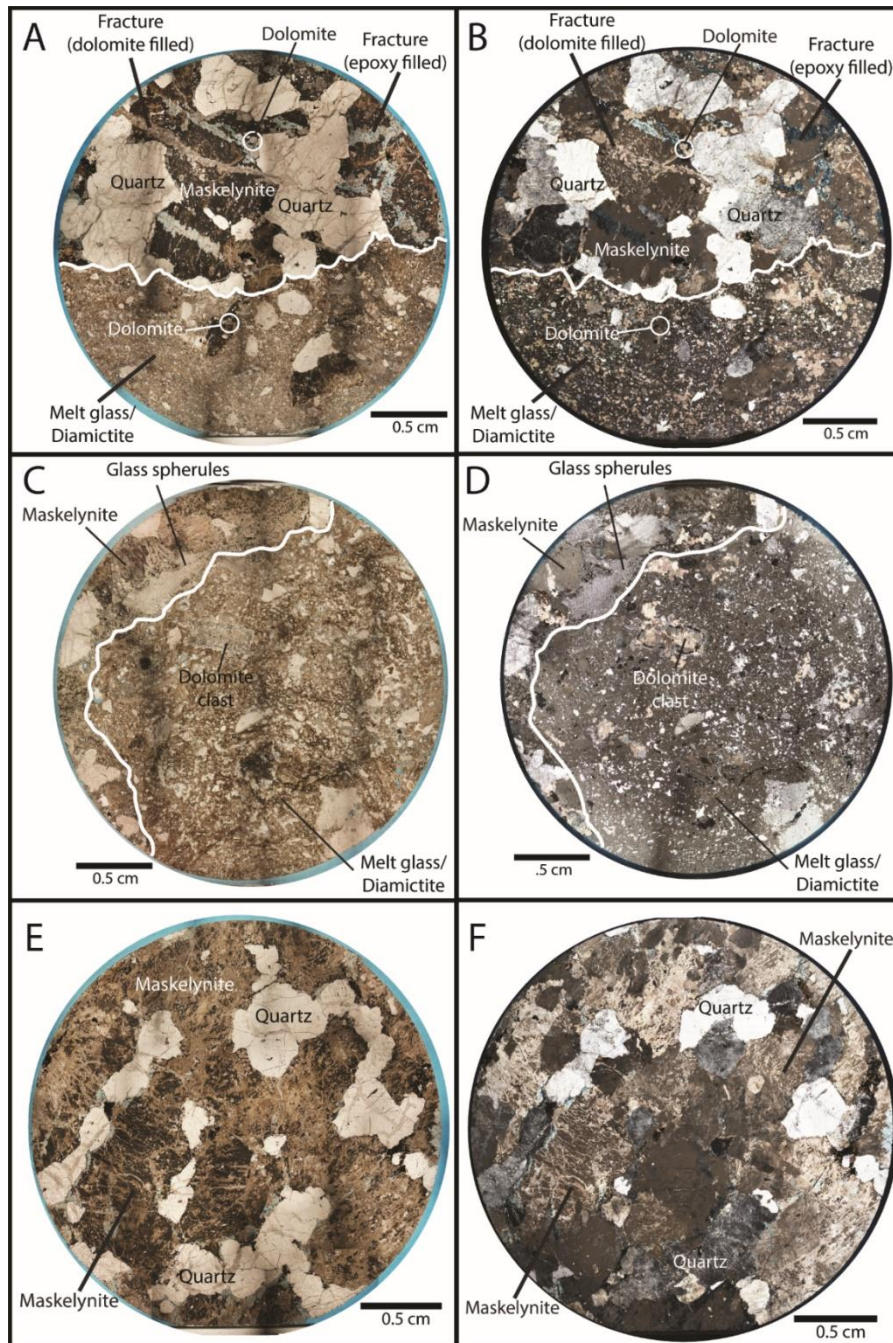


Figure 4.2: Photomosaics of thin sections from the Nicor Chestnut 18-4 core. A: Sample S4 9022' (Plane polarized light). B: Sample S4 9022' (Cross polarized light). C: Sample S6B 9027' (Plane polarized light). D: Sample S6B 9027' (Cross polarized light). E: Sample S7 9031' (Plane polarized light). F: Sample S7 9031' (Cross polarized light).

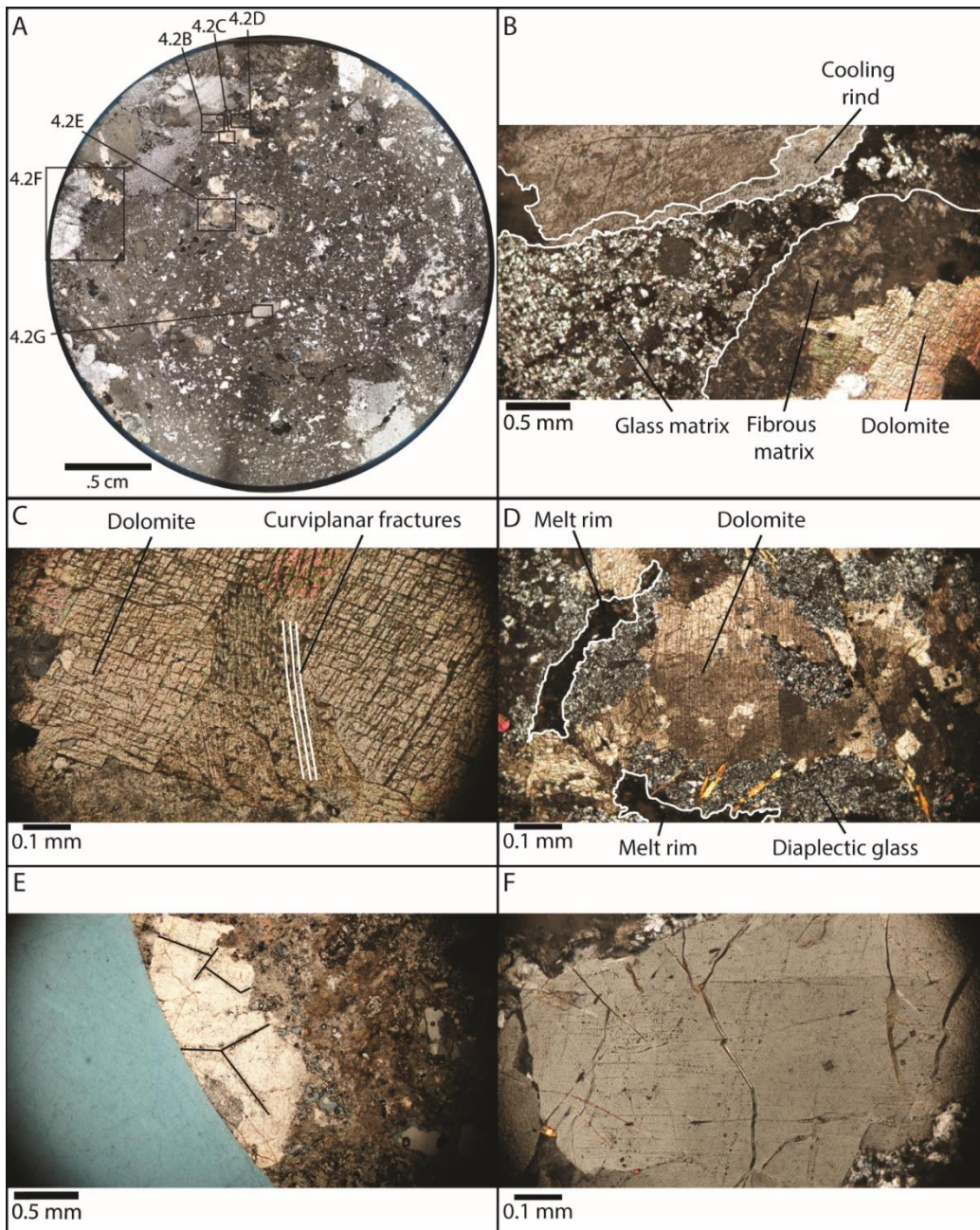


Figure 4.3. Thin section S6B (9027') with key features highlighted. 4.3A: Overview (Cross polarized light). 4.3B: melt injection texture (Cross polarized light). 4.3C: Curvilinear fractures within dolomite (Cross polarized light). 4.3D: Melt texture around shocked dolomite clast. (Cross polarized light). 4.3E: Mosaic texture within quartz crystal (Plane polarized light). 4.3F: Inclusions within quartz along crystallographic axis (Cross polarized light).

#### 4.2.2 SLATE ISLANDS

Hand samples of both syenite (Fig. 4.4) and suevite (4.5) were collected for analysis. Fig. 4.4 shows the characteristic red color of syenite hand samples. Hand samples that appeared to be syenite in the field were revealed in thin section to be a quartz-rich syenite porphyry (Figs. 4.4, 4.6), for the sake of simplicity they will be referred to as syenite in this thesis. Fig. 4.5 shows a representative sample of suevite. The sample contains brecciated clasts of multiple lithologies welded together by melt glass. All of the main lithologies on the archipelago (including syenite, rhyolite, banded iron formation, gabbro and chert) are represented in the breccia clasts. The sample itself is a beach cobble found adjacent to the outcrop. The suevite samples collected from the outcrop were weathered and thus difficult to photograph, many had fragmented by the time they were returned to UT Austin. The cobble in Fig. 4.5 had been naturally polished by the waves and was the most photogenic of any collected suevite, it was the only sample to show the polymict breccia texture.

Thin sections were made of representative samples of suevite and syenite from the Slate Islands. Samples G1 and S1 were chosen for thin section analysis (Figs. 4.6, 4.7). Syenite samples are composed of plagioclase, orthoclase and quartz crystals in an orthoclase matrix (Figs. 4.6). Suevite samples are composed of a glass matrix surrounding clasts of the various bedrock units found on the Slate Islands (Fig. 4.7). In thin section both show the highly deformed and fractured texture characteristic of the Ames Astrobleme samples.



Figure 4.4. Hand sample of syenite. Sample S1 showing syenite appearance.

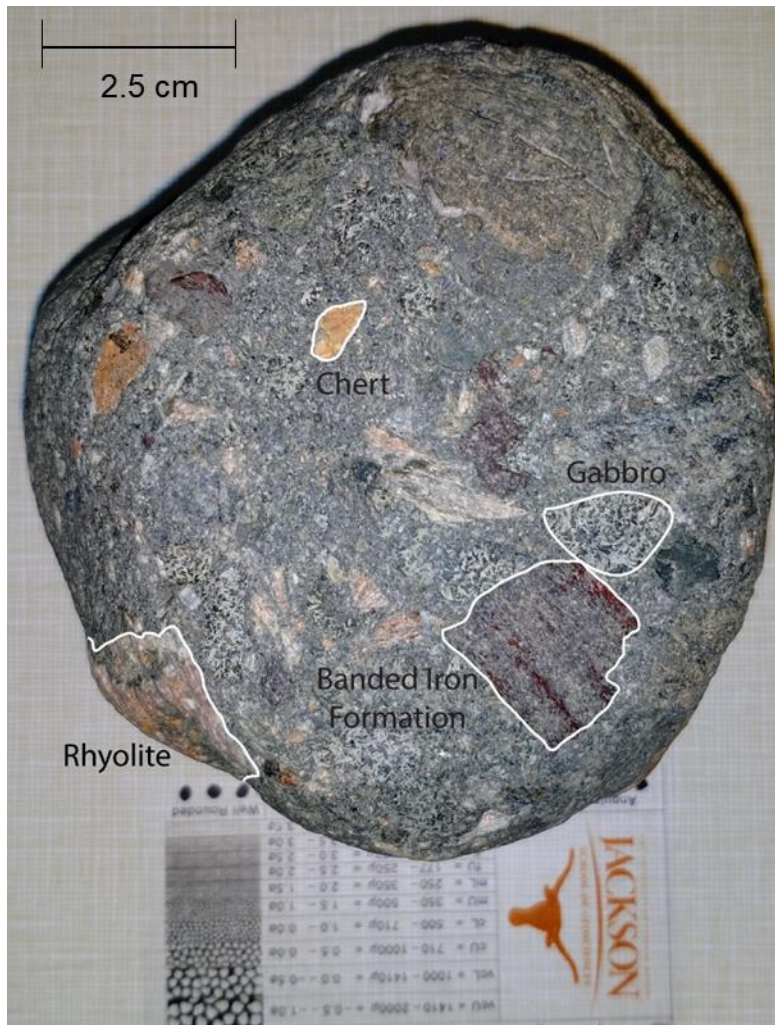


Figure 4.5. Hand sample of suevite with examples of clast lithology labeled. See Section 2.4 for likely identities of the clasts.

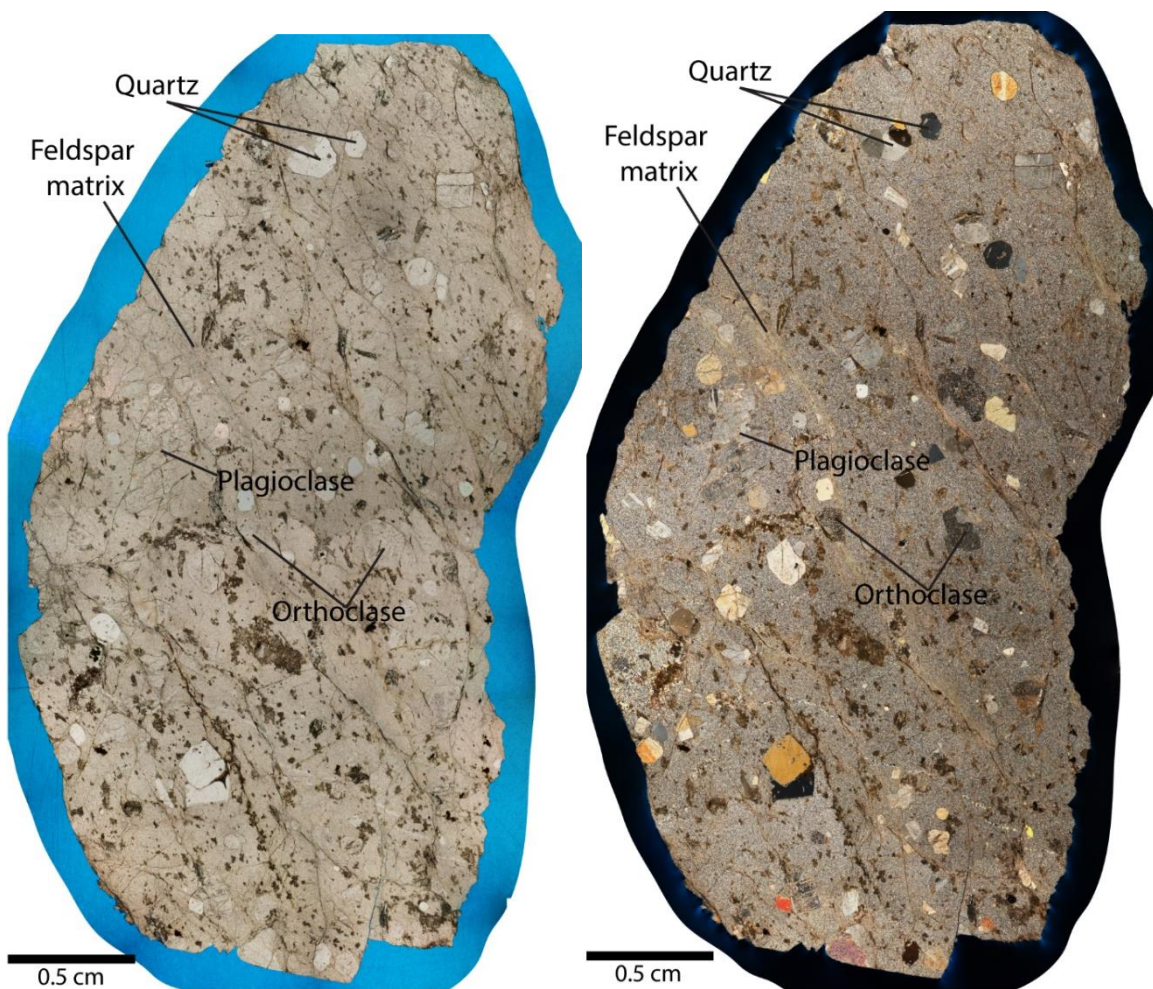


Figure 4.6 Thin section of syenite sample S1. Texture is characteristic of an alkali porphyry rather than a 'true' syenite. Compare with figure 4.3A. Left: plane polarized light. Right: cross polarized light.

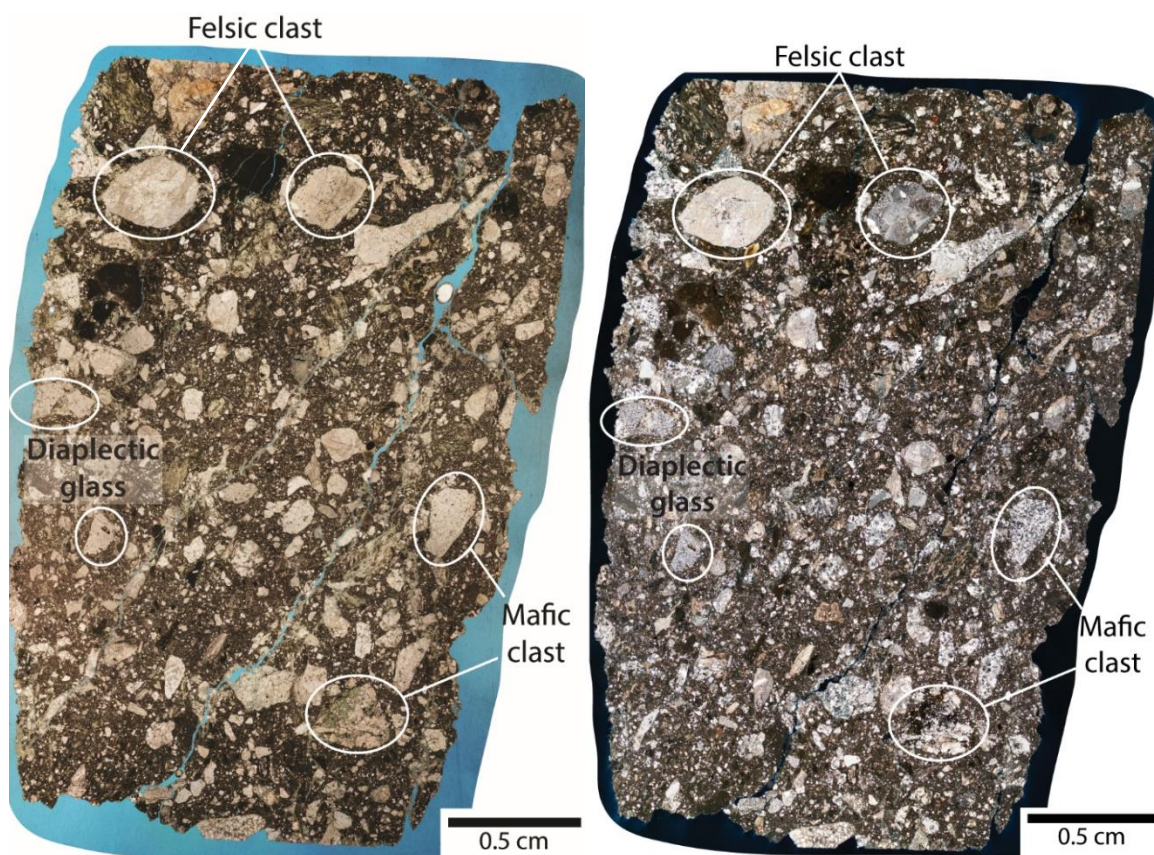


Figure 4.7 Thin section of suevite sample G1 showing the texture characteristic of a polymict lithic breccia. Note brecciated texture of sample. Felsic clasts are either syenite or rhyolite, mafic clasts are either gabbro or basalt. Left: plane polarized light. Right: cross polarized light.

### 4.3 U-Pb Zircon Geochronology

#### 4.3.1 AMES ASTROBLEME

All of the U-Pb data collected from zircons from the Ames Astrobleme is presented here. The Ames Astrobleme data collected at UT-Austin via LA-ICP-MS and Heidelberg University via SIMS is presented in Table 4.1 and 4.2. The data are also

presented here as both Concordia (Fig. 4.8) and age distribution plots (Fig. 4.9). Note that different measurements have different identifying labels.

Based on the data, certain trends were identified, the significance of which will be elaborated upon in Chapter 5. On Concordia, a linear trend in the data was identified and a Discordia line is drawn through the data using the Isoplot 3.7 software published by Berkley Geochronology Center. Certain data points which clearly did not match the trend were excluded from the correlation. 33/37 data points were used to determine the discordant trend. The software also identified the best fit upper and lower intercepts between the discordia line and the concordia curve, those intercepts are  $1428 \pm 31$  Ma and  $372 \pm 42$  Ma.

The age distribution plot in Fig. 4.9 identifies unique populations of zircons. Fig. 4.9 presents only the determined “Best Age” for LA-ICP-MS analyses, which is the  $^{206}\text{Pb}/^{238}\text{U}$  Age for ages  $<800$  Ma and  $^{207}\text{Pb}/^{206}\text{Pb}$  age for those  $>800$  Ma. If no “Best Age” could be determined due to high level of discordance, the  $^{206}\text{Pb}/^{238}\text{U}$  age is reported (Table 4.1, 4.2). The age distribution plot showing all determined ages is presented in Appendix 6.3 (Fig. 6.4). Three unique populations of zircons are likely: (1) an ‘older’ group with ages from 1294 Ma to 1492 Ma, (2) a ‘middle’ group with ages from 1073 Ma to 1108 Ma, and (3) a ‘young’ group with ages from 341.3 Ma- 411.4 Ma.

CL images of select zircons are presented in Fig. 4.10; the remainder are presented in Appendix 6.2. Zircons were chosen for Fig. 4.10 due to their significant relationship to trends in the data. All zircons analyzed in this study appear as euhedral to subhedral grains; completely recrystallized granular zircons (such as those seen in

Schmieder et al., 2015, Figs. 6E-I), were not identified. Fig. 4.10 shows CL images for three such zircons, all other CL images for the Ames Astrobleme zircons are in Appendix 6.2.

Table 4.1: Ames Astrobleme U-Pb zircon geochronology analysis by LA-ICP-MS (University of Texas at Austin). All uncertainties are reported at the 2-sigma level. See Appendix 6.3 for complete details.

| Sample Spot #: | Zircon Grain <sup>a</sup> | Best age (Ma) <sup>b</sup> | 2 $\sigma$ error | Th/U | 2 $\sigma$ error |
|----------------|---------------------------|----------------------------|------------------|------|------------------|
| S52026_8       | AAOK_11                   | 342.0                      | 5.4              | 0.2  | 4.4              |
| AAOK2016_1     | AAOK_9                    | 364.8                      | 4.7              | 0.3  | 0.2              |
| AAOK2016_2     | AAOK_9                    | 369.3                      | 8.3              | 0.4  | 0.1              |
| AAOK2016_8     | AAOK_12                   | 377.9                      | 5.3              | 0.6  | 0.1              |
| AAOK2016_11    | AAOK_5                    | 928.0 <sup>c</sup>         | 19.0             | 2.0  | 0.02             |
| AAOK2016_10    | AAOK_13                   | 1108.0 <sup>c</sup>        | 14.0             | 1.7  | 0.01             |
| S39018_29_1    | AAOK_14                   | 1362.0                     | 36.0             | 1.4  | 0.01             |
| S39018_29_5    | AAOK_14                   | 1372.0                     | 25.0             | 1.2  | 0.02             |
| AAOK2016_4     | AAOK_10                   | 1379.0                     | 17.0             | 1.2  | 0.03             |
| AAOK2016_3     | AAOK_7                    | 1390.0                     | 20.0             | 1.1  | 0.01             |
| AAOK2016_6     | AAOK_10                   | 1396.0                     | 24.0             | 0.8  | 0.02             |
| AAOK2016_5     | AAOK_10                   | 1407.0                     | 30.0             | 1.2  | 0.01             |
| AAOK2016_7     | AAOK_10                   | 1414.0                     | 22.0             | 1.0  | 0.03             |
| AAOK2016_9     | AAOK_8                    | 1449.0                     | 19.0             | 1.0  | 0.04             |
| S52026_5       | AAOK_15                   | 1457.0                     | 44.0             | 1.4  | 0.03             |

a: Zircon grain corresponds with labeled grains in Figure 4.10 and Appendix 6.1

b: Unless otherwise noted, ages younger <800 Ma are given as <sup>206</sup>Pb/<sup>238</sup>U Age (Ma), ages >800 Ma are determined via data reduction software

c: No best age could be determined due to high level of discordance. Age reported is <sup>206</sup>Pb/<sup>238</sup>U Age (Ma).

Table 4.2: Ames Astrobleme U-Pb zircon geochronology analysis by SIMS (Heidelberg University). All uncertainties are reported at the 1-sigma level. See Appendix 6.3 for complete details.

| Sample Spot #: | Zircon Grain <sup>a</sup> | Best age (Ma) <sup>b</sup> | 2 $\sigma$ error | Th/U | 2 $\sigma$ error | % <sup>206</sup> Pb* | 2 $\sigma$ error |
|----------------|---------------------------|----------------------------|------------------|------|------------------|----------------------|------------------|
| Ames_z3@3      | AAOK_9                    | 341.3                      | 9.7              | 0.1  | 0.0              | 99.5                 | 0.1              |
| Ames_z3@2      | AAOK_9                    | 355.8                      | 14.1             | 0.0  | 0.0              | 99.8                 | <0.1             |
| Ames_z7@2      | AAOK_6                    | 357.6                      | 11.3             | 0.1  | 0.0              | 99.6                 | 0.1              |
| Ames_z3@1      | AAOK_9                    | 363.7                      | 10.5             | 0.0  | 0.0              | 99.7                 | 0.1              |
| Ames_z7@1      | AAOK_6                    | 368.4                      | 10.9             | 0.2  | 0.0              | 100.0                | <0.1             |
| Ames_z7@4      | AAOK_6                    | 369.4                      | 11.4             | 0.1  | 0.0              | 99.6                 | 0.2              |
| Ames_z7@3      | AAOK_6                    | 372.0                      | 11.4             | 0.3  | 0.0              | 99.7                 | 0.1              |
| Ames2_z1@2     | AAOK_1                    | 411.1                      | 12.1             | 0.2  | 0.0              | 99.5                 | 0.1              |
| Ames2_z1@1     | AAOK_1                    | 411.4                      | 10.7             | 0.1  | 0.0              | 99.0                 | 0.2              |
| Ames_z6@2      | AAOK_5                    | 587.3                      | 21.4             | 0.6  | 0.0              | 94.3                 | 0.3              |
| Ames_z6@1      | AAOK_5                    | 713.6                      | 21.9             | 0.6  | 0.0              | 91.5                 | 1.0              |
| Ames_z5@1      | AAOK_4                    | 937.0                      | 94.8             | 0.5  | 0.0              | 97.4                 | 0.4              |
| Ames2_z2@1     | AAOK_2                    | 1095                       | 13               | 0.4  | 0.0              | 99.8                 | <0.1             |
| Ames2_z2@2     | AAOK_2                    | 1073                       | 16               | 0.7  | 0.0              | 99.6                 | <0.1             |
| Ames_z4@2      | AAOK_10                   | 1324                       | 25               | 0.5  | 0.0              | 99.4                 | 0.1              |
| Ames_z4@1      | AAOK_10                   | 1294                       | 25               | 0.3  | 0.0              | 98.8                 | 0.1              |
| Ames_z4@3      | AAOK_10                   | 1335                       | 23               | 0.4  | 0.0              | 99.6                 | 0.1              |
| Ames_z8@1      | AAOK_8                    | 1339                       | 24               | 0.4  | 0.0              | 99.8                 | 0.1              |
| Ames_z2@2      | AAOK_7                    | 1354                       | 17               | 0.3  | 0.0              | 98.4                 | 0.1              |
| Ames_z1@1      | AAOK_3                    | 1385                       | 70               | 0.3  | 0.0              | 99.2                 | 0.1              |
| Ames_z2@1      | AAOK_7                    | 1402                       | 21               | 0.5  | 0.0              | 99.1                 | 0.1              |
| Ames_z1@2      | AAOK_3                    | 1492                       | 162              | 0.4  | 0.0              | 93.0                 | 0.4              |

a: Zircon grain corresponds with labeled grains in Figure 4.10 and Appendix 6.2

b: Unless otherwise noted, ages younger <800 Ma are given as <sup>206</sup>Pb/<sup>238</sup>U Age (Ma), ages >800 Ma are given as <sup>207</sup>Pb/<sup>206</sup>Pb Age (Ma).

### Ames Astrobleme U-Pb Ages

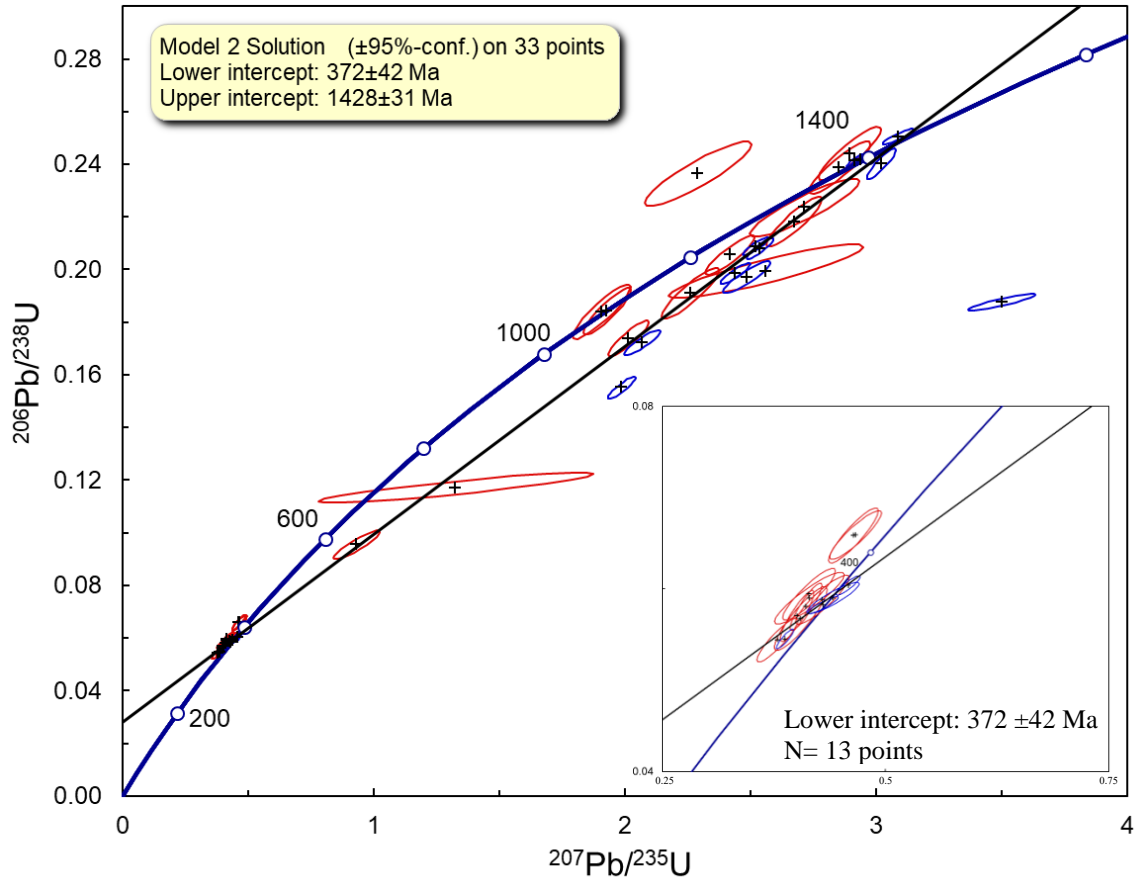


Figure 4.8 Concordia plot of data from all analyzed zircons from Ames Astrobleme. Red ellipses indicate zircons analyzed via SIMS, blue ellipses indicate zircons analyzed via LA-ICP-MS. Blue error ellipses are  $2\sigma$ , red error ellipses are  $1\sigma$ . Inset highlights cluster of ages at lower intercept.

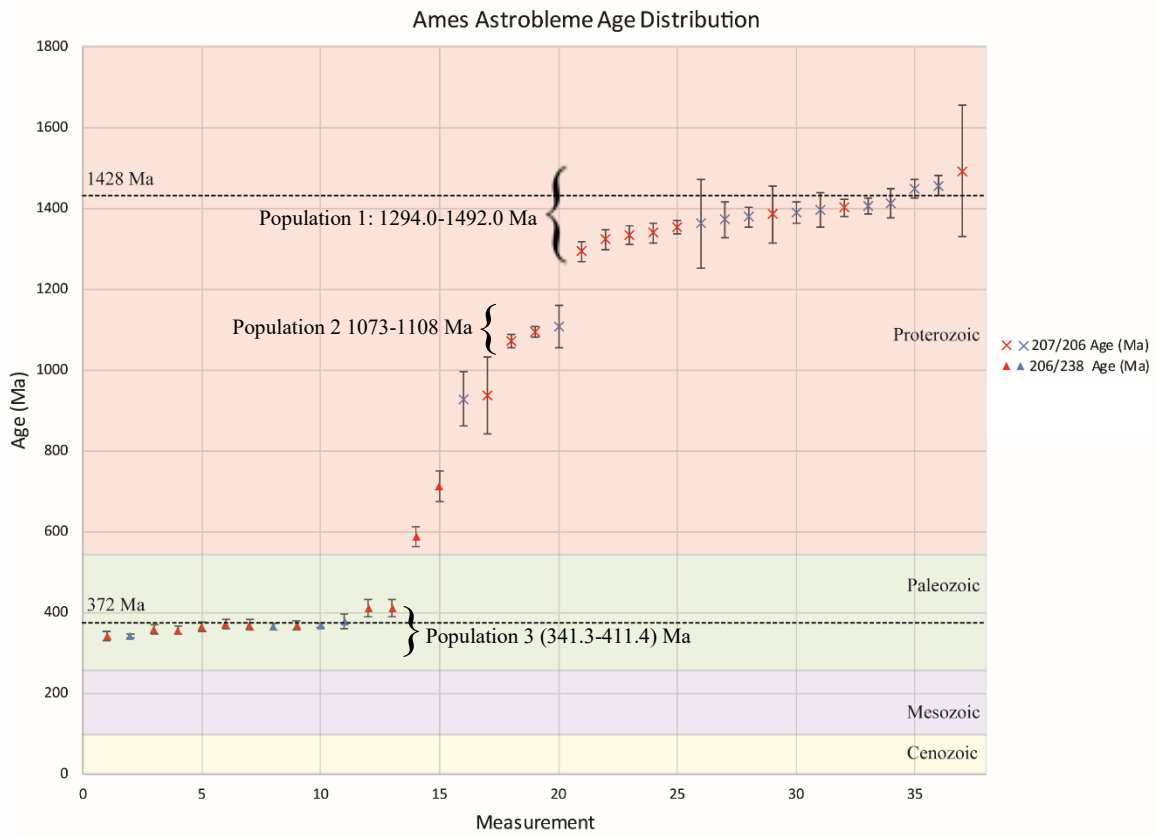


Figure 4.9 Ames Astrobleme U-Pb simplified zircon age distribution plot. Red data points indicate zircons analyzed via SIMS, blue data points indicate zircons analyzed via LA-ICP-MS. Dashed lines indicated values of upper and lower discordia line intercepts as seen in Fig. 4.8. Figure shows only best ages from analyses, see Appendix 6.3 for full data.

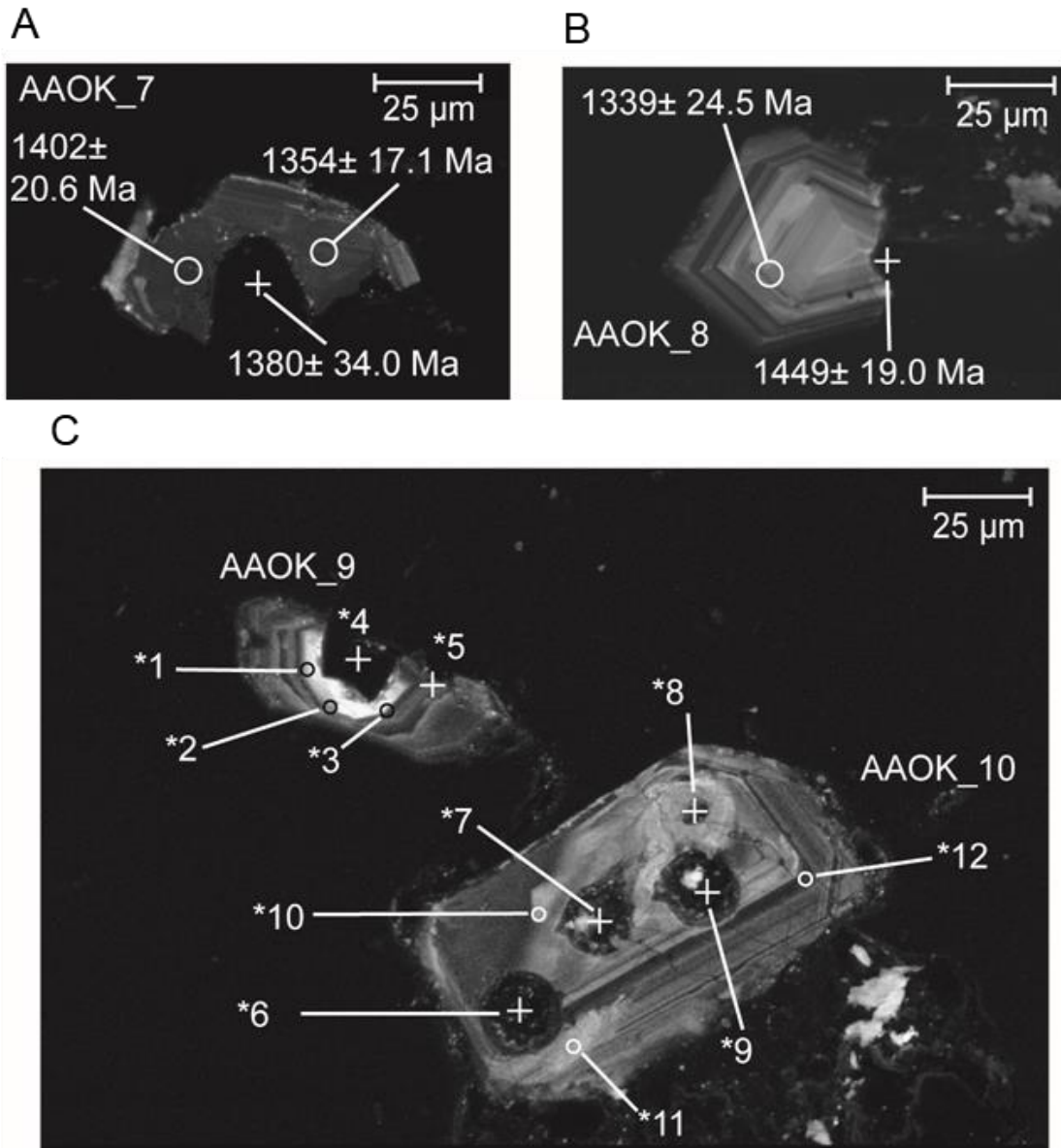


Figure 4.10: Images of select zircons from Ames Astrobleme showing locations where age measurements were taken. Crosses indicate location of measurement via Laser Ablation-ICP-MS, circled areas indicate location of measurement via SIMS. A: Zircon AOK\_7 CL image. B: Zircon AOK\_8 CL image. C: Zircon AOK\_9 and AOK\_10 CL image. Numbered spots are the following ages: \*1:  $363.7 \pm 10.5$  Ma, \*2:  $355.8 \pm 14.1$  Ma, \*3:  $341.3 \pm 9.7$  Ma, \*4:  $364.8 \pm 4.7$  Ma, \*5:  $369.3 \pm 8.3$  Ma, \*6:  $1379 \pm 17$  Ma, \*7:  $1414 \pm 22$  Ma, \*8:  $1407 \pm 30$  Ma, \*9:  $1396 \pm 24$  Ma, \*10:  $1335 \pm 23$  Ma, \*11:  $1294 \pm 25$  Ma, \*12:  $1324 \pm 25$  Ma.

### 4.3.2 SLATE ISLANDS

All of the U-Pb data collected from zircons from the Slate Islands Archipelago is presented here. Data collected at the University of Texas at Austin via LA-ICP-MS is displayed in Table 4.3. Data collected at the Heidelberg University is displayed in Table 4.4. The data are also presented here as both Concordia (Figs. 4.11, 4.12) and age distribution plots (Fig. 4.13). Note that different measurements have different identifying labels. Samples have been further identified based on grain number to allow for convenience when comparing different analyses.

On Concordia, a linear trend in the data was identified and a Discordia line drawn through the data using the Isoplot 3.7 software published by Berkley Geochronology Center. Certain data points which clearly did not match the trend were excluded from the correlation. The software also identified the best fit upper and lower intercepts with the concordia curve, those intercepts are  $2706\pm 20$  Ma and  $469\pm 45$  Ma.

The age distribution plot in Fig. 4.13 identifies unique populations of zircons. Fig. 4.13 presents only the determined 'best ages' as defined earlier. The age distribution plot showing all determined ages is in Appendix 6.4 (Fig. 6.5).

Four or more unique populations of zircon ages are likely present in the analyses: (1) an 'Archean' group with ages from 2710 to 2632 Ma, (2) a 'Paleozoic' group with ages from 1703 to 1603 Ma, (3) a 'Phanerozoic' group with ages from 665.6 to 319.8 Ma, and (4) a 'modern' group with ages from  $<34.39$  Ma. This theme will be discussed in more detail in Chapter 5.

CL images of select zircons are presented in Fig. 4.14; the remainder are presented in Appendix 6.2. Zircons were chosen for Fig. 4.14 to represent all identified age populations. As with the Ames zircons, Slate Island grains are also euhedral to subhedral in shape. Granular zircons (such as those seen in Schmieder et al., 2015, Figs. 6E-6I), were not identified. Fig. 4.14A shows two measurements on zircon SION\_G2\_20, a ‘young’ zircon’ which have best ages of  $31.4 \pm 1.4$  Ma and  $34.4 \pm 1.2$  Ma. Fig. 4.14B shows two measurements on zircon SION\_G1\_7 which have best ages of  $498 \pm 16$  Ma and  $468 \pm 12$  Ma. Fig. 4.14C shows a measurement on zircon SION\_G2\_26 which has a best age of  $592 \pm 17$ . Fig. 4.14D shows two measurements on zircon SION\_G2\_21, which have best ages of  $1692 \pm 27$  Ma and  $1703 \pm 29$  Ma. Fig. 4.14E shows a measurement on zircon SION\_G2\_10, an ‘old’ zircon, which has a best age of  $2687 \pm 15$  Ma. Fig. 4.14F shows a measurement on zircon SION\_G2\_5, an ‘old’ zircon, which has a best age of  $2701 \pm 8$  Ma.

Table 4.3: Slate Islands U-Pb zircon geochronology analysis by LA-ICP-MS (University of Texas at Austin). All uncertainties are reported at the 2-sigma level. See Appendix 6.4 for complete details.

| Sample Spot #:             | Zircon Grain <sup>a</sup> | Best age (Ma) <sup>b</sup> | 2 $\sigma$ error | Th/U | 2 $\sigma$ error |
|----------------------------|---------------------------|----------------------------|------------------|------|------------------|
| SLON2017_G3_2 <sup>d</sup> | SION_G2_27                | 432.0                      | 25.0             | 3.0  | 0.1              |
| SLON2017_G4_3 <sup>d</sup> | SION_G2_28                | 452.7                      | 9.1              | 3.5  | 0.1              |
| SLON2017_G4_4 <sup>d</sup> | SION_G2_29                | 1220                       | 17               | 1.8  | 0.1              |
| SLON2017_S2_5 <sup>c</sup> | SION_S2_5                 | 1603                       | 68               | 0.6  | <0.1             |
| SLON2017_S1_5 <sup>c</sup> | SION_S1_7                 | 1655                       | 32               | 0.7  | <0.1             |
| SLON2017_G4_5 <sup>d</sup> | SION_G2_31                | 1680                       | 50               | 0.5  | <0.1             |
| SLON2017_S2_3 <sup>c</sup> | SION_S2_3                 | 2632                       | 18               | 0.9  | <0.1             |
| SLON2017_S1_3 <sup>c</sup> | SION_S1_8                 | 2655                       | 12               | 0.8  | <0.1             |
| SLON2017_S1_2 <sup>c</sup> | SION_S1_8                 | 2667                       | 11               | 0.7  | <0.1             |
| SLON2017_S2_1 <sup>c</sup> | SION_S2_1                 | 2669                       | 11               | 1.1  | <0.1             |
| SLON2017_S1_6 <sup>c</sup> | SION_S1_9                 | 2676                       | 17               | 1.6  | 0.1              |
| SLON2017_S1_4 <sup>c</sup> | SION_S1_10                | 2682                       | 16               | 1.1  | <0.1             |
| SLON2017_S1_7 <sup>c</sup> | SION_S1_11                | 2685                       | 16               | 1.6  | 0.2              |
| SLON2017_S2_6 <sup>c</sup> | SION_S2_7                 | 2689                       | 14               | 0.9  | <0.1             |
| SLON2017_G3_1 <sup>d</sup> | SION_S1_12                | 2691                       | 17               | 0.8  | <0.1             |
| SLON2017_S1_1 <sup>c</sup> | SION_G2_30                | 2695                       | 12               | 2.1  | <0.1             |
| SLON2017_S1_8 <sup>c</sup> | SION_S1_13                | 2699                       | 14               | 1.3  | 0.1              |
| SLON2017_S2_2 <sup>c</sup> | SION_S2_8                 | 2701                       | 12               | 1.7  | 0.1              |
| SLON2017_S2_4 <sup>c</sup> | SION_S2_9                 | 2701                       | 13               | 0.7  | <0.1             |
| SLON2017_G3_3 <sup>d</sup> | SION_G2_32                | 2707                       | 22               | 0.7  | 0.1              |

a: Zircon grain corresponds with labeled grains in Figure 4.13 and Appendix 6.2. SION refers to Slate Islands Ontario. G1, G2, S1 and S2 refer to sample locations in Fig. 3.3

b: Unless otherwise noted, ages younger <800 Ma are given as <sup>206</sup>Pb/<sup>238</sup>U Age (Ma), ages >800 Ma are determined via data reduction software

c: Source lithology for zircons is syenite.

d: Source rock for zircons is suevite.

Table 4.4: Slate Islands Archipelago U-Pb zircon geochronology analysis by SIMS (Heidelberg University). All uncertainties are reported at the 1-sigma level. See Appendix 6.4 for complete details.

| Sample Spot #:          | Zircon Grain <sup>a</sup> | Best Age <sup>b</sup> | 1 $\sigma$<br>error | Th/<br>U | 1 $\sigma$ error | % <sup>206</sup> Pb* | 1 $\sigma$<br>error |
|-------------------------|---------------------------|-----------------------|---------------------|----------|------------------|----------------------|---------------------|
| SIsc@4 <sup>d</sup>     | SION_G1_4                 | 4.6                   | 0.2                 | 0.3      | <0.01            | 89.2                 | 2.4                 |
| SIbc@20 <sup>d</sup>    | SION_G2_20                | 31.4                  | 1.4                 | 0.5      | 0.01             | 89.1                 | 3.2                 |
| SIbc_s2@20 <sup>d</sup> | SION_G2_20                | 34.4                  | 1.2                 | 0.5      | 0.01             | 96.3                 | 1.2                 |
| SIbc@15 <sup>d</sup>    | SION_G2_15                | 248.1                 | 23.2                | 0.7      | 0.07             | 98.2                 | 0.5                 |
| SIbc@17 <sup>d</sup>    | SION_G2_17                | 319.8                 | 10.2                | 0.4      | 0.03             | 95.0                 | 0.6                 |
| SIbc@7 <sup>d</sup>     | SION_G2_7                 | 331.9                 | 10.8                | 0.7      | 0.01             | 99.7                 | 0.1                 |
| SIbc@6a <sup>d</sup>    | SION_G2_6                 | 336.4                 | 12.0                | 0.5      | <0.01            | 99.4                 | 0.2                 |
| SIbc@1 <sup>d</sup>     | SION_G2_1                 | 337.9                 | 11.4                | 0.5      | <0.01            | 99.9                 | <0.1                |
| SIbc@9 <sup>d</sup>     | SION_G2_9                 | 385.3                 | 11.8                | 0.1      | <0.01            | 98.8                 | 0.2                 |
| SIsc@7b <sup>d</sup>    | SION_G1_7                 | 467.8                 | 12.1                | 0.0      | <0.01            | 99.7                 | 0.1                 |
| SIbc@12 <sup>d</sup>    | SION_G2_12                | 472.8                 | 15.9                | 0.2      | <0.01            | 99.6                 | 0.2                 |
| SIbc@4 <sup>d</sup>     | SION_G2_4                 | 487.3                 | 13.2                | 0.2      | 0.01             | 99.1                 | 0.1                 |
| SIsc@7a <sup>d</sup>    | SION_G1_7                 | 498.5                 | 15.9                | 0.0      | <0.01            | 99.9                 | <0.1                |
| SIbc@11 <sup>d</sup>    | SION_G2_11                | 555.3                 | 15.5                | 0.1      | <0.01            | 100.0                | <0.1                |
| SIbc@14 <sup>d</sup>    | SION_G2_14                | 578.0                 | 16.3                | 0.1      | <0.01            | 99.1                 | 0.1                 |
| SIbc@25 <sup>d</sup>    | SION_G2_25                | 585.1                 | 16.3                | 0.2      | 0.01             | 99.7                 | 0.1                 |
| SIbc@24 <sup>d</sup>    | SION_G2_24                | 588.1                 | 21.9                | 0.5      | 0.01             | 99.8                 | 0.1                 |
| SIbc@26 <sup>d</sup>    | SION_G2_26                | 591.7                 | 17.3                | 0.1      | <0.01            | 99.7                 | 0.1                 |
| SIbc@19 <sup>d</sup>    | SION_G2_19                | 619.1                 | 19.3                | 0.6      | 0.01             | 99.5                 | 0.2                 |
| SIbc@18 <sup>d</sup>    | SION_G2_18                | 626.4                 | 17.9                | 0.9      | 0.01             | 99.8                 | 0.1                 |
| SIbc@22 <sup>d</sup>    | SION_G2_22                | 641.0                 | 18.0                | 0.4      | 0.01             | 99.7                 | 0.2                 |
| SIbc@3 <sup>d</sup>     | SION_G2_3                 | 665.6                 | 23.3                | 0.2      | <0.01            | 99.8                 | 0.1                 |
| SIbc@2 <sup>d</sup>     | SION_G2_2                 | 745.2                 | 21.2                | 0.1      | <0.01            | 99.9                 | <0.1                |
| SIbc_s2@21 <sup>d</sup> | SION_G2_21                | 1692                  | 26                  | 0.1      | <0.01            | 99.6                 | 0.2                 |
| SIbc@23 <sup>d</sup>    | SION_G2_23                | 1699                  | 33                  | 0.5      | 0.02             | 99.2                 | 0.1                 |
| SIbc@21 <sup>d</sup>    | SION_G2_21                | 1703                  | 29                  | 0.1      | <0.01            | 98.6                 | 0.1                 |
| SIbc@8 <sup>d</sup>     | SION_G2_8                 | 2058                  | 13                  | 0.1      | <0.01            | 99.9                 | <0.1                |
| SIbc@16 <sup>d</sup>    | SION_G2_16                | 2398                  | 13                  | 0.2      | <0.01            | 99.9                 | <0.1                |
| SIS1_z4@1 <sup>c</sup>  | SION_S1_4                 | 2428                  | 12                  | 0.1      | <0.01            | 99.4                 | <0.1                |
| SIS1_z5@1 <sup>c</sup>  | SION_S1_5                 | 2465                  | 15                  | 0.4      | 0.01             | 99.5                 | <0.1                |
| SIS2_z1@1 <sup>c</sup>  | SION_S2_1                 | 2547                  | 11                  | 0.5      | 0.01             | 98.9                 | 0.1                 |
| SIS1_z6@1 <sup>c</sup>  | SION_S1_6                 | 2633                  | 13                  | 0.5      | 0.02             | 99.2                 | 0.1                 |
| SIS1_z3@1 <sup>3c</sup> | SION_S1_3                 | 2645                  | 13                  | 3.0      | 0.04             | 99.5                 | 0.1                 |

Table 4.4 Continued

| Sample Spot #:         | Zircon Grain <sup>a</sup> | Best Age <sup>b</sup> | 1 $\sigma$ error | Th/U | 1 $\sigma$ error | % <sup>206</sup> Pb* | 1 $\sigma$ error |
|------------------------|---------------------------|-----------------------|------------------|------|------------------|----------------------|------------------|
| SIS1_z2@1 <sup>c</sup> | SION_S1_2                 | 2650                  | 11               | 0.8  | 0.01             | 99.8                 | <0.1             |
| SIS2_z3@1 <sup>c</sup> | SION_S2_3                 | 2657                  | 15               | 0.4  | 0.01             | 99.6                 | 0.1              |
| SIsc@3 <sup>d</sup>    | SION_G1_3                 | 2680                  | 15               | 0.2  | <0.01            | 99.8                 | 0.1              |
| SIS2_z1@2 <sup>c</sup> | SION_S2_1                 | 2682                  | 19               | 0.4  | 0.01             | 99.9                 | <0.1             |
| SIS2_z4@1 <sup>c</sup> | SION_S2_4                 | 2685                  | 10               | 0.2  | 0.01             | 99.7                 | <0.1             |
| SIS2_z2@1 <sup>c</sup> | SION_S2_2                 | 2686                  | 14               | 0.2  | <0.01            | 99.6                 | <0.1             |
| SIsc@5 <sup>d</sup>    | SION_G1_5                 | 2687                  | 15               | 0.7  | 0.01             | 99.3                 | 0.1              |
| SIbc@10 <sup>d</sup>   | SION_G2_10                | 2688                  | 24               | 0.3  | 0.01             | 99.8                 | <0.1             |
| SIsc@6 <sup>d</sup>    | SION_G1_6                 | 2696                  | 15               | 0.4  | <0.01            | 99.9                 | <0.1             |
| SIsc@2 <sup>d</sup>    | SION_G1_2                 | 2697                  | 17               | 0.3  | <0.01            | 99.9                 | <0.1             |
| SIS1_z1@1 <sup>c</sup> | SION_S1_1                 | 2701                  | 8                | 0.4  | 0.01             | 99.9                 | <0.1             |
| SIbc@5 <sup>d</sup>    | SION_G2_5                 | 2701                  | 9                | 0.4  | 0.02             | 99.9                 | <0.1             |
| SIsc@1 <sup>d</sup>    | SION_G1_1                 | 2710                  | 21               | 0.3  | <0.01            | 99.7                 | 0.1              |

a: Zircon grain corresponds with labeled grains in Figure 4.13 and Appendix 6.2. SION refers to Slate Islands, Ontario. G1, G2, S1 and S2 refer to sample locations in Fig. 3.3

b: Unless otherwise noted, ages younger <800 Ma are given as <sup>206</sup>Pb/<sup>238</sup>U Age (Ma), ages >800 Ma are given as <sup>207</sup>Pb/<sup>206</sup>Pb Age (Ma).

c: Source lithology for zircons is syenite.

d: Source rock for zircons is suevite.

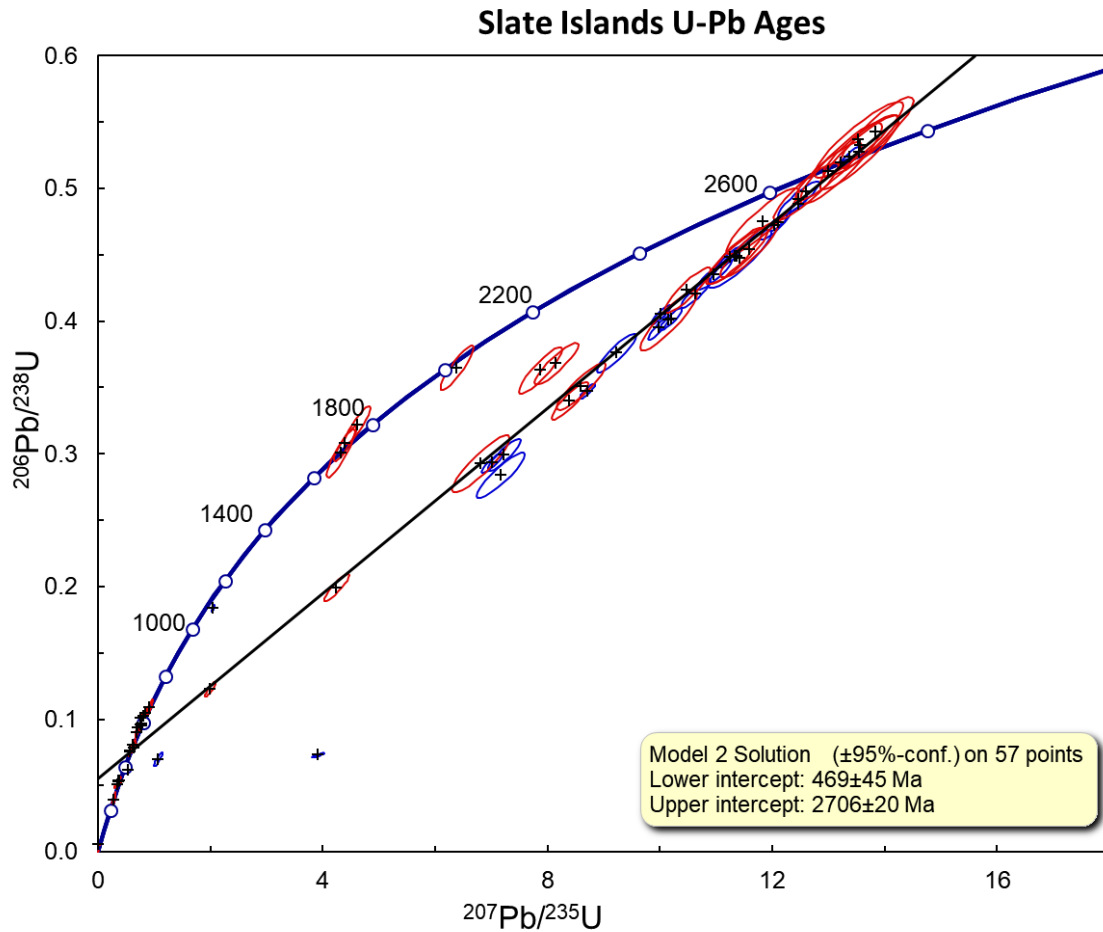


Figure 4.11 Concordia plot of data collected from zircons from Slate Islands. Red ellipses indicate zircons analyzed via SIMS, blue ellipses indicate zircons analyzed via LA-ICP-MS. Blue error ellipses are  $2\sigma$ , red error ellipses are  $1\sigma$ .

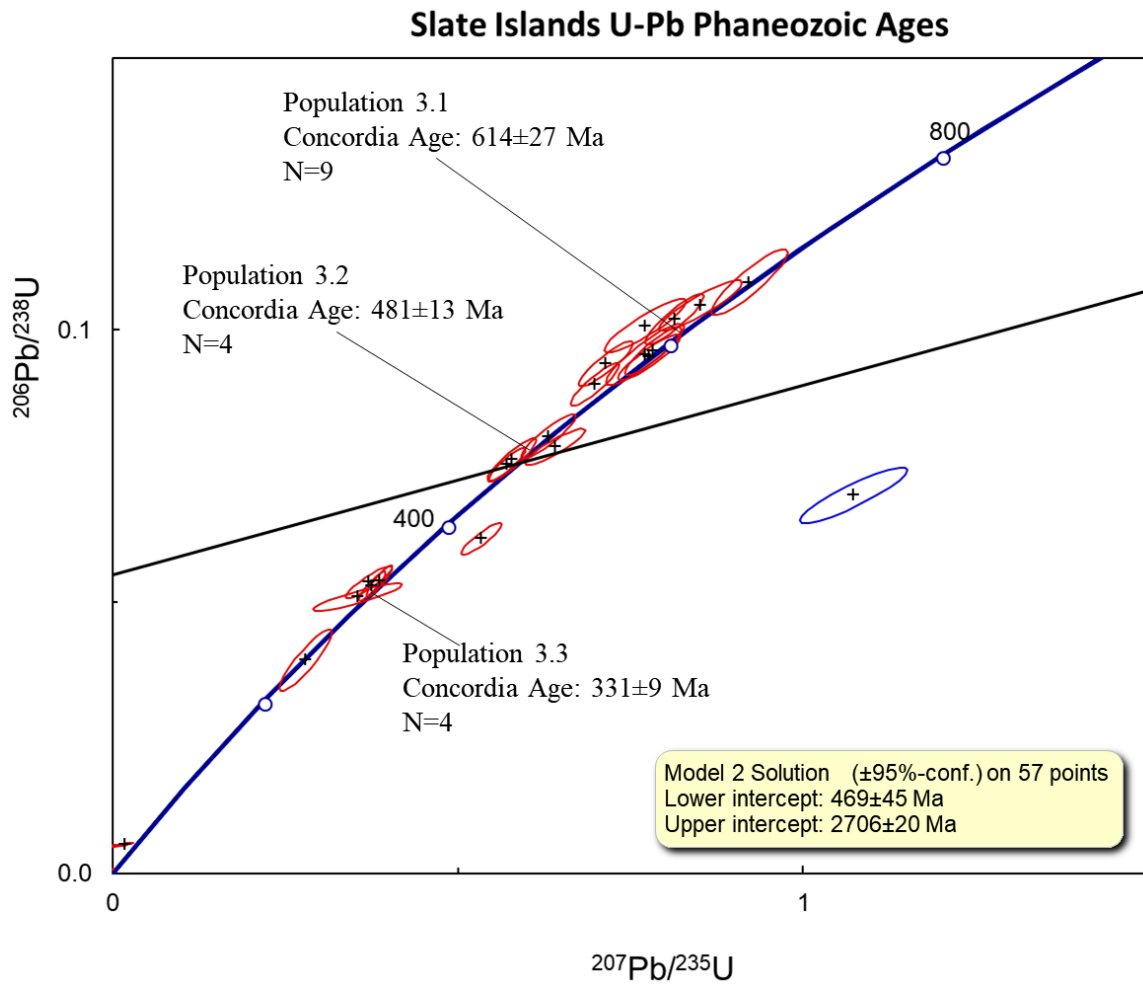


Figure 4.12 Concordia plot of data collected from zircons from Slate Islands highlighting Phanerozoic ages. Red ellipses indicate zircons analyzed via SIMS, blue ellipses indicate zircons analyzed via LA-ICP-MS. Blue error ellipses are  $2\sigma$ , red error ellipses are  $1\sigma$ .

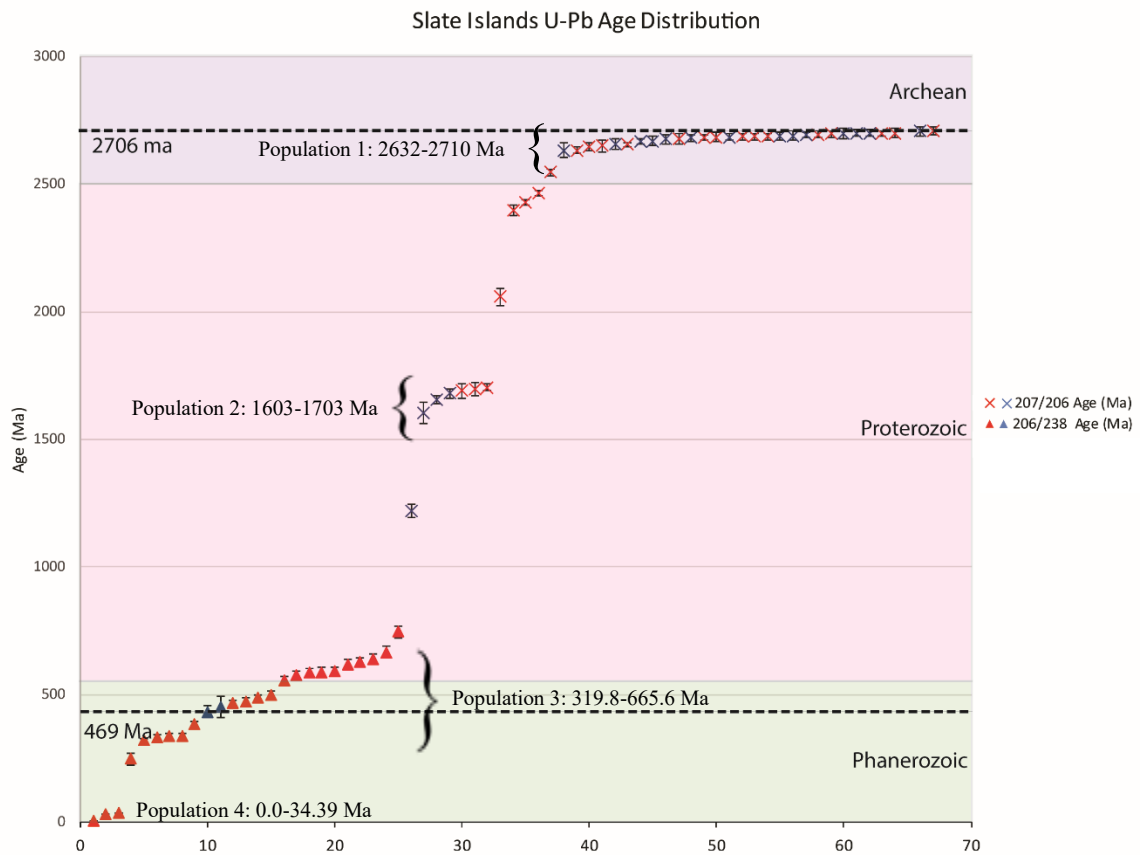


Figure 4.13 Age distribution plot of data collected from zircons from the Slate Islands. Red data points indicate zircons analyzed via SIMS, blue data points indicate zircons analyzed via LA-ICP-MS. Dashed lines indicated values of upper and lower discordia line intercepts as seen in Fig. 4.11. Figure shows only best ages from analyses, see Appendix 6.4 for full data.

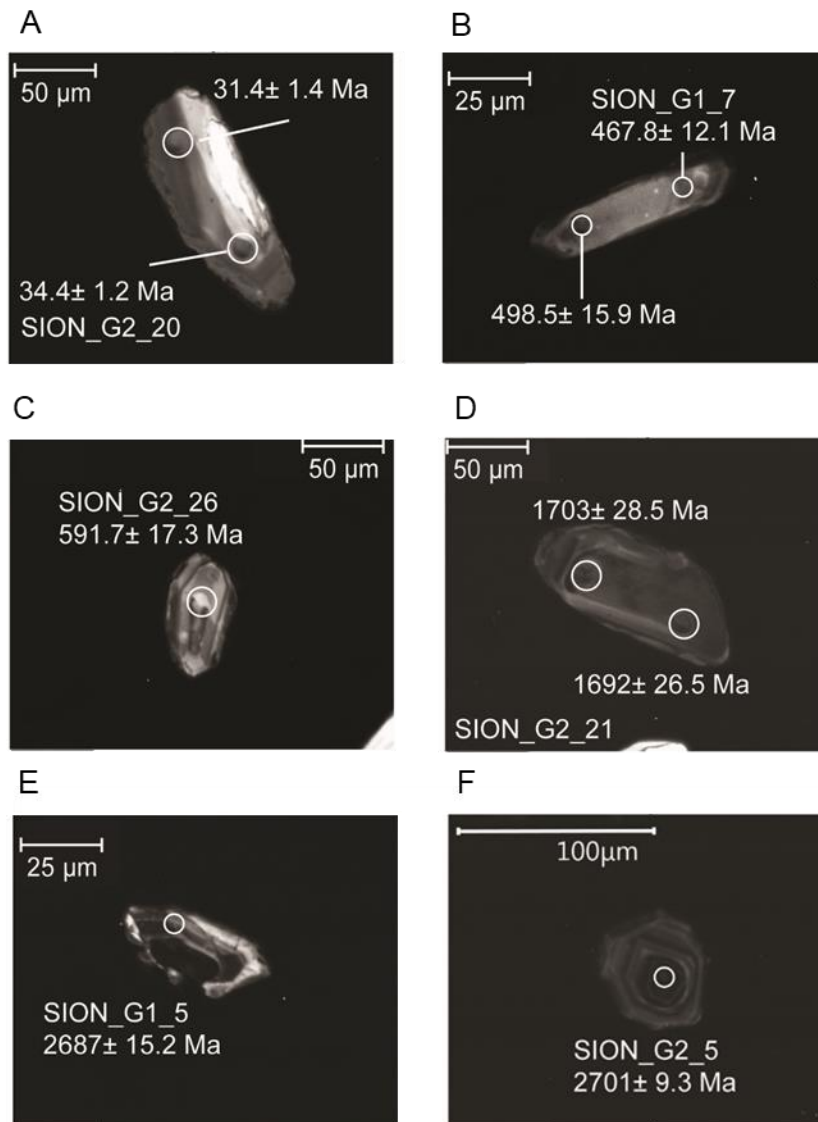


Figure 4.14: Images of select zircons from the Slate Islands. Circled areas indicate location of measurement via SIMS. A: Zircon SION\_G2\_20 CL image. B: Zircon SION\_G1\_7 image. C: Zircon SION\_G2\_26 CL image. D: Zircon SION\_G2\_21 CL image. E: Zircon SION\_G1\_5 CL image. F: Zircon SION\_G2\_5 CL image.

## 4.4 $^{40}\text{Ar}/^{39}\text{Ar}$ Geochronology via step heating

### 4.4.1 AMES ASTROBLEME

The  $^{40}\text{Ar}/^{39}\text{Ar}$  data collected from plagioclase feldspar from the Ames Astrobleme is presented here. The complete data from the step-heating experiments is presented in Appendix 6.5. The results of the step heating experiment for each sample were plotted as age spectrum plots (Figs 4.15-4.19). Ages were calculated from the presence of plateaus with 5 or more steps on the age spectrum diagrams. Age spectrum plots typically show a perfectly horizontal plateau during the initial release of argon. The technicians explained this was argon which was not released during pre-heating and is an artifact of the analysis. All five samples show a high apparent age at low temperatures (the hill), followed by a decrease to a relatively stable plateau. The ages determined via heating plateaus ranged from  $250.54 \pm 0.03$  Ma to  $314.19 \pm 1.37$  Ma. There is no trend in the ages in relation to their position within the sampled drill core. The data for each sample was also plotted as an inverse isochron plot, which indicates the amount mixing between the radiogenic and atmospheric argon component. The plots show that the grains have almost no atmospheric argon, and any argon is almost entirely radiogenic. This gives us the confidence to say that these grains have remained a closed system since the last heating episode. The geologic context of this determined ages will be further explored in chapter 5.

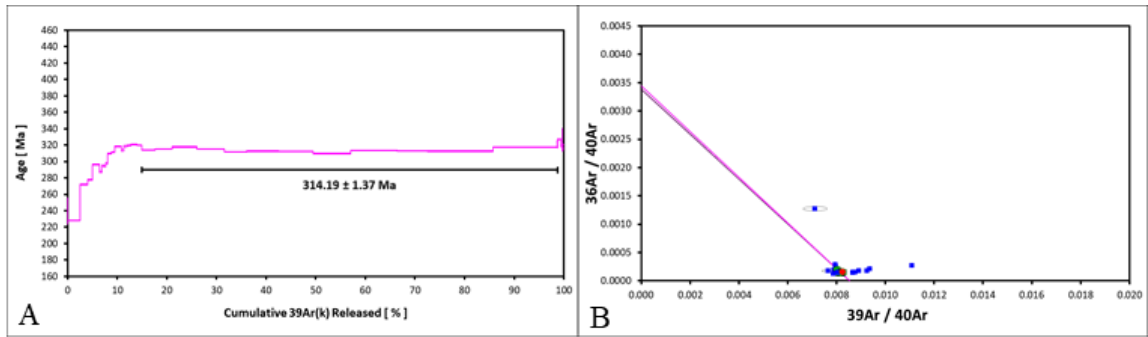


Figure 4.15:  $^{40}\text{Ar}/^{39}\text{Ar}$  analysis of Ames Astrobleme S1 9014.9'. A: Age spectrum following step heating experiment. B: Inverse isochron plot

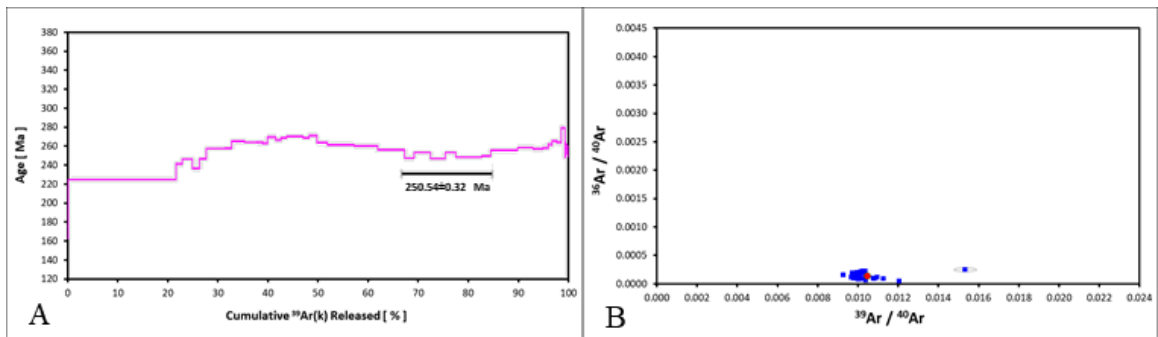


Figure 4.16:  $^{40}\text{Ar}/^{39}\text{Ar}$  analysis of Ames Astrobleme S4 9020'. A: Age spectrum following step heating experiment. B: inverse isochron plot.

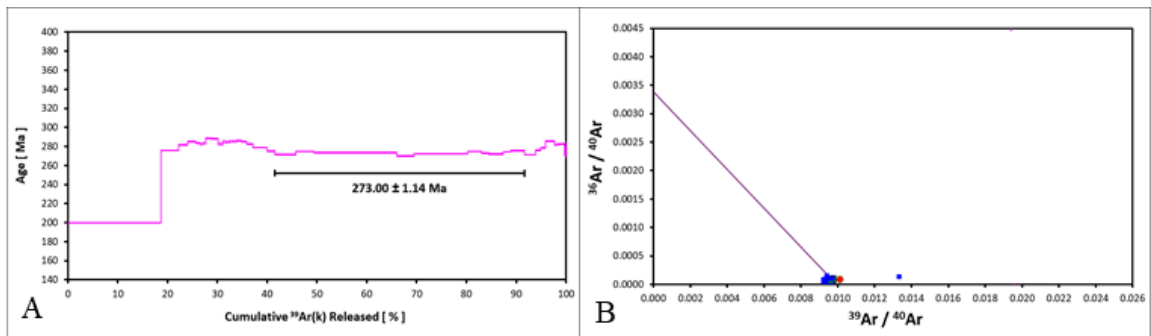


Figure 4.17:  $^{40}\text{Ar}/^{39}\text{Ar}$  analysis of Ames Astrobleme S6 9027'. A: Age spectrum following step heating experiment. B: Inverse isochron plot

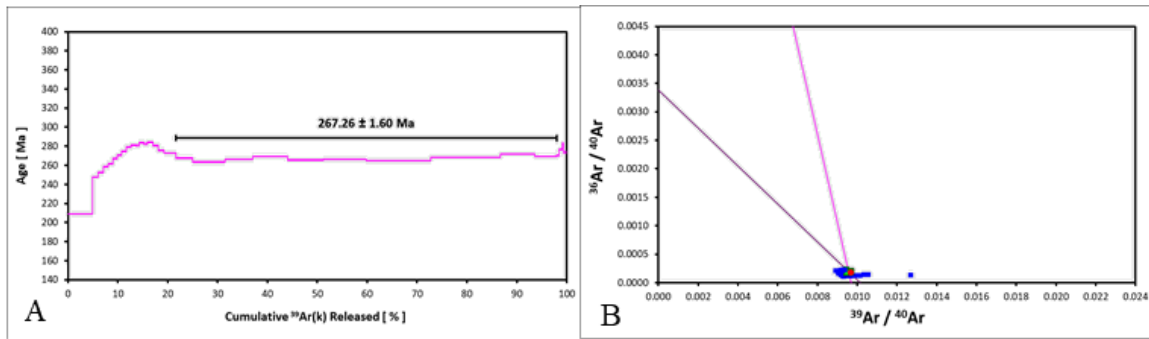


Figure 4.18:  $^{40}\text{Ar}/^{39}\text{Ar}$  analysis of Ames Astrobleme S7 9031'. A: Age spectrum following step heating experiment. B: Inverse isochron plot

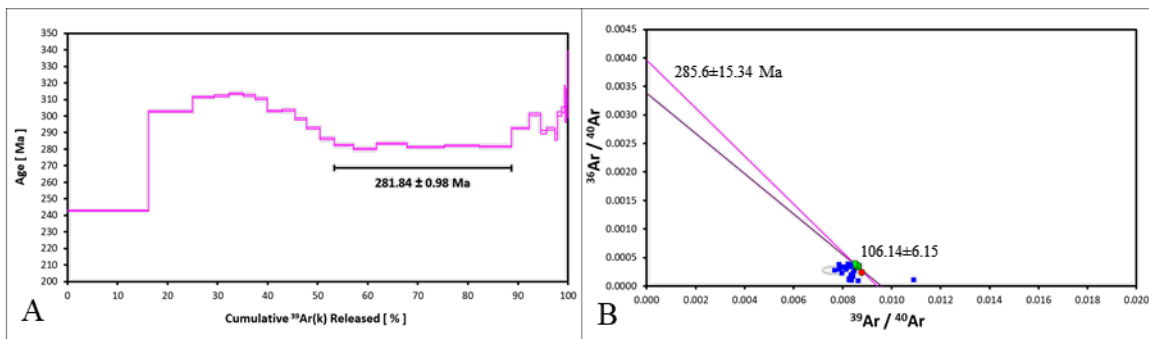


Figure 4.19:  $^{40}\text{Ar}/^{39}\text{Ar}$  analysis of Ames Astrobleme S9 9034'. A: Age spectrum following step heating experiment. B: Inverse isochron plot

#### 4.4.2 SLATE ISLANDS ARCHIPELAGO

Due to issues with sample preparation and quality, the step heating experiment was performed on only one sample from the Slate Islands (S3); the results of that experiment are presented in Fig. 4.20. K-feldspar was not able to be separated from the other samples, and they were deemed too altered to provide useful information. The complete data from the step heating experiments is presented in Appendix 6.6. The age

spectrum plot is more complicated than that of the Ames samples, reflecting the age and history of the Slate Islands. The age spectrum shows an increasing apparent age at low temperatures, a drop to a horizontal plateau at medium temperatures, and then a complex increasing and decreasing pattern at high temperatures. The plateau from this single experiment suggested an age of  $1621 \pm 130$ . The data for the sample was also plotted as an inverse isochron plot, which indicates the amount mixing between the radiogenic and atmospheric argon component. The plot shows that the grain has almost no atmospheric argon, and any argon present is almost entirely radiogenic. The geologic context of the determined age will be further explored in chapter 5.

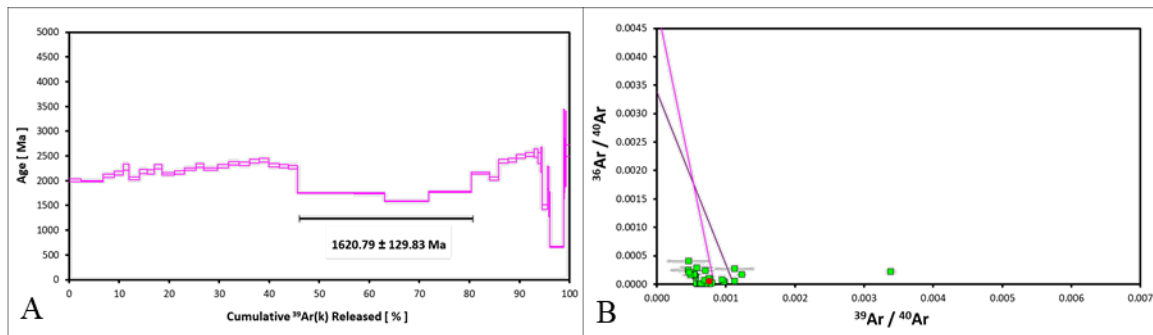


Figure 4.20:  $^{40}\text{Ar}/^{39}\text{Ar}$  analysis of Slate Islands syenite S2. A: Age spectrum following step heating experiment. B: Inverse isochron plot

Table 4.5: Summary of results from step heating experiments.

| <b>Sample</b>          | <b>Plateau<br/>40Ar/39Ar<br/>age (Ma) <sup>a</sup></b> | <b>Plateau<br/>quality (%) <sup>b</sup></b> | <b>Oldest step</b> | <b>Youngest step</b> |
|------------------------|--|---|--------------------|----------------------|
| <b>Ames Astrobleme</b> |  |   |                    |                      |
| S1 9014.9'             | 314.2±1.4  | 84.5  | 330.2±10.4         | 228.2±0.3            |
| S4 9020'               | 250.5±0.3  | 68.3  | 279.0±1.0          | 168.9±6.1            |
| S6 9027'               | 273.0±1.1  | 50.1  | 288.4±0.1          | 199.7±0.2            |
| S7 9031'               | 267.3±1.6  | 76.9  | 284.1±0.5          | 209.1±0.3            |
| S9 9034'               | 281.8±0.1  | 35.4  | 319.3±20.5         | 242.7±0.3            |
| <b>Slate Islands</b>   |  |   |                    |                      |
| S Two                  | 1620.8±129.8   | 34.8  | 2648.4±765.0       | 1466.7±49.9          |

a. Plateau age defined as five steps with statistically identical age.

b. Calculated as percent of released argon in plateau.

## **4.5 Summary**

All of the data collected for this project has been presented here. For both field sites, the data collected from analysis of zircons and feldspars provides a wide range of ages. Ages range from Precambrian, which correspond to hypothesized bedrock formation ages to the mid Phanerozoic. In the case of both sites, the majority of collected ages fall outside the OME. The full data interpreted in terms of the geologic context of each area as presented in Chapter 5.

## **V: DISCUSSION AND INTERPRETATION**

### **5.1 Overview**

This chapter discusses the implications of the data presented in the previous chapter. Here will be discussed the notable patterns in the data compared with the geologic context of each field area. Each identified age population will be matched with the most likely explanation given its location and age. Special consideration will be given to the data patterns as they relate to the OME. Lastly, an explanation will be offered for certain data that does not appear to match established geologic scenarios.

### **5.2 Ames Astrobleme Discussion**

#### **5.2.1 AGE POPULATION IDENTIFICATION**

The geochronologic data from the Ames Astrobleme reveals trends from across the established age ranges of units involved in the structure. The oldest zircon date obtained is  $1492 \pm 162$  Ma, while the youngest is  $341.3 \pm 9.7$  Ma. Two distinct age populations can be identified from the data. The old population (“Population 1”) consists of seventeen measurements which range in age from  $1492 \pm 162$  Ma to  $1294 \pm 25$  Ma. The young population (“Population 3”) consists of thirteen measurements which range in age from  $411.4 \pm 10.7$  Ma to  $341.3 \pm 9.7$  Ma. The remaining seven measurements fall between

the two populations and form the discordant linear trend seen in Figs. 4.8 and 5.1. These three populations are both readily identified from both the Concordia and age distribution diagrams.

The ages determined from  $^{40}\text{Ar}/^{39}\text{Ar}$  analysis of plagioclase feldspar (“Population 3”) are younger than the youngest zircon age. These ages range from  $314.1 \pm 1.4$  Ma to  $250.5 \pm 0.3$ . This postdates the youngest zircon measurement by ~70 million years. (Fig. 5.1)

### **5.2.2 GEOLOGIC SIGNIFICANCE OF AGE POPULATIONS**

Of primary importance to this thesis is the relationship between the age populations and the OME. To remind the reader, the OME occurred between 480-450 Ma. None of the dates obtained, either from analysis of zircons or feldspars, fall within this time span. This is especially confusing considering the formation age of the astrobleme is constrained to within 470-450 Ma by biostratigraphy. Thus, the ages determined do not confirm the hypothesized OME age of the astrobleme formation.

Although unnecessary, it is beneficial to remind the reader to the significance of the determined ages. These ages represent the most recent time when the mineral was heated above a specific temperature. In the simplest systems this corresponds to the time when the mineral cooled from its source melt. A first order interpretation might be to suggest that the three age populations represent the timing of three distinct igneous intrusions. This interpretation is not supported by the petrographic analysis. There is no

evidence to suggest that there exists more than one igneous source (the granodiorite) for the analyzed minerals.

Given our understanding of both the nature of the granodiorite clasts and the basement geology of Oklahoma, we can determine that the age of population 1 represents the initial cooling age of the granodiorite. This lithologic unit is not given a formal name in the relevant literature. Fischer (1997) and Koeberl et al., (1997, 2001) refer only to “pre-Cambrian granitics”. Given the lack of appropriate seismic data it may be impossible to connect the astrobleme granodiorite with any named geologic unit. Still, comparisons between the astrobleme granodiorite and nearby lithologies (both temporarily and spatially) can still be made.

The nearest named geologic formations with a similar age and composition are the Spavinaw granite which underlies northeast Oklahoma, southeast Kansas and southwest Missouri (Bickford and Lewis, 1979, Kisvarsanvi, 1990) and the Woodson County Granite of southeast Kansas (Denison, 1966). The formation age of these two units overlaps with the astrobleme granodiorite, but they each have a higher felsic component. There is also no reason to think that the units are connected by some vast buried igneous system. Our understanding interprets these units as isolated sills or batholiths (Muehlberger et al., 1967, Pearson et al., 2014). Pearson et al., (2014, from Higley et al., 2014 based on Whitmeyer and Karlstrom, 2007) interpret this and other nearby granitoids as being part of an intrusive series of A type granitoids which were emplaced within the Yavapai, Mazatzal and Granite-Rhyolite Provinces. It is likely that this ‘astrobleme granodiorite’ is part of this larger series.

The two younger age populations represent not an age of formation, but the time when the area was most recently above the closure temperatures for that particular radiometric system. As mentioned, neither age population 2 or 3 fall within the range of the timeframe of the OME. The  $^{40}\text{Ar}/^{39}\text{Ar}$  ages of population 3 are similar to those obtained by Koeberl et al., (1997, 2001). This was interpreted as being due to thermally elevated fluids mobilized due to the Nemaha Uplift. Yet population 2 is more enigmatic. This age does not correspond to any established tectonic events in central or southern North America. This time period overlaps with the larger Appalachian orogeny, but there is no reason to expect that the northwest Oklahoma region was affected by the formation of the Appalachians. There is also no reason to think that a previously unidentified igneous body intruded the area and caused only some of the zircons to be reset. Also, if age population 2 represents a time of elevated temperature, there is no explanation as to how the individual zircon grains suggest such a wide range of dates (70.1 Ma) despite all being within 7 m of each other. This leaves us with the unsettling conclusion that age population 2 does not represent the time of the most recent thermal episode. This conclusion will be explored further in section 5.4.

There is an alternative explanation for the discrepancies between the impact age as determined by biostratigraphy and the age of the most recent thermal event as determined by zircon analysis. This thesis has accepted the conclusion of Repetski (1997), that the conodonts found in the crater shale are of Middle Ordovician age and were deposited after the crater has formed. The question must be asked, what if that conclusion was wrong? Perhaps Dr. Repetski mis-identified the conodonts. No researcher

has yet addressed this question, and it is beyond the scope of both this thesis and my expertise as a paleontologist, but it remains a possibility to test in future analysis.

Now consider a second scenario, that the conodonts analyzed by Repetski were correctly identified as being Middle Ordovician in age, and that the impact occurred at 372 Ma. In this scenario, shales corresponding to the McLish Formation were part of the target rocks which were struck by the impactor, along with Arbuckle dolostone and the 'astrobleme granodiorite'. Conodonts which survived the impact were deposited along the crater rim, and later were washed back into the crater. Thus, fossils from ~460 Ma were included with shales deposited at ~370 Ma.

The evidence collected by other researchers does not support this explanation. As mentioned, the upper most crater deposits are layered dolomites. It is these, and not the crater shales, which are interpreted as the washback deposits from the settling of the crater rim. The crater shale is also interpreted as being deposited under calm conditions. Repetski describes conodont elements with basal attachment structures and bedding plane assemblages of oriented elements. The shale also contained carbonaceous and pyritized phyllocarid fragments. Altogether, this indicates a calm, anaerobic sea floor with a lack of significant current activity. This completely refutes the hypothesis that the conodont elements were reworked (and certainly were not involved in the asteroid impact!). We are instead forced to accept, for the time being, both the Middle Ordovician age indicated by the conodonts and the Devonian age of the thermal heating, without either being out of place.



Figure 5.1 Ames Astrobleme U-Pb zircon age distribution plot with  $^{40}\text{Ar}/^{39}\text{Ar}$  step heating age ranges. The distinct age populations, upper and lower discordia intercepts, and the range of the OME have been highlighted.

## 5.3 Slate Islands Archipelago

### 5.3.1 AGE POPULATION IDENTIFICATION

The age data from the Slate Islands Archipelago reveals trends from across the established age ranges of units involved in the structure (Fig. 5.3). The oldest date obtained is  $2710 \pm 21$  Ma, while the youngest date obtained is  $4.6 \pm 0.2$  Ma. As mentioned in the previous chapter, three distinct age populations can be identified from the data. The oldest population (“Population 1”) consists of 28 measurements which range in age from  $2710 \pm 21$  Ma to  $2632 \pm 18$  Ma. Population 2 consists of six measurements which range in age from  $1703 \pm 26$  Ma to  $1603 \pm 68$  Ma. Population 3 consists of 20 measurements which can be subdivided as follows: population 3.1 ranges in age from  $641.0 \pm 18.0$  Ma to  $578.0 \pm 16.3$  Ma; population 3.2 ranges in age from  $487.3 \pm 13.2$  Ma to  $432.0 \pm 25.0$  Ma; population 3.3 ranges in age from  $337.9 \pm 11.4$  Ma to  $319.8 \pm 10.2$  Ma. The youngest group (“Population 4”) consists of three measurements which range in age from  $34.4 \pm 1.2$  Ma to  $4.6 \pm 0.2$  Ma. The remaining measurements fall between the populations and form the discordant linear trend seen in Fig. 4.11. These populations are both readily identified from both Concordia and age distribution diagrams.

The ages determined from  $^{40}\text{Ar}/^{39}\text{Ar}$  analysis of K feldspar from the one analyzed sample is  $1621 \pm 130$  Ma. This measurement falls within the age range of population 2 and will be included in that population moving forward.

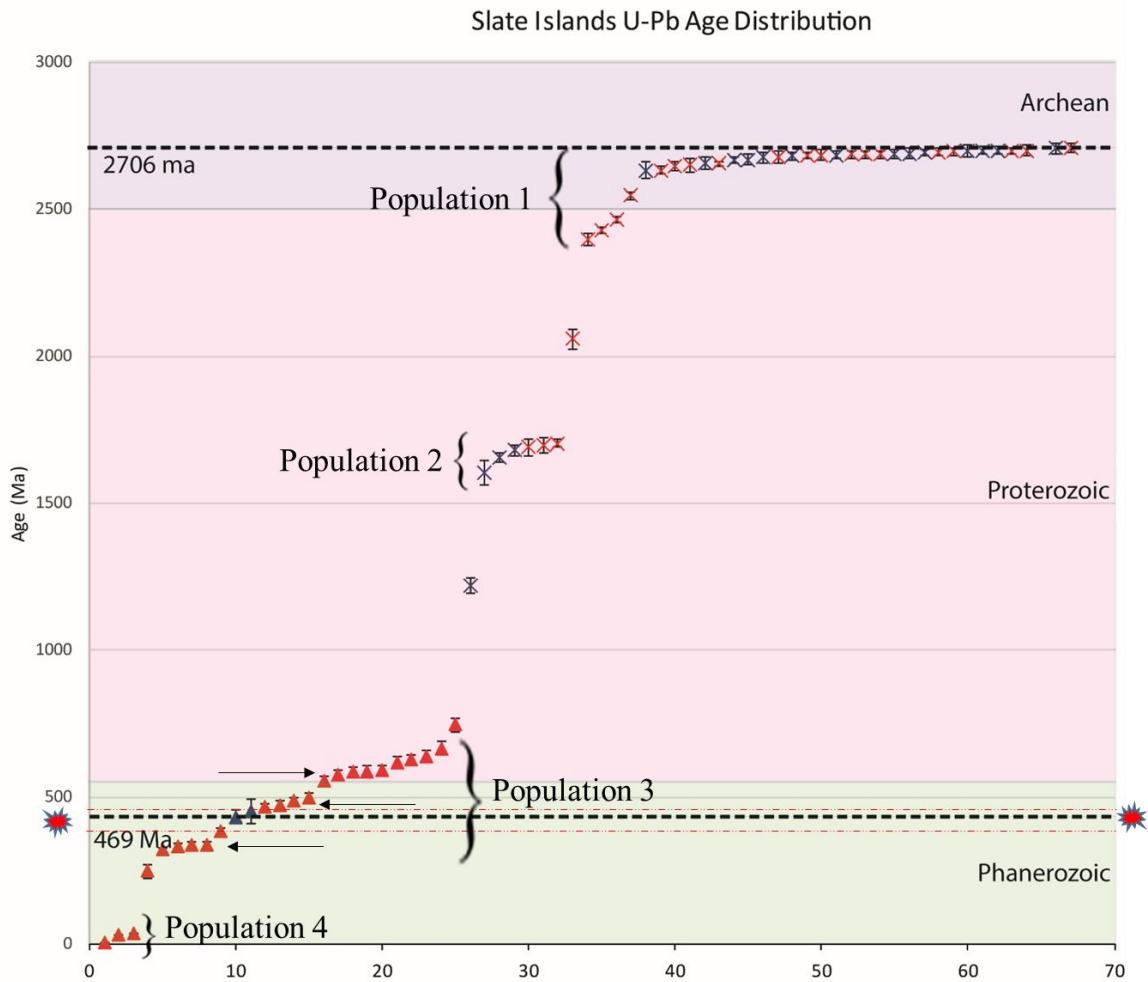


Figure 5.2 Slate Islands Archipelago U-Pb zircon age distribution plot. The distinct age populations (including subdivisions of population 3), upper and lower discordia intercepts, and the range of the OME have highlighted.

### 5.3.2 GEOLOGIC SIGNIFICANCE OF AGE POPULATIONS

Of primary importance to this thesis is the relationship between the age populations and the OME. The ages in subpopulation 3.2 all fall within the timeframe of the OME, within the margin of error. This is encouraging considering the lack of

stratigraphic constraints on the age of the impact structure formation. If this was the only (or even dominant) age population, it would provide strong evidence that the Slate Islands archipelago formation is due to the OME. Yet this data must be interpreted in the context of all the ages which do not fall within the OME.

Similar to the Ames Astrobleme, only the oldest population can be conclusively tied to the initial formation of the bedrock syenite or rhyolite. These units were interpreted by Sage (1991) as coeval with units from the Kenoran orogeny in northern Minnesota/ southwest Ontario. The ages of population 1 confirms this.

Population 2 does not match any of the broader geologic groups on the island or in the geographic vicinity. It is younger than the sedimentary rocks of the Animikie group (2500- 1800 Ma, Lundquist, 2006), the Penokean Orogeny (1890-1830 Ma, Schneider et al., 2002, Schulz and Cannon, 2007) and the Wisconsin magmatic terrane (1860-1835 Ma, Sims et al., 1989), but older than the Olser group/Midcontinent Rift System (1105-1087 Ma, Ojakangas et al., 2001 and references therein). There is some slight overlap between the age of population 2 and movement along the Great Lakes Tectonic Zone (Tohver et al., 2007). I speculate that the ages are due to the intrusion of one of the local rock units, which either caused resetting of some of the bedrock zircons or was itself captured in the later impactites. The fact that the  $^{40}\text{Ar}/^{39}\text{Ar}$  age of the analyzed syenite orthoclase was reset to this time period supports this hypothesis. Future work involving a more exhaustive sampling of all rock types and units on the island will allow the source of population 2 to be properly identified.

Population 3 (and its subpopulations) is more enigmatic than population 2. All the measurements within population 3 appear to be concordant (Figs. 4.11, 4.12), so lead loss due to partial resetting must be ruled out as an explanation. The first explanation to consider is that some of the ages within population 3 record the time of formation for the impact structure. It clearly cannot be all of the ages, as there is a ~345 million year range and the impact was geologically instantaneous. As mentioned, subpopulation 3.2 matches the age of the OME, and could represent zircons reset by that impact. Also, the best fit for the discordia line has a lower intercept which matches subpopulation 3.2, suggesting that it is the most significant thermal event from within the whole of population 3. This lends credence to the idea that the Slate Island Impact Structure was formed during the time of the OME.

The other two subpopulations (3.1 and 3.3) are more difficult to match known geologic events. The area around Lake Superior has been tectonically stable since the Mid-Continent Rift system. The closest tectonic events include the Grenville and Appalachian orogenies along the east coast of North America. Neither of these are satisfactory explanations, as none of the measurements are of Grenville age, and the Appalachian front is >1,000 km away at its closest. Subpopulation 3.1 is roughly coincident with the break of Rodinia (750-600 Ma, Li et al., 2008, references therein). The edge of this rifting is the Grenville province to the east, and the Arbuckle aulacogen to the south, and is as equally implausible. There is no reason to think that activities along the edge of North America could affect the area around the Slate Islands. At this time, there is no tectonic explanation for the ages of subpopulation 3.3.

A possible explanation for the ages in population 4 is that it is actually population 4 which records the time of the asteroid impact. The evidence suggests this is highly unlikely. If population 4 was the true age of the asteroid impact, we would expect to see the discordant trend pointing toward population 4, not 3. Also, we would expect that far more of the zircons would be dated to  $<34$  Ma, which we do not. It is highly unlikely that population 4 represents the true formation age of the impact structure. A second possible explanation for population 4 is the North Appalachian Anomaly, a hot spot currently hypothesized to be beneath the Adirondack Mountains/Central New England (Levin et al., 2018). At 34 Ma, this hot spot may have been near the location of the Slate Islands, although our current understanding of the hot spot's trajectory would place it too far north to be a significant influence on the Slate Islands. This is an unlikely explanation for the age of population 4, but one to consider moving forward.

#### **5.4 A Non-Tectonic Explanation for the Geologic Disparities**

An alternative explanation for the incongruities is that the anomalous zircons have experienced significant lead loss. A key assumption of any radiometric dating technique is that the minerals being analyzed form a closed system, that there has been no loss of the radiogenic isotope since the most recent heating event. However, we know that the lithologies involved in the impact crater formation, at both sites, are highly fractured (see Figs. 4.2, 4.6). It is possible that microscopic fractures within the zircon crystals are causing the loss of radiogenic lead.

Similar issues with improper U-Pb resetting have arisen with when trying to date other impact structures (eg: Krogh et al., 1993, Kamo et al., 1996, Kalleson et al., 2009, Schmeider et al., 2013, 2015). For example, Schmeider et al., (2015) identified a correlation between increasing severity of shock metamorphism and with progressive resetting. That study used U-Pb analysis of zircon to determine a formation date for the Acraman impact structure in South Australia that was outside of the established stratigraphic constraints. In this study, CL images show that older zircons have zonation which is 'clearer', i.e., more visible (consider Fig. 6.2, grain AAOK\_10 and Fig. 6.3, grain SION\_G1\_1, SION\_G1\_3, SION\_G1\_5, and SION\_S1\_1). These competently zoned grains are characteristic of original, igneous zircons which have not undergone metamorphosis. Several of the younger grains show 'mottled' zonation (ie, zoning appears to be present but is difficult to observe) or no zoning at all. (Consider Fig. 6.2, grain AAOK\_1 and Fig. 6.3, grain SION\_G1\_7, SION\_G2\_9, SION\_G2\_12, and SION\_G2\_15). This is indicative of metamorphism having occurred, of pre-existing zircons having their ages reset.

Thus, the age populations which do not correspond to known geologic events may still be related to the OME. Zircons determined to be slightly older than the OME may be providing a slightly erroneous date, one which was measured between an ancient, igneous core and a metamorphosed rim (consider Fig. 6.3, SION\_G2\_25). Zircons determined to be slightly younger than the OME might be experiencing lead loss due to the effects of shock metamorphism on the zircon crystal lattice. This same conclusion was reached by

other researchers studying large impact structures, such as Krogh et al., (1993), Kamo et al., (1996), and Schmieder et al (2015).

## **5.5 Summary and Future Work**

This project attempted to determine the formation age of two North American impact structures which had been hypothesized to have formed during the Ordovician Meteor Event. Samples of felsic bedrock and impact-generated melt rocks were collected from the two sites and minerals for radiometric dating were separated from them. Zircons were analyzed via LA-ICP-MS at University of Texas at Austin and SIMS at the University of Hiedelberg, while feldspars were analyzed via step heating analysis at Oregon State University.

The returned data reveals new information about the thermal and geologic histories of the two field sites. In both cases, the initial cooling age of the oldest igneous facies is revealed, and in the case of the Slate Islands, a new, Phanerozoic age is suggested for one of the bedrock units. It is the youngest dates which appear problematic given the regional geologic context. For the Ames Astrobleme, the identified Phanerozoic thermal event does not correspond to the stratigraphically established age of the astrobleme. In the case of the Slate Islands, the data suggests four distinct thermal events, only two of which can be explained by known geologic events. Although the analysis did not provide definitive proof that the Slate Islands formed during the OME, there is strong evidence to which agrees with that hypothesis. The young zircons which were reset to ~470 Ma, and

the fact the discordant zircons indicate a major resetting at ~470 Ma, strongly suggests that the most important thermal event in the area happened during the OME. Since the asteroid impact which formed the islands is the only known major thermal event in the area, it can be surmised that the Slate Islands did form during the OME. All that remains is to explain the reason why some of the young zircon suggest a thermal event at other dates.

It is likely that the discrepancy between the stratigraphic constraints on the impact structures and the ages determined in this study is due to a combination of factors. Post impact thermal alteration is probable at the two sites, especially at the Ames Astrobleme. Post impact alteration due to the effects of shock metamorphism is also likely; would have the effect of making the determined ages younger than they should be. Thus, although the ages determined suggest actual geologic events, the interpretation is complex, and one must be wary and not interpret the results at face value.

Future work will reduce the confusion surrounding the obtained ages. In the Slate Islands, extensive sampling and dating of each lithologic unit will allow for better identification of the unit's origins. By dating shocked zircons from multiple sources, multiple discordant trends might reveal the timing of the most significant recent thermal event, in theory, the impact which formed the Slate Islands. Lastly, it may be possible to constrain the post impact lead loss given the state of shock metamorphism in individual zircon grains. If this can be achieved, then we can compensate for that loss and adjust the determined age to properly match the geologic event which it represents. From there, we

can determine the proper age of the thermal events which affected the zircons and determine the actual age of the impact structure formation.

## VI: APPENDICES

### 6.1 Hand samples from Ames Astrobleme

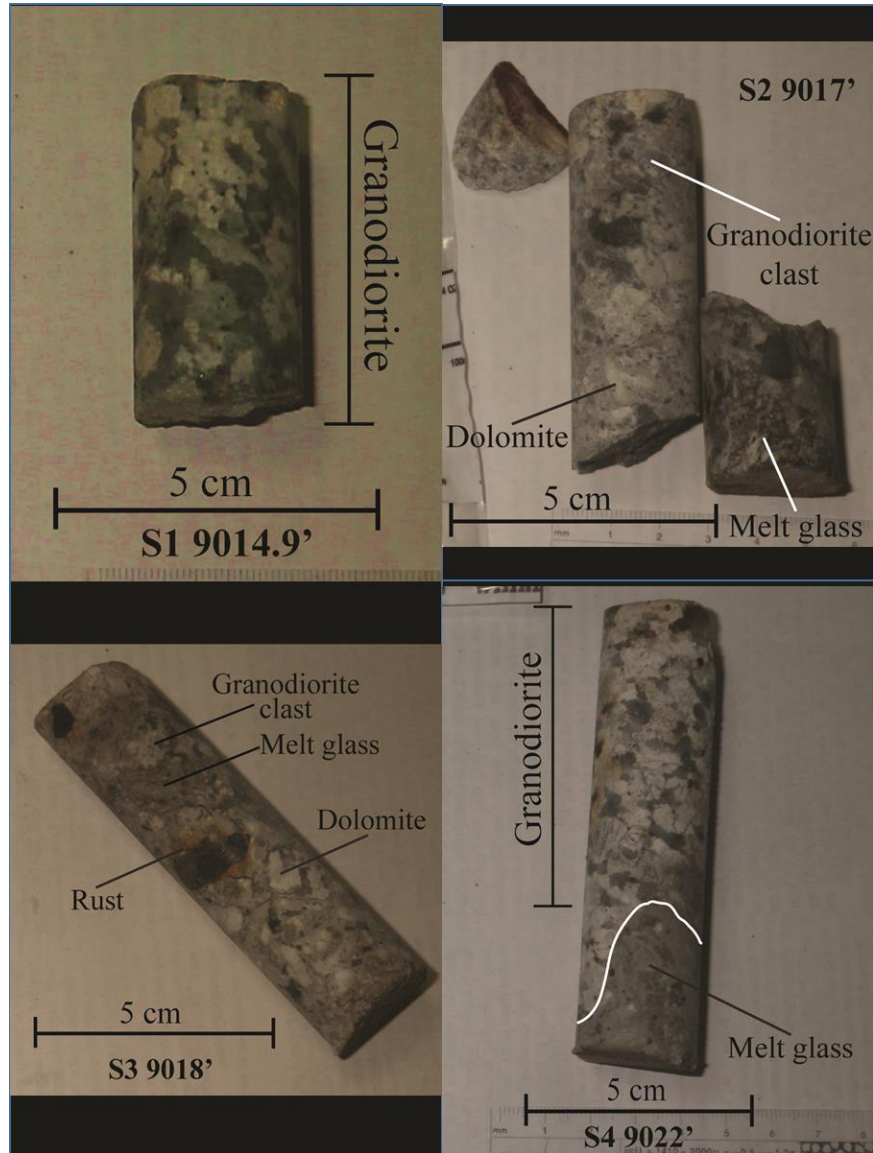


Figure 6.1: Images of hand samples collected from Ames Astrobleme Nicor Chestnut Core.

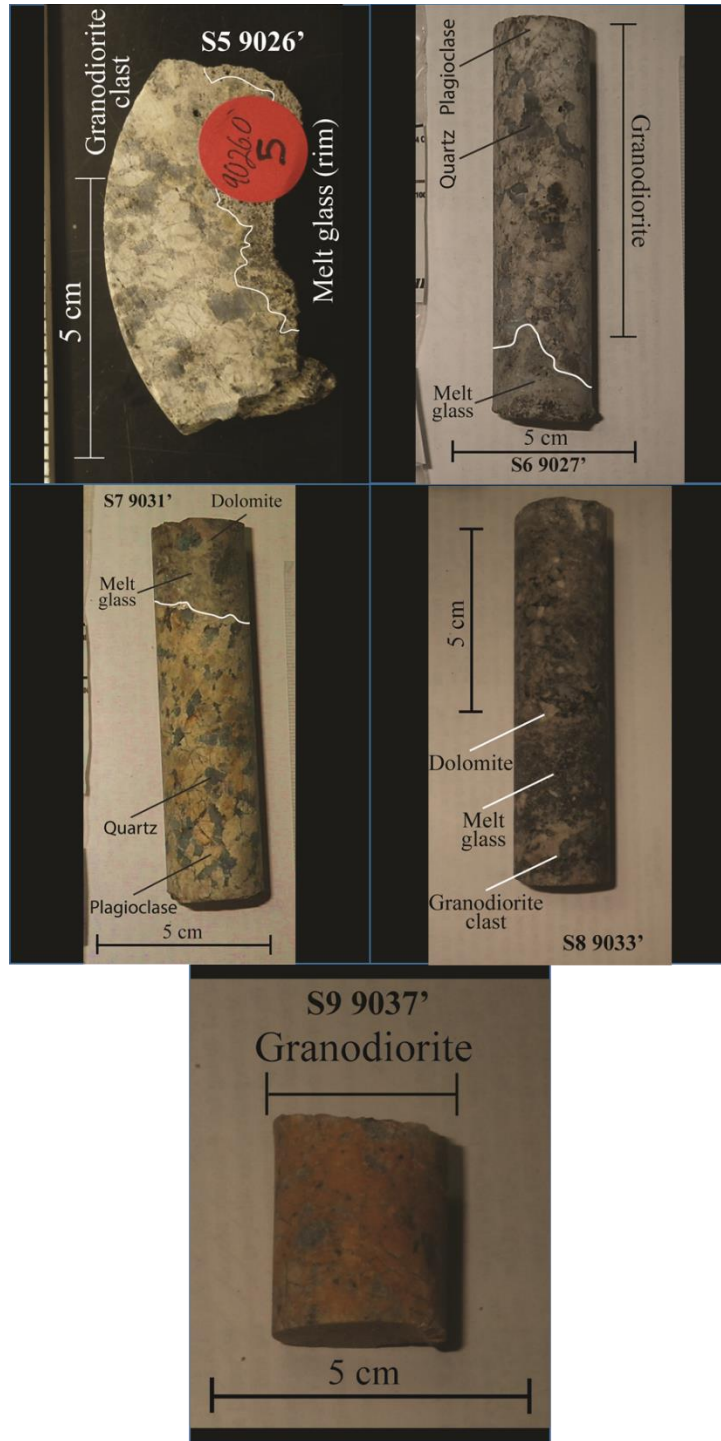


Figure 6.1: Continued

## 6.2 CL Images of Analyzed Zircons

### 6.2.1 CL IMAGES OF ZIRCONS FROM AMES ASTROBLEME CL IMAGES OF ZIRCONS FROM AMES ASTROBLEME.

The next page contains CL images of ten zircons from Ames Astrobleme analyzed as part of this project. Unfortunately, certain zircons were destroyed during laser ablation, and CL images of those zircons were not obtained. Crosses indicate location of measurement via Laser Ablation-ICP-MS, circled areas indicate location of measurement via SIMS. See accompanying chart for ages of numbered spots.

Table 6.1 Ages of Zircon analysis corresponding with Figure 6.2

| Zircon Grain | Spot number | Analysis number | Analysis type | Age (Ma) | Uncertainty (Ma) |
|--------------|-------------|-----------------|---------------|----------|------------------|
| AAOK_4       | *1:         | Ames_z5@1       | SIMS          | 937      | 95               |
| AAOK_5       | *2:         | AAOK2016_11     | LA-ICP-MS     | 928      | 19               |
|              | *3:         | Ames_z6@2       | SIMS          | 587.3    | 21.4             |
|              | *4:         | Ames_z6@1       | SIMS          | 713.6    | 21.9             |
|              | *5:         | Ames_z7@2       | SIMS          | 357.6    | 11.3             |
| AAOK_6       | *6:         | Ames_z7@1       | SIMS          | 368.4    | 10.9             |
|              | *7:         | Ames_z7@4       | SIMS          | 369.4    | 11.4             |
|              | *8:         | Ames_z7@3       | SIMS          | 372.0    | 11.4             |
|              | *9:         | Ames_z7@2       | SIMS          | 363.7    | 11.3             |
| AAOK_9       | *10:        | Ames_z3@2       | SIMS          | 355.8    | 14.1             |
|              | *11:        | Ames_z3@3       | SIMS          | 341.3    | 9.7              |
|              | *12:        | AAOK2016_1      | LA-ICP-MS     | 364.8    | 4.7              |
|              | *13:        | AAOK2016_2      | LA-ICP-MS     | 369.3    | 8.3              |
| AAOK_10      | *14:        | AAOK2016_4      | LA-ICP-MS     | 1379     | 17               |
|              | *15:        | AAOK2016_7      | LA-ICP-MS     | 1414     | 22               |
|              | *16:        | AAOK2016_5      | LA-ICP-MS     | 1407     | 30               |
|              | *17:        | AAOK2016_6      | LA-ICP-MS     | 1396     | 24               |
|              | *18:        | Ames_z4@3       | SIMS          | 1335     | 23               |
|              | *19:        | Ames_z4@1       | SIMS          | 1294     | 25               |
|              | *20:        | Ames_z4@2       | SIMS          | 1324     | 25               |

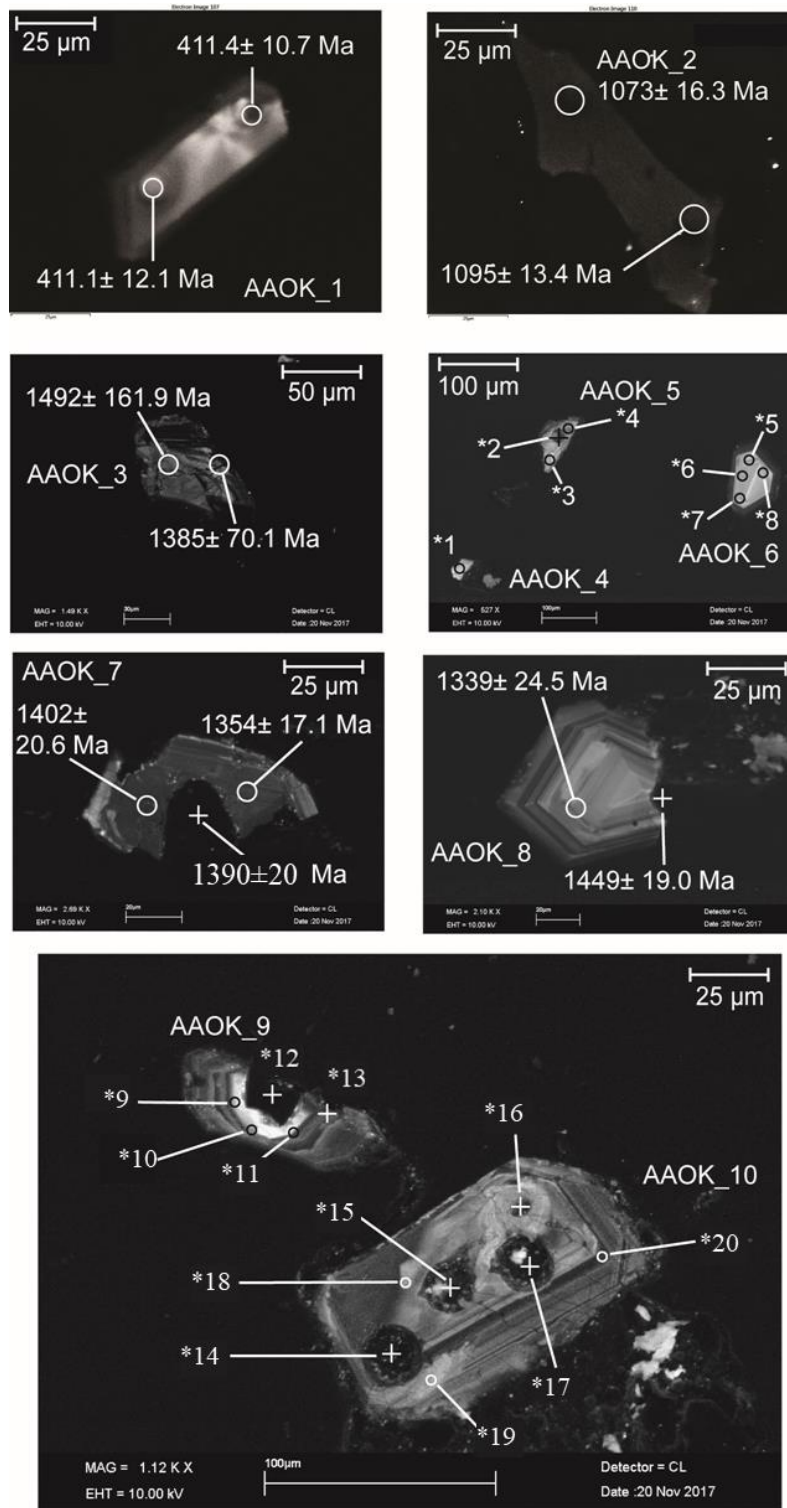


Figure 6.2: CL images of zircons analyzed from Ames Astrobleme.

### 6.2.2 CL IMAGES OF ZIRCONS FROM THE SLATE ISLANDS ARCHIPELAGO

The next several pages contains CL images of twenty-nine zircons from the Slate Islands analyzed as part of this project. Unfortunately, certain zircons were destroyed during laser ablation, and CL images of those zircons were not obtained. Crosses indicate location of measurement via Laser Ablation-ICP-MS, circled areas indicate location of measurement via SIMS. All zircons were imaged under identical probe conditions. Several zircons showed very limited luminescence, and as such, are difficult to see against the background.

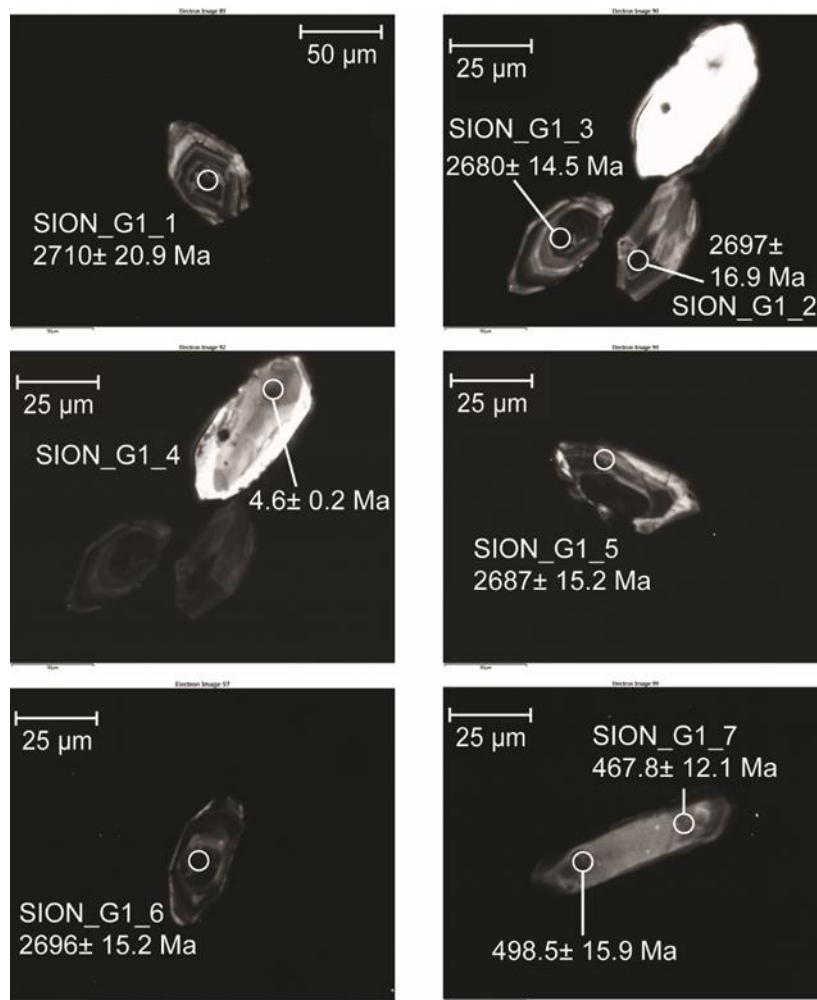


Figure 6.3: CL images of zircons analyzed from the Slate Islands.

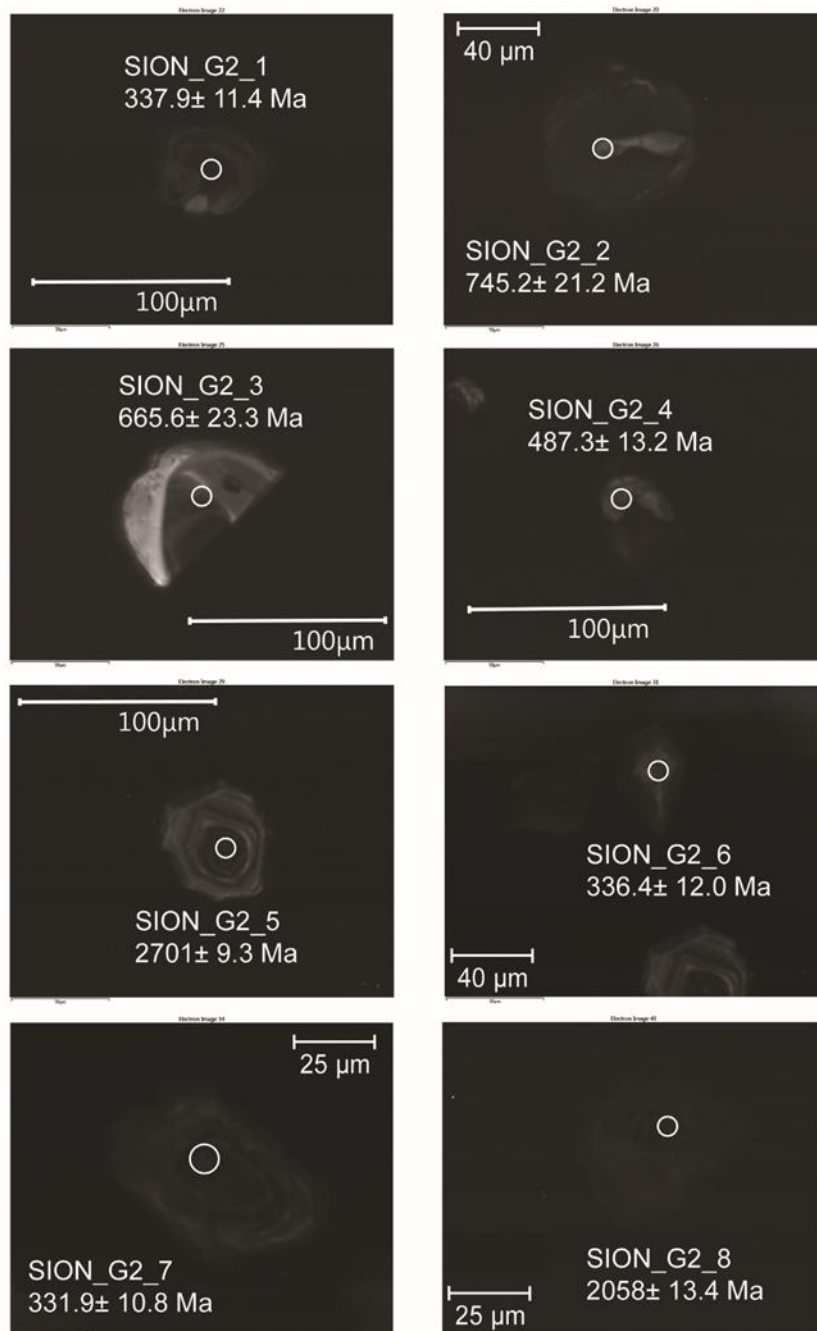


Figure 6.3 Continued

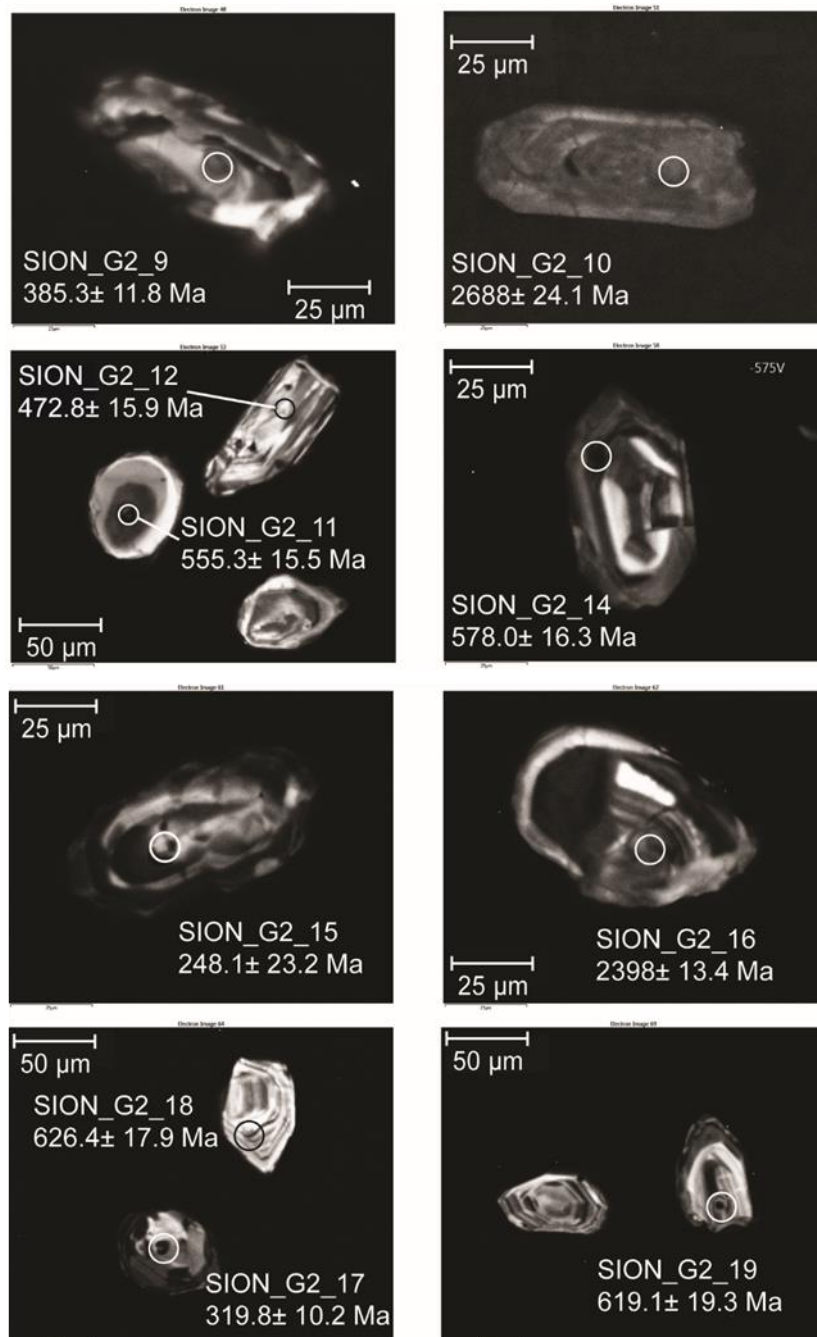


Figure 6.3 Continued

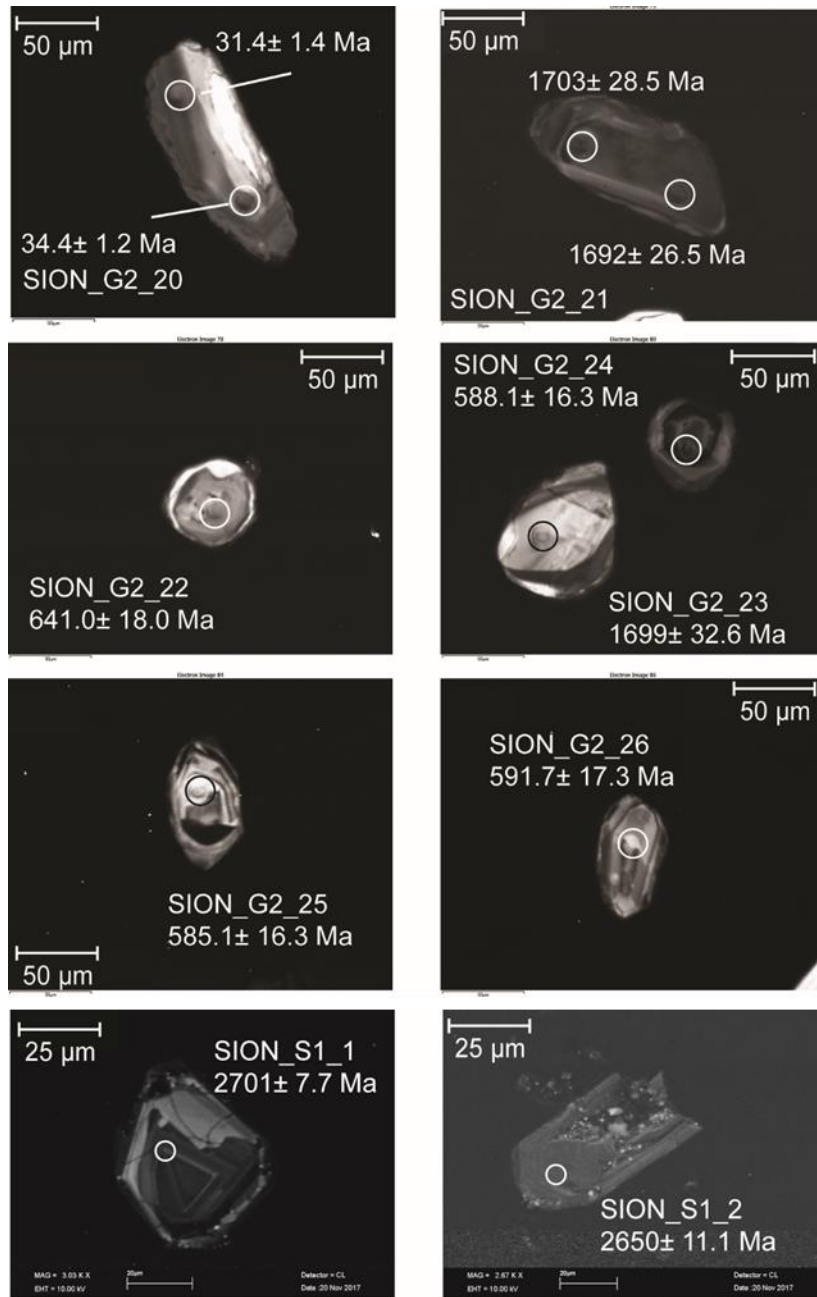


Figure 6.3 Continued

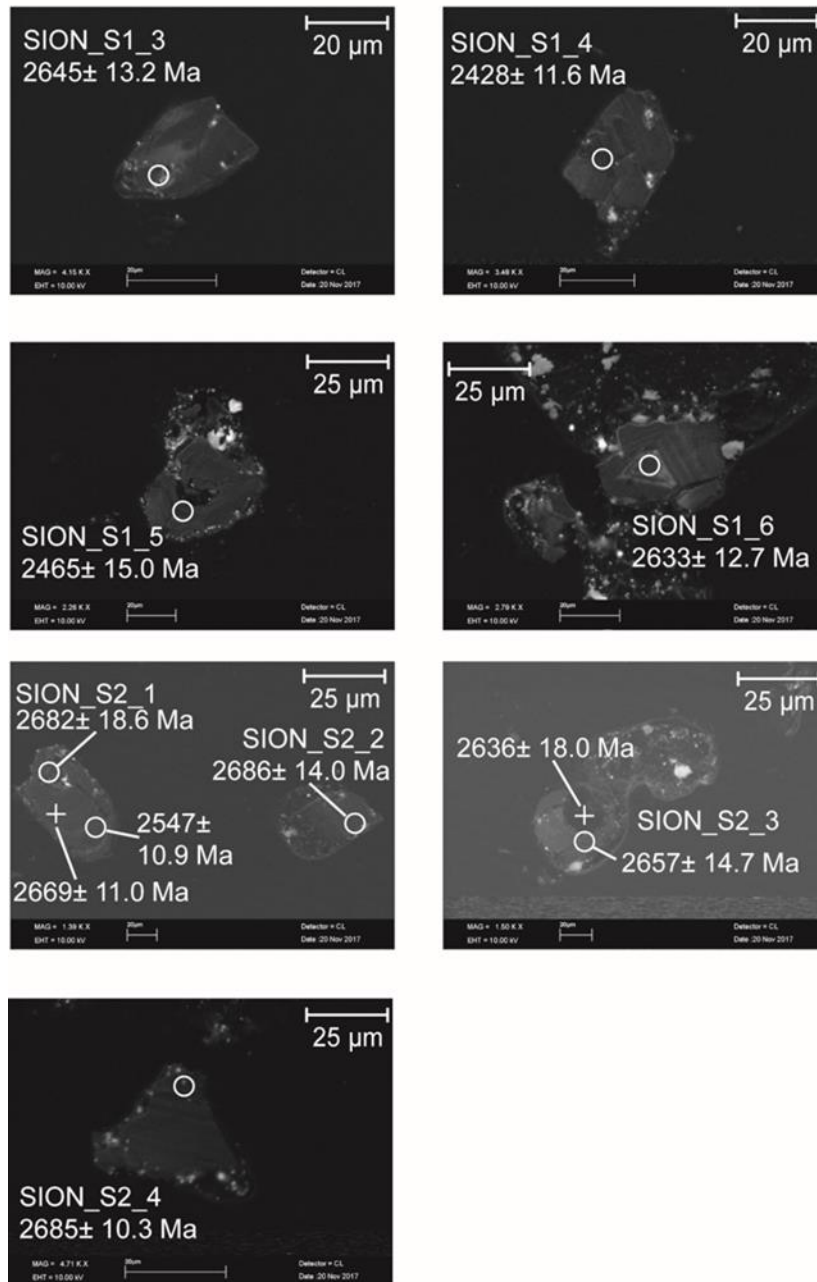


Figure 6.3 Continued

### 6.3 Data from U-Pb analysis of zircons from Ames Astrobleme

Table 6.2 Data from U-Pb analysis via LA-ICP-MS performed at the University of Texas at Austin

| Sample Spot #:           | Grain # | [U] ppm | U/Th | 2 $\sigma$ error | <sup>207</sup> Pb/ <sup>235</sup> U | 2 $\sigma$ error | <sup>206</sup> Pb/ <sup>238</sup> U | 2 $\sigma$ error | RHO  |
|--------------------------|---------|---------|------|------------------|-------------------------------------|------------------|-------------------------------------|------------------|------|
| S52026_8                 | AAOK_11 | 694.0   | 4.36 | 4.36             | 0.39                                | 0.01             | 0.05                                | <0.01            | 0.54 |
| AAOK2016_1               | AAOK_9  | 86.0    | 3.36 | 0.21             | 0.43                                | 0.01             | 0.06                                | <0.01            | 0.20 |
| AAOK2016_2               | AAOK_9  | 67.0    | 2.37 | 0.08             | 0.44                                | 0.02             | 0.06                                | <0.01            | 0.31 |
| AAOK2016_8               | AAOK_12 | 207.0   | 1.81 | 0.10             | 0.46                                | 0.01             | 0.06                                | <0.01            | 0.34 |
| AAOK2016_11 <sup>a</sup> | AAOK_5  | 212.0   | 0.51 | 0.02             | 1.99                                | 0.05             | 0.16                                | <0.01            | 0.89 |
| AAOK2016_10 <sup>a</sup> | AAOK_13 | 50.4    | 0.58 | 0.01             | 3.50                                | 0.11             | 0.19                                | <0.01            | 0.71 |
| S39018_29_1              | AAOK_14 | 215.0   | 0.72 | 0.01             | 2.07                                | 0.06             | 0.17                                | <0.01            | 0.78 |
| S39018_29_5              | AAOK_14 | 426.0   | 0.87 | 0.02             | 2.52                                | 0.04             | 0.21                                | <0.01            | 0.64 |
| AAOK2016_4               | AAOK_10 | 175.6   | 0.85 | 0.03             | 2.92                                | 0.03             | 0.24                                | <0.01            | 0.47 |
| AAOK2016_3               | AAOK_7  | 147.3   | 0.94 | 0.01             | 2.94                                | 0.03             | 0.24                                | <0.01            | 0.43 |
| AAOK2016_6               | AAOK_10 | 211.0   | 1.22 | 0.02             | 2.54                                | 0.04             | 0.21                                | <0.01            | 0.72 |
| AAOK2016_5               | AAOK_10 | 37.7    | 0.84 | 0.01             | 3.09                                | 0.05             | 0.25                                | <0.01            | 0.32 |
| AAOK2016_7               | AAOK_10 | 678.0   | 1.04 | 0.03             | 2.44                                | 0.05             | 0.20                                | <0.01            | 0.82 |
| AAOK2016_9               | AAOK_15 | 547.0   | 1.03 | 0.04             | 3.02                                | 0.05             | 0.24                                | <0.01            | 0.81 |
| S52026_5                 | AAOK_16 | 248.0   | 0.70 | 0.03             | 2.49                                | 0.08             | 0.20                                | 0.01             | 0.68 |

Table 6.2 Continued

| Sample Spot #:           | $^{207}\text{Pb}/^{235}\text{U}$<br>Age (Ma) | 2 $\sigma$<br>error | $^{206}\text{Pb}/^{238}\text{U}$<br>Age (Ma) | 2 $\sigma$<br>error | $^{207}\text{Pb}/^{206}\text{Pb}$<br>Age (Ma) | 2 $\sigma$<br>error | Best<br>age<br>(Ma) | 2 $\sigma$<br>error | %<br>Discordance* | Rim/Core   |
|--------------------------|--|---------------------|--|---------------------|---|---------------------|---------------------|---------------------|-------------------|------------|
| S52026_8                 | 331.7  | 5.8                 | 342.0  | 5.4                 | 270.0   | 40.0                | 342.0               | 5.4                 | 3.1               |            |
| AAOK2016_1               | 361.7  | 9.7                 | 364.8  | 4.7                 | 67.0  | 67.0                | 364.8               | 4.7                 | <0.1              | Single Age |
| AAOK2016_2               | 369.0  | 17.0                | 369.3  | 8.3                 | 110.0   | 110.0               | 369.3               | 8.3                 | <0.1              | Single Age |
| AAOK2016_8               | 382.3  | 7.5                 | 377.9  | 5.3                 | 52.0  | 52.0                | 377.9               | 5.3                 | 1.2               | Single Age |
| AAOK2016_11 <sup>a</sup> | 1112.0                                       | 16.0                | 928.0  | 19.0                | 24.0  | 24.0                | 928.0               | 19.0                | 37.9              | Single Age |
| AAOK2016_10 <sup>a</sup> | 1519.0                                       | 24.0                | 1108.0                                       | 14.0                | 42.0  | 42.0                | 1108.0              | 14.0                | 48.9              | Single Age |
| S39018_29_1              | 1134.0                                       | 20.0                | 1023.0                                       | 22.0                | 1362.0  | 36.0                | 1362.0              | 36.0                | 24.9              |            |
| S39018_29_5              | 1276.0                                       | 12.0                | 1222.0                                       | 15.0                | 1372.0  | 25.0                | 1372.0              | 25.0                | 10.9              |            |
| AAOK2016_4               | 1385.3                                       | 7.2                 | 1394.0                                       | 10.0                | 17.0  | 17.0                | 1379.0              | 17.0                | <0.1              | Single Age |
| AAOK2016_3               | 1391.6                                       | 8.4                 | 1394.8                                       | 9.7                 | 20.0  | 20.0                | 1390.0              | 20.0                | <0.1              | Single Age |
| AAOK2016_6               | 1281.0                                       | 13.0                | 1218.0                                       | 18.0                | 24.0  | 24.0                | 1396.0              | 24.0                | 12.8              | Single Age |
| AAOK2016_5               | 1427.0                                       | 12.0                | 1442.0                                       | 13.0                | 30.0  | 30.0                | 1407.0              | 30.0                | <0.1              | Single Age |
| AAOK2016_7               | 1252.0                                       | 14.0                | 1167.0                                       | 18.0                | 22.0  | 22.0                | 1414.0              | 22.0                | 17.5              | Single Age |
| AAOK2016_9               | 1410.0                                       | 12.0                | 1385.0                                       | 25.0                | 19.0  | 19.0                | 1449.0              | 19.0                | 4.4               | Single Age |
| S52026_5                 | 1259.0                                       | 22.0                | 1157.0                                       | 27.0                | 1457.0  | 44.0                | 1457.0              | 44.0                | 20.6              |            |

a: The ages obtained from these samples did not match the overall linear trend in the data, and were not included in the calculation of the discordia line.

Table 6.3 Data from U-Pb analysis via SIMS performed at the Heidelberg University

| Sample Name:            | Grain # | UO <sub>2</sub> /U | 1σ error | Th/U | 1σ error | <sup>206</sup> Pb/ <sup>238</sup> U | 1σ error | <sup>207</sup> Pb/ <sup>235</sup> U | 1σ error |
|-------------------------|---------|--------------------|----------|------|----------|-------------------------------------|----------|-------------------------------------|----------|
| Ames_z3@3               | AAOK_9  | 1.55               | 0.02     | 0.07 | 0.002    | 0.05                                | 0.002    | 0.38                                | 0.02     |
| Ames_z3@2               | AAOK_9  | 1.50               | 0.05     | 0.01 | 0.000    | 0.06                                | 0.002    | 0.40                                | 0.02     |
| Ames_z7@2               | AAOK_6  | 1.64               | 0.04     | 0.10 | 0.002    | 0.06                                | 0.002    | 0.40                                | 0.01     |
| Ames_z3@1               | AAOK_9  | 1.46               | 0.02     | 0.04 | 0.006    | 0.06                                | 0.002    | 0.41                                | 0.01     |
| Ames_z7@1               | AAOK_6  | 1.53               | 0.03     | 0.22 | 0.009    | 0.06                                | 0.002    | 0.43                                | 0.02     |
| Ames_z7@4               | AAOK_6  | 1.44               | 0.02     | 0.10 | 0.003    | 0.06                                | 0.002    | 0.41                                | 0.03     |
| Ames_z7@3               | AAOK_6  | 1.47               | 0.03     | 0.27 | 0.011    | 0.06                                | 0.002    | 0.41                                | 0.02     |
| Ames2_z1@2              | AAOK_1  | 1.43               | 0.02     | 0.15 | 0.002    | 0.07                                | 0.002    | 0.46                                | 0.02     |
| Ames2_z1@1              | AAOK_1  | 1.50               | 0.02     | 0.14 | 0.002    | 0.07                                | 0.002    | 0.47                                | 0.02     |
| Ames_z6@2               | AAOK_5  | 1.90               | 0.03     | 0.57 | 0.010    | 0.10                                | 0.004    | 0.93                                | 0.06     |
| Ames_z6@1               | AAOK_5  | 1.90               | 0.04     | 0.65 | 0.010    | 0.12                                | 0.004    | 1.33                                | 0.36     |
| Ames_z5@1 <sup>a</sup>  | AAOK_4  | 1.37               | 0.02     | 0.51 | 0.008    | 0.24                                | 0.008    | 2.29                                | 0.14     |
| Ames2_z2@1 <sup>a</sup> | AAOK_2  | 1.41               | 0.01     | 0.38 | 0.003    | 0.18                                | 0.006    | 1.93                                | 0.06     |
| Ames2_z2@2 <sup>a</sup> | AAOK_2  | 1.43               | 0.02     | 0.69 | 0.008    | 0.18                                | 0.007    | 1.91                                | 0.08     |
| Ames_z4@2               | AAOK_10 | 1.62               | 0.02     | 0.47 | 0.008    | 0.21                                | 0.005    | 2.42                                | 0.06     |
| Ames_z4@1               | AAOK_10 | 1.58               | 0.02     | 0.34 | 0.005    | 0.17                                | 0.004    | 2.01                                | 0.05     |
| Ames_z4@3               | AAOK_10 | 1.44               | 0.02     | 0.35 | 0.004    | 0.19                                | 0.006    | 2.26                                | 0.08     |
| Ames_z8@1               | AAOK_8  | 1.53               | 0.02     | 0.36 | 0.006    | 0.24                                | 0.007    | 2.90                                | 0.08     |
| Ames_z2@2               | AAOK_7  | 1.51               | 0.02     | 0.30 | 0.003    | 0.24                                | 0.007    | 2.85                                | 0.08     |
| Ames_z1@1               | AAOK_3  | 1.44               | 0.01     | 0.31 | 0.004    | 0.22                                | 0.007    | 2.72                                | 0.14     |
| Ames_z2@1               | AAOK_7  | 1.49               | 0.02     | 0.47 | 0.008    | 0.22                                | 0.006    | 2.67                                | 0.07     |
| Ames_z1@2               | AAOK_3  | 1.87               | 0.06     | 0.37 | 0.012    | 0.20                                | 0.007    | 2.56                                | 0.26     |

Table 6.3 Continued

| Sample Name:            | Common $^{206}\text{Pb}/^{204}\text{Pb}$ | Common $^{207}\text{Pb}/^{204}\text{Pb}$ | Common $^{208}\text{Pb}/^{204}\text{Pb}$ | $^{206}\text{Pb}/^{238}\text{U}$<br>Age (Ma) | 1 $\sigma$<br>error | $^{207}\text{Pb}/^{235}\text{U}$<br>Age (Ma) | 1 $\sigma$<br>error | $^{207}\text{Pb}/^{206}\text{Pb}$<br>Age (Ma) | 1 $\sigma$<br>error | % Radiogenic $^{206}\text{Pb}$ | 1 $\sigma$<br>error |
|-------------------------|--|--|--|--|---------------------|--|---------------------|---|---------------------|--------------------------------|---------------------|
| Ames_z3@3               | 18.86                                    | 15.62                                    | 38.34                                    | 341.3  | 9.7                 | 326.2  | 11.2                | 219.3   | 58.0                | 99.5                           | 0.1                 |
| Ames_z3@2               | 18.86                                    | 15.62                                    | 38.34                                    | 355.8  | 14.1                | 345.1  | 14.2                | 273.3   | 27.6                | 99.8                           | <0.1                |
| Ames_z7@2               | 18.86                                    | 15.62                                    | 38.34                                    | 357.6  | 11.3                | 342.2  | 9.0                 | 238.8   | 51.1                | 99.6                           | 0.1                 |
| Ames_z3@1               | 18.86                                    | 15.62                                    | 38.34                                    | 363.7  | 10.5                | 349.4  | 8.5                 | 255.7   | 28.9                | 99.7                           | 0.1                 |
| Ames_z7@1               | 18.86                                    | 15.62                                    | 38.34                                    | 368.4  | 10.9                | 362.4  | 14.1                | 324.5   | 69.5                | 100.0                          | <0.1                |
| Ames_z7@4               | 18.86                                    | 15.62                                    | 38.34                                    | 369.4  | 11.4                | 352.1  | 18.5                | 239.4   | 112.0               | 99.6                           | 0.2                 |
| Ames_z7@3               | 18.86                                    | 15.62                                    | 38.34                                    | 372.0  | 11.4                | 351.8  | 14.0                | 220.9   | 72.6                | 99.7                           | 0.1                 |
| Ames2_z1@2              | 18.86                                    | 15.62                                    | 38.34                                    | 411.1  | 12.1                | 386.9  | 12.7                | 244.9   | 55.6                | 99.5                           | 0.1                 |
| Ames2_z1@1              | 18.86                                    | 15.62                                    | 38.34                                    | 411.4  | 10.7                | 388.7  | 13.3                | 255.5   | 67.2                | 99.0                           | 0.2                 |
| Ames_z6@2               | 18.86                                    | 15.62                                    | 38.34                                    | 587.3  | 21.4                | 669.1  | 32.0                | 955.1   | 101.8               | 94.3                           | 0.3                 |
| Ames_z6@1               | 18.86                                    | 15.62                                    | 38.34                                    | 713.6  | 21.9                | 857.0  | 157.4               | 1249.0  | 508.9               | 91.5                           | 1.0                 |
| Ames_z5@1 <sup>a</sup>  | 18.86                                    | 15.62                                    | 38.34                                    | 1367.0                                       | 42.5                | 1209.0                                       | 43.3                | 937.0   | 94.8                | 97.4                           | 0.4                 |
| Ames2_z2@1 <sup>a</sup> | 18.86                                    | 15.62                                    | 38.34                                    | 1089.0                                       | 32.1                | 1091.0                                       | 21.8                | 1095.0  | 13.4                | 99.8                           | <0.1                |
| Ames2_z2@2 <sup>a</sup> | 18.86                                    | 15.62                                    | 38.34                                    | 1089.0                                       | 37.4                | 1083.0                                       | 26.5                | 1073.0  | 16.4                | 99.6                           | <0.1                |
| Ames_z4@2               | 18.86                                    | 15.62                                    | 38.34                                    | 1205.0                                       | 26.4                | 1248.0                                       | 19.3                | 1324.0  | 24.8                | 99.4                           | 0.1                 |
| Ames_z4@1               | 18.86                                    | 15.62                                    | 38.34                                    | 1033.0                                       | 24.5                | 1120.0                                       | 18.2                | 1294.0  | 24.7                | 98.8                           | 0.1                 |
| Ames_z4@3               | 18.86                                    | 15.62                                    | 38.34                                    | 1126.0                                       | 34.8                | 1200.0                                       | 23.4                | 1335.0  | 23.0                | 99.6                           | 0.1                 |
| Ames_z8@1               | 18.86                                    | 15.62                                    | 38.34                                    | 1408.0                                       | 34.4                | 1381.0                                       | 21.4                | 1339.0  | 24.5                | 99.8                           | 0.1                 |
| Ames_z2@2               | 18.86                                    | 15.62                                    | 38.34                                    | 1380.0                                       | 34.0                | 1370.0                                       | 21.2                | 1354.0  | 17.1                | 98.4                           | 0.1                 |
| Ames_z1@1               | 18.86                                    | 15.62                                    | 38.34                                    | 1300.0                                       | 38.5                | 1333.0                                       | 39.2                | 1385.0  | 70.1                | 99.2                           | 0.1                 |
| Ames_z2@1               | 18.86                                    | 15.62                                    | 38.34                                    | 1272.0                                       | 33.0                | 1321.0                                       | 20.1                | 1402.0  | 20.6                | 99.1                           | 0.1                 |
| Ames_z1@2               | 18.86                                    | 15.62                                    | 38.34                                    | 1171.0                                       | 36.3                | 1289.0                                       | 73.0                | 1492.0  | 161.9               | 93.0                           | 0.4                 |

a: The ages obtained from these samples did not match the overall linear trend in the data, and were not included in the calculation of the discordia line.

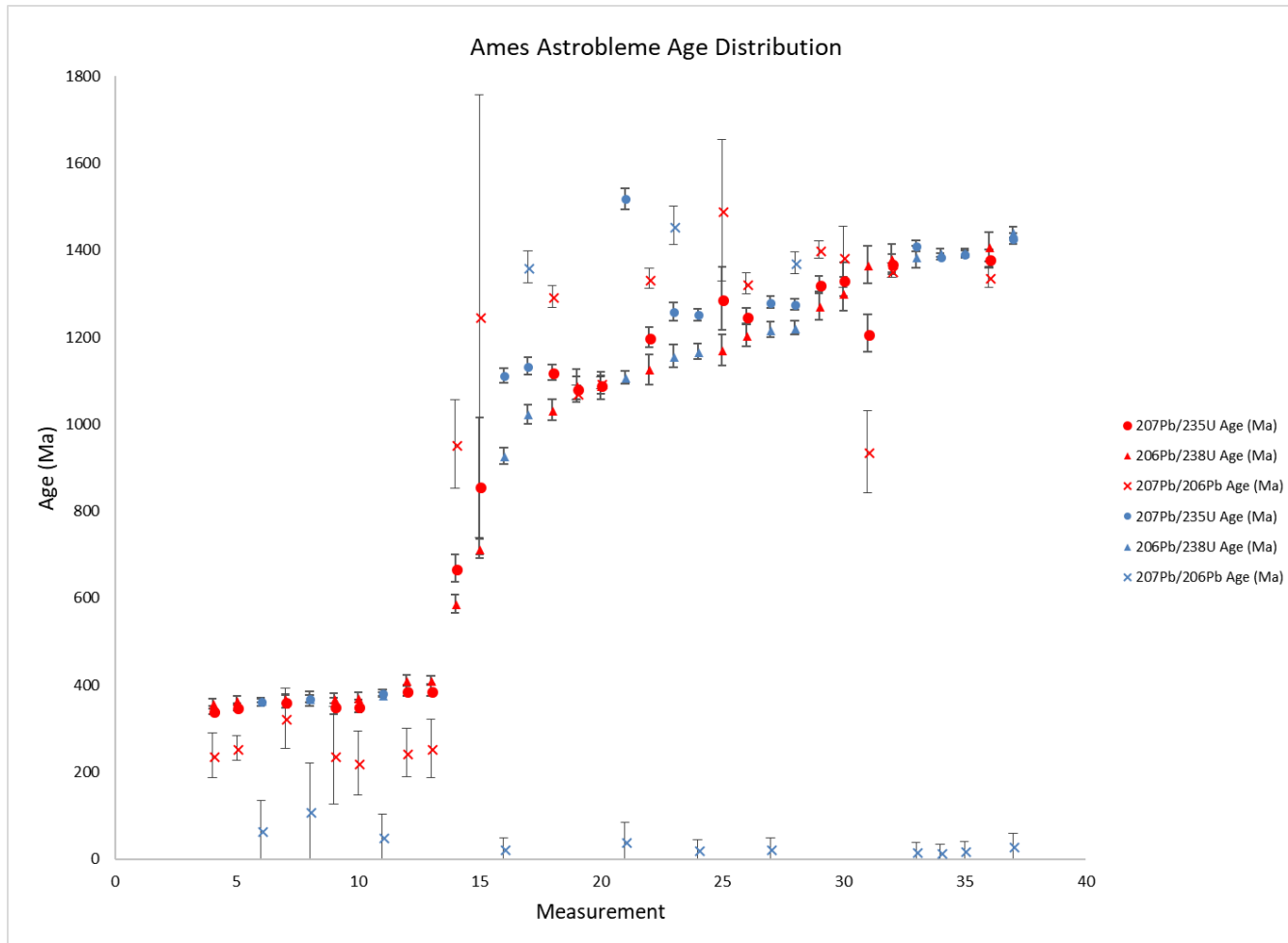


Figure 6.4: Age distribution plot of all measurements from Ames Astrobleme zircons. Red data points indicate zircons analyzed via SIMS, blue data points indicate zircons analyzed via LA-ICP-MS. Error bars designate  $2\sigma$ .

## 6.4 Data from U-Pb analysis of zircons from Slate Islands Archipelago

Table 6.4 Data from U-Pb analysis via LA-ICP-MS performed at the University of Texas at Austin

| Sample Spot #:             | Grain #    | [U] ppm | U/Th | 2 $\sigma$ error | <sup>207</sup> Pb/ <sup>235</sup> U | 2 $\sigma$ error | <sup>206</sup> Pb/ <sup>238</sup> U | 2 $\sigma$ error | RHO  |
|----------------------------|------------|---------|------|------------------|-------------------------------------|------------------|-------------------------------------|------------------|------|
| SLON2017_G3_2 <sup>1</sup> | SION_G2_27 | 792.0   | 3.01 | 0.11             | 1.07                                | 0.06             | 0.07                                | <0.01            | 0.97 |
| SLON2017_G4_3 <sup>1</sup> | SION_G2_28 | 19.7    | 3.53 | 0.09             | 3.91                                | 0.09             | 0.07                                | <0.01            | 0.09 |
| SLON2017_G4_4 <sup>1</sup> | SION_G2_29 | 645.0   | 1.79 | 0.05             | 2.05                                | 0.02             | 0.18                                | <0.01            | 0.64 |
| SLON2017_S2_5              | SION_S2_5  | 559.0   | 0.62 | 0.03             | 7.17                                | 0.35             | 0.28                                | 0.01             | 0.94 |
| SLON2017_S1_5              | SION_S1_7  | 621.0   | 0.67 | 0.03             | 7.02                                | 0.16             | 0.29                                | 0.01             | 0.86 |
| SLON2017_G4_5              | SION_G2_31 | 97.7    | 0.48 | 0.01             | 7.23                                | 0.24             | 0.30                                | 0.01             | 0.93 |
| SLON2017_S2_3              | SION_S2_3  | 535.0   | 0.86 | 0.04             | 9.23                                | 0.29             | 0.38                                | 0.01             | 0.93 |
| SLON2017_S1_3              | SION_S1_8  | 338.4   | 0.79 | 0.03             | 10.02                               | 0.14             | 0.40                                | 0.01             | 0.85 |
| SLON2017_S1_2              | SION_S1_8  | 289.2   | 0.72 | 0.02             | 11.25                               | 0.18             | 0.45                                | 0.01             | 0.91 |
| SLON2017_S2_1              | SION_S2_1  | 467.0   | 1.08 | 0.02             | 8.71                                | 0.11             | 0.35                                | <0.01            | 0.89 |
| SLON2017_S1_6              | SION_S1_9  | 372.0   | 1.63 | 0.13             | 10.96                               | 0.26             | 0.44                                | 0.01             | 0.92 |
| SLON2017_S1_4              | SION_S1_10 | 130.8   | 1.08 | 0.04             | 10.64                               | 0.22             | 0.42                                | 0.01             | 0.89 |
| SLON2017_S1_7              | SION_S1_11 | 439.0   | 1.58 | 0.19             | 12.47                               | 0.30             | 0.49                                | 0.01             | 0.93 |
| SLON2017_S2_6              | SION_S2_7  | 521.0   | 0.90 | 0.03             | 10.20                               | 0.16             | 0.40                                | 0.01             | 0.87 |
| SLON2017_G3_1              | SION_S1_12 | 124.8   | 0.84 | 0.03             | 9.98                                | 0.15             | 0.39                                | 0.01             | 0.81 |
| SLON2017_S1_1              | SION_G2_30 | 297.0   | 2.12 | 0.03             | 12.47                               | 0.12             | 0.49                                | <0.01            | 0.73 |
| SLON2017_S1_8              | SION_S1_13 | 218.0   | 1.32 | 0.10             | 13.38                               | 0.17             | 0.52                                | 0.01             | 0.79 |
| SLON2017_S2_2              | SION_S2_8  | 384.1   | 1.75 | 0.06             | 12.05                               | 0.22             | 0.47                                | 0.01             | 0.92 |
| SLON2017_S2_4              | SION_S2_9  | 331.0   | 0.70 | 0.02             | 12.11                               | 0.13             | 0.47                                | <0.01            | 0.80 |
| SLON2017_G3_3              | SION_G2_32 | 163.0   | 0.68 | 0.06             | 11.42                               | 0.46             | 0.45                                | 0.02             | 0.98 |

Table 6.4 Continued

| Sample Spot #:             | $^{207}\text{Pb}/^{235}\text{U}$<br>Age (Ma) | 2 $\sigma$ error | $^{206}\text{Pb}/^{238}\text{U}$<br>Age (Ma) | 2 $\sigma$ error | $^{207}\text{Pb}/^{206}\text{Pb}$<br>Age (Ma) | 2 $\sigma$ error | Best<br>age<br>(Ma) | 2 $\sigma$ error | %<br>Discordance* | Rim/Core   |
|----------------------------|--|------------------|--|------------------|---|------------------|---------------------|------------------|-------------------|------------|
| SLON2017_G3_2 <sup>a</sup> | 723.0  | 32.0             | 432.0  | 25.0             | 24.0  | 24.0             | 432.0               | 25.0             | 40.2              | Single Age |
| SLON2017_G4_3 <sup>a</sup> | 1610.0                                       | 19.0             | 452.7  | 9.1              | 41.0  | 41.0             | 452.7               | 9.1              | 71.9              | Single Age |
| SLON2017_G4_4 <sup>a</sup> | 1131.6                                       | 6.3              | 1086.0                                       | 11.0             | 17.0  | 17.0             | 1220.0              | 17.0             | 11.0              | Single Age |
| SLON2017_S2_5              | 2117.0                                       | 44.0             | 1603.0                                       | 68.0             | 28.0  | 28.0             | 1603.0              | 68.0             | 40.2              | Single Age |
| SLON2017_S1_5              | 2106.0                                       | 21.0             | 1655.0                                       | 32.0             | 19.0  | 19.0             | 1655.0              | 32.0             | 36.0              | Single Age |
| SLON2017_G4_5              | 2121.0                                       | 33.0             | 1680.0                                       | 50.0             | 21.0  | 21.0             | 1680.0              | 50.0             | 35.6              | Single Age |
| SLON2017_S2_3              | 2350.0                                       | 29.0             | 2050.0                                       | 57.0             | 18.0  | 18.0             | 2632.0              | 18.0             | 22.1              | Single Age |
| SLON2017_S1_3              | 2435.0                                       | 13.0             | 2189.0                                       | 27.0             | 12.0  | 12.0             | 2655.0              | 12.0             | 17.6              | Single Age |
| SLON2017_S1_2              | 2543.0                                       | 14.0             | 2389.0                                       | 29.0             | 11.0  | 11.0             | 2667.0              | 11.0             | 10.4              | Single Age |
| SLON2017_S2_1              | 2305.0                                       | 11.0             | 1919.0                                       | 22.0             | 11.0  | 11.0             | 2669.0              | 11.0             | 28.1              | Single Age |
| SLON2017_S1_6              | 2516.0                                       | 22.0             | 2326.0                                       | 43.0             | 17.0  | 17.0             | 2676.0              | 17.0             | 13.1              | Single Age |
| SLON2017_S1_4              | 2488.0                                       | 20.0             | 2262.0                                       | 40.0             | 16.0  | 16.0             | 2682.0              | 16.0             | 15.7              | Single Age |
| SLON2017_S1_7              | 2634.0                                       | 24.0             | 2575.0                                       | 46.0             | 16.0  | 16.0             | 2685.0              | 16.0             | 4.1               | Single Age |
| SLON2017_S2_6              | 2449.0                                       | 15.0             | 2174.0                                       | 31.0             | 14.0  | 14.0             | 2689.0              | 14.0             | 19.2              | Single Age |
| SLON2017_G3_1              | 2431.0                                       | 15.0             | 2142.0                                       | 33.0             | 17.0  | 17.0             | 2691.0              | 17.0             | 20.4              | Single Age |
| SLON2017_S1_1              | 2640.2                                       | 8.6              | 2562.0                                       | 20.0             | 12.0  | 12.0             | 2695.0              | 12.0             | 4.9               | Single Age |
| SLON2017_S1_8              | 2705.0                                       | 12.0             | 2713.0                                       | 29.0             | 14.0  | 14.0             | 2699.0              | 14.0             | <0.1              | Single Age |
| SLON2017_S2_2              | 2605.0                                       | 17.0             | 2489.0                                       | 38.0             | 12.0  | 12.0             | 2701.0              | 12.0             | 7.8               | Single Age |
| SLON2017_S2_4              | 2611.0                                       | 10.0             | 2499.0                                       | 21.0             | 13.0  | 13.0             | 2701.0              | 13.0             | 7.5               | Single Age |
| SLON2017_G3_3              | 2548.0                                       | 40.0             | 2377.0                                       | 81.0             | 22.0  | 22.0             | 2707.0              | 22.0             | 12.2              | Single Age |

a: The ages obtained from these samples did not match the overall linear trend in the data and were not included in the calculation of the discordia line.

Table 6.5 Data from U-Pb analysis via SIMS performed at the Heidelberg University

| Sample Name: | Grain #    | UO <sub>2</sub> /U | 1σ error | Th/U | 1σ error | <sup>206</sup> Pb/ <sup>238</sup> U | 1σ error | <sup>207</sup> Pb/ <sup>235</sup> U | 1σ error |
|--------------|------------|--------------------|----------|------|----------|-------------------------------------|----------|-------------------------------------|----------|
| SIsc@4       | SION_G1_4  | 1.39               | 0.02     | 0.30 | 0.002    | 0.00                                | <0.001   | <0.01                               | 0.002    |
| SIbc@20      | SION_G2_20 | 1.47               | 0.02     | 0.50 | 0.008    | 0.00                                | <0.001   | <0.01                               | 0.021    |
| SIbc_s2@20   | SION_G2_20 | 1.44               | 0.02     | 0.49 | 0.006    | 0.01                                | <0.001   | 0.02                                | 0.008    |
| SIbc@15      | SION_G2_15 | 1.44               | 0.01     | 0.65 | 0.074    | 0.04                                | 0.004    | 0.28                                | 0.025    |
| SIbc@17      | SION_G2_17 | 1.44               | 0.02     | 0.42 | 0.032    | 0.05                                | 0.002    | 0.36                                | 0.042    |
| SIbc@6a      | SION_G2_7  | 1.44               | 0.03     | 0.66 | 0.011    | 0.05                                | 0.002    | 0.38                                | 0.013    |
| SIbc@7       | SION_G2_6  | 1.44               | 0.04     | 0.49 | 0.003    | 0.05                                | 0.002    | 0.37                                | 0.022    |
| SIbc@1       | SION_G2_1  | 1.44               | 0.03     | 0.53 | 0.005    | 0.05                                | 0.002    | 0.39                                | 0.012    |
| SIbc@9       | SION_G2_9  | 1.44               | 0.02     | 0.11 | 0.002    | 0.06                                | 0.002    | 0.53                                | 0.019    |
| SIsc@7b      | SION_G1_7  | 1.44               | 0.02     | 0.03 | 0.001    | 0.08                                | 0.002    | 0.57                                | 0.018    |
| SIbc@12      | SION_G2_12 | 1.44               | 0.03     | 0.18 | 0.003    | 0.08                                | 0.003    | 0.58                                | 0.024    |
| SIsc@7a      | SION_G2_4  | 1.44               | 0.04     | 0.17 | 0.005    | 0.08                                | 0.002    | 0.64                                | 0.029    |
| SIbc@4       | SION_G1_7  | 1.44               | 0.03     | 0.04 | 0.002    | 0.08                                | 0.003    | 0.63                                | 0.026    |
| SIbc@11      | SION_G2_11 | 1.44               | 0.01     | 0.08 | 0.004    | 0.09                                | 0.003    | 0.70                                | 0.023    |
| SIbc@14      | SION_G2_14 | 1.44               | 0.02     | 0.11 | 0.001    | 0.09                                | 0.003    | 0.71                                | 0.026    |
| SIbc@24      | SION_G2_25 | 1.44               | 0.01     | 0.23 | 0.007    | 0.10                                | 0.003    | 0.78                                | 0.030    |
| SIbc@19      | SION_G2_24 | 1.44               | 0.03     | 0.52 | 0.008    | 0.10                                | 0.004    | 0.77                                | 0.037    |
| SIbc@25      | SION_G2_26 | 1.44               | 0.01     | 0.13 | 0.001    | 0.10                                | 0.003    | 0.78                                | 0.027    |
| SIbc@26      | SION_G2_19 | 1.44               | 0.02     | 0.59 | 0.012    | 0.10                                | 0.003    | 0.77                                | 0.039    |
| SIbc@18      | SION_G2_18 | 1.44               | 0.01     | 0.87 | 0.011    | 0.10                                | 0.003    | 0.81                                | 0.028    |
| SIbc@22      | SION_G2_22 | 1.44               | 0.01     | 0.44 | 0.007    | 0.10                                | 0.003    | 0.85                                | 0.040    |
| SIbc@3       | SION_G2_3  | 1.44               | 0.02     | 0.24 | 0.004    | 0.11                                | 0.004    | 0.92                                | 0.037    |

a: The ages obtained from these samples did not match the overall linear trend in the data and were not included in the calculation of the discordia line.

Table 6.5 Continued

| Sample Name: | Common<br>$^{206}\text{Pb}/^{204}\text{Pb}$ | Common<br>$^{207}\text{Pb}/^{204}\text{Pb}$ | Common<br>$^{208}\text{Pb}/^{204}\text{Pb}$ | $^{206}\text{Pb}/^{238}\text{U}$<br>Age (Ma) | 1 $\sigma$<br>error | $^{207}\text{Pb}/^{235}\text{U}$ Age<br>(Ma) | 1 $\sigma$<br>error | $^{207}\text{Pb}/^{206}\text{Pb}$ Age<br>(Ma) | 1 $\sigma$<br>error | % Radiogenic<br>$^{206}\text{Pb}$ | 1 $\sigma$<br>error |
|--------------|---|---|---|--|---------------------|--|---------------------|---|---------------------|-----------------------------------|---------------------|
| SIsc@4       | 18.86                                       | 15.62                                       | 38.34                                       | 4.6  | 0.2                 | <0.01  | 2.3                 | <0.01   | <0.01               | 89.2                              | 2.4                 |
| SIbc@20      | 18.86                                       | 15.62                                       | 38.34                                       | 31.4   | 1.4                 | <0.01  | 21.7                | <0.01   | <0.01               | 89.1                              | 3.2                 |
| SIbc_s2@20   | 18.86                                       | 15.62                                       | 38.34                                       | 34.4   | 1.2                 | 18.2   | 8.2                 | <0.01   | <0.01               | 96.3                              | 1.2                 |
| SIbc@15      | 18.86                                       | 15.62                                       | 38.34                                       | 248.1  | 23.2                | 250.5  | 19.8                | 273.5   | 209.9               | 98.2                              | 0.5                 |
| SIbc@17      | 18.86                                       | 15.62                                       | 38.34                                       | 319.8  | 10.2                | 308.5  | 31.8                | 223.9   | 250.7               | 95.0                              | 0.6                 |
| SIbc@6a      | 18.86                                       | 15.62                                       | 38.34                                       | 331.9  | 10.8                | 324.0  | 9.3                 | 267.6   | 35.9                | 99.7                              | 0.1                 |
| SIbc@7       | 18.86                                       | 15.62                                       | 38.34                                       | 336.4  | 12.0                | 320.5  | 16.3                | 206.1   | 97.4                | 99.4                              | 0.2                 |
| SIbc@1       | 18.86                                       | 15.62                                       | 38.34                                       | 337.9  | 11.4                | 331.7  | 9.1                 | 288.5   | 26.0                | 99.9                              | <0.1                |
| SIbc@9       | 18.86                                       | 15.62                                       | 38.34                                       | 385.3  | 11.8                | 434.8  | 12.8                | 706.0   | 47.5                | 98.8                              | 0.2                 |
| SIsc@7b      | 18.86                                       | 15.62                                       | 38.34                                       | 467.8  | 12.1                | 459.0  | 11.4                | 414.7   | 40.3                | 99.7                              | 0.1                 |
| SIbc@12      | 18.86                                       | 15.62                                       | 38.34                                       | 472.8  | 15.9                | 463.4  | 15.1                | 416.7   | 61.8                | 99.6                              | 0.2                 |
| SIsc@7a      | 18.86                                       | 15.62                                       | 38.34                                       | 487.3  | 13.2                | 502.8  | 17.8                | 574.3   | 59.5                | 99.1                              | 0.1                 |
| SIbc@4       | 18.86                                       | 15.62                                       | 38.34                                       | 498.5  | 15.9                | 496.6  | 16.2                | 487.6   | 40.6                | 99.9                              | <0.1                |
| SIbc@11      | 18.86                                       | 15.62                                       | 38.34                                       | 555.3  | 15.5                | 537.7  | 14.0                | 463.5   | 36.4                | 100.0                             | <0.1                |
| SIbc@14      | 18.86                                       | 15.62                                       | 38.34                                       | 578.0  | 16.3                | 547.3  | 15.5                | 421.5   | 40.3                | 99.1                              | 0.1                 |
| SIbc@24      | 18.86                                       | 15.62                                       | 38.34                                       | 585.1  | 16.3                | 584.0  | 17.1                | 580.1   | 52.0                | 99.7                              | 0.1                 |
| SIbc@19      | 18.86                                       | 15.62                                       | 38.34                                       | 588.1  | 21.9                | 580.2  | 21.4                | 549.6   | 50.3                | 99.8                              | 0.1                 |
| SIbc@25      | 18.86                                       | 15.62                                       | 38.34                                       | 591.7  | 17.3                | 587.1  | 15.4                | 569.4   | 36.4                | 99.7                              | 0.1                 |
| SIbc@26      | 18.86                                       | 15.62                                       | 38.34                                       | 619.1  | 19.3                | 580.5  | 22.5                | 432.0   | 74.1                | 99.5                              | 0.2                 |
| SIbc@18      | 18.86                                       | 15.62                                       | 38.34                                       | 626.4  | 17.9                | 604.5  | 15.6                | 523.1   | 37.8                | 99.8                              | 0.1                 |
| SIbc@22      | 18.86                                       | 15.62                                       | 38.34                                       | 641.0  | 18.0                | 625.3  | 21.8                | 568.7   | 72.7                | 99.7                              | 0.2                 |
| SIbc@3       | 18.86                                       | 15.62                                       | 38.34                                       | 665.6  | 23.3                | 663.4  | 19.3                | 656.1   | 32.5                | 99.8                              | 0.1                 |

Table 6.5 Continued

| Sample Name:            | Grain #    | UO <sub>2</sub> /U | 1σ error | Th/U | 1σ error | <sup>206</sup> Pb/ <sup>238</sup> U | 1σ error | <sup>207</sup> Pb/ <sup>235</sup> U | 1σ error |
|-------------------------|------------|--------------------|----------|------|----------|-------------------------------------|----------|-------------------------------------|----------|
| SIbc@23 <sup>a</sup>    | SION_G2_2  | 1.44               | 0.02     | 0.15 | 0.002    | 0.31                                | 0.009    | 4.40                                | 0.132    |
| SIbc@8 <sup>a</sup>     | SION_G2_21 | 1.44               | 0.02     | 0.54 | 0.017    | 0.32                                | 0.009    | 4.62                                | 0.154    |
| SIbc_s2@21 <sup>a</sup> | SION_G2_23 | 1.44               | 0.03     | 0.14 | 0.003    | 0.30                                | 0.012    | 4.32                                | 0.165    |
| SIbc@2                  | SION_G2_21 | 1.44               | 0.02     | 0.14 | 0.003    | 0.12                                | 0.004    | 2.00                                | 0.061    |
| SIS1_z3@1 <sup>a</sup>  | SION_G2_8  | 1.44               | 0.02     | 0.21 | 0.004    | 0.36                                | 0.011    | 6.39                                | 0.194    |
| SIbc@16                 | SION_G2_16 | 1.44               | 0.02     | 0.15 | 0.001    | 0.20                                | 0.007    | 4.25                                | 0.147    |
| SIS1_z5@1 <sup>1</sup>  | SION_S1_4  | 1.44               | 0.02     | 0.43 | 0.006    | 0.36                                | 0.012    | 7.87                                | 0.257    |
| SIS1_z6@1 <sup>1</sup>  | SION_S1_5  | 1.44               | 0.02     | 0.47 | 0.013    | 0.37                                | 0.010    | 8.16                                | 0.258    |
| SIbc@21                 | SION_S2_1  | 1.44               | 0.03     | 0.49 | 0.016    | 0.29                                | 0.014    | 6.81                                | 0.340    |
| SIS1_z4@1               | SION_S1_6  | 1.44               | 0.03     | 3.05 | 0.039    | 0.35                                | 0.012    | 8.60                                | 0.290    |
| SIS2_z1@1               | SION_S1_3  | 1.44               | 0.01     | 0.79 | 0.014    | 0.34                                | 0.010    | 8.40                                | 0.215    |
| SIS1_z2@1               | SION_S1_2  | 1.44               | 0.01     | 0.37 | 0.009    | 0.42                                | 0.011    | 10.49                               | 0.270    |
| SIS2_z3@1               | SION_S2_3  | 1.44               | 0.02     | 0.22 | 0.003    | 0.48                                | 0.017    | 11.83                               | 0.426    |
| SIsc@2                  | SION_G1_3  | 1.44               | 0.02     | 0.41 | 0.009    | 0.54                                | 0.019    | 13.54                               | 0.516    |
| SIS2_z1@2               | SION_S2_1  | 1.44               | 0.02     | 0.18 | 0.006    | 0.45                                | 0.014    | 11.34                               | 0.327    |
| SIS2_z4@1               | SION_S2_4  | 1.44               | 0.02     | 0.16 | 0.003    | 0.45                                | 0.014    | 11.37                               | 0.368    |
| SIS2_z2@1               | SION_S2_2  | 1.44               | 0.02     | 0.75 | 0.011    | 0.50                                | 0.014    | 12.60                               | 0.380    |
| SIsc@5                  | SION_G1_5  | 1.44               | 0.01     | 0.31 | 0.006    | 0.51                                | 0.015    | 13.00                               | 0.390    |
| SIbc@10                 | SION_G2_10 | 1.44               | 0.02     | 0.36 | 0.005    | 0.40                                | 0.015    | 10.16                               | 0.336    |
| SIsc@6                  | SION_G1_6  | 1.44               | 0.01     | 0.27 | 0.002    | 0.52                                | 0.020    | 13.22                               | 0.480    |
| SIsc@3                  | SION_G1_2  | 1.44               | 0.01     | 0.38 | 0.006    | 0.53                                | 0.015    | 13.57                               | 0.438    |
| SIS1_z1@1               | SION_S1_1  | 1.44               | 0.02     | 0.43 | 0.019    | 0.45                                | 0.014    | 11.59                               | 0.338    |
| SIbc@5                  | SION_G2_5  | 1.44               | 0.02     | 0.25 | 0.004    | 0.54                                | 0.018    | 13.85                               | 0.439    |
| SIsc@1                  | SION_G1_1  | 1.44               | 0.02     | 0.32 | 0.006    | 0.53                                | 0.018    | 13.55                               | 0.464    |

Table 6.5 Continued

| Sample Name:            | Common $^{206}\text{Pb}/^{204}\text{Pb}$ | Common $^{207}\text{Pb}/^{204}\text{Pb}$ | Common $^{208}\text{Pb}/^{204}\text{Pb}$ | $^{206}\text{Pb}/^{238}\text{U}$ Age (Ma) | 1 $\sigma$ error | $^{207}\text{Pb}/^{235}\text{U}$ Age (Ma) | 1 $\sigma$ error | $^{207}\text{Pb}/^{206}\text{Pb}$ Age (Ma) | 1 $\sigma$ error | % Radiogenic $^{206}\text{Pb}$ | 1 $\sigma$ error |
|-------------------------|--|--|--|---|------------------|---|------------------|--|------------------|--------------------------------|------------------|
| SIbc@23 <sup>a</sup>    | 18.86                                    | 15.62                                    | 38.34                                    | 1729                                      | 42               | 1712                                      | 25               | 1692                                       | 26               | 99.9                           | <0.1             |
| SIbc@8 <sup>a</sup>     | 18.86                                    | 15.62                                    | 38.34                                    | 1798                                      | 46               | 1752                                      | 28               | 1699                                       | 33               | 99.6                           | 0.2              |
| SIbc_s2@21 <sup>a</sup> | 18.86                                    | 15.62                                    | 38.34                                    | 1693                                      | 60               | 1697                                      | 31               | 1703                                       | 28               | 99.2                           | 0.1              |
| SIbc@2                  | 18.86                                    | 15.62                                    | 38.34                                    | 745.2                                     | 21.2             | 1114                                      | 21               | 1928                                       | 18               | 98.6                           | 0.1              |
| SIS1_z3@1 <sup>a</sup>  | 18.86                                    | 15.62                                    | 38.34                                    | 2005                                      | 53               | 2031                                      | 27               | 2058                                       | 13               | 99.9                           | <0.1             |
| SIbc@16                 | 18.86                                    | 15.62                                    | 38.34                                    | 1171                                      | 37               | 1683                                      | 28               | 2398                                       | 13               | 99.9                           | <0.1             |
| SIS1_z5@1 <sup>a</sup>  | 18.86                                    | 15.62                                    | 38.34                                    | 1995                                      | 56               | 2217                                      | 29               | 2428                                       | 12               | 99.4                           | <0.1             |
| SIS1_z6@1 <sup>a</sup>  | 18.86                                    | 15.62                                    | 38.34                                    | 2019                                      | 49               | 2249                                      | 29               | 2465                                       | 15               | 99.5                           | <0.1             |
| SIbc@21                 | 18.86                                    | 15.62                                    | 38.34                                    | 1653                                      | 71               | 2087                                      | 44               | 2547                                       | 11               | 98.9                           | 0.1              |
| SIS1_z4@1               | 18.86                                    | 15.62                                    | 38.34                                    | 1938                                      | 56               | 2297                                      | 31               | 2633                                       | 13               | 99.2                           | 0.1              |
| SIS2_z1@1               | 18.86                                    | 15.62                                    | 38.34                                    | 1887                                      | 46               | 2275                                      | 23               | 2645                                       | 13               | 99.5                           | 0.1              |
| SIS1_z2@1               | 18.86                                    | 15.62                                    | 38.34                                    | 2275                                      | 51               | 2479                                      | 24               | 2650                                       | 11               | 99.8                           | <0.1             |
| SIS2_z3@1               | 18.86                                    | 15.62                                    | 38.34                                    | 2507                                      | 72               | 2591                                      | 34               | 2657                                       | 15               | 99.6                           | 0.1              |
| SIsc@2                  | 18.86                                    | 15.62                                    | 38.34                                    | 2770                                      | 79               | 2718                                      | 36               | 2680                                       | 14               | 99.8                           | 0.1              |
| SIS2_z1@2               | 18.86                                    | 15.62                                    | 38.34                                    | 2391                                      | 62               | 2552                                      | 27               | 2682                                       | 19               | 99.9                           | <0.1             |
| SIS2_z4@1               | 18.86                                    | 15.62                                    | 38.34                                    | 2391                                      | 63               | 2554                                      | 30               | 2685                                       | 10               | 99.7                           | <0.1             |
| SIS2_z2@1               | 18.86                                    | 15.62                                    | 38.34                                    | 2603                                      | 62               | 2650                                      | 28               | 2686                                       | 14               | 99.6                           | <0.1             |
| SIsc@5                  | 18.86                                    | 15.62                                    | 38.34                                    | 2669                                      | 63               | 2679                                      | 28               | 2687                                       | 15               | 99.3                           | 0.1              |
| SIbc@10                 | 18.86                                    | 15.62                                    | 38.34                                    | 2172                                      | 69               | 2449                                      | 31               | 2688                                       | 24               | 99.8                           | <0.1             |
| SIsc@6                  | 18.86                                    | 15.62                                    | 38.34                                    | 2695                                      | 86               | 2696                                      | 34               | 2696                                       | 15               | 99.9                           | <0.1             |
| SIsc@3                  | 18.86                                    | 15.62                                    | 38.34                                    | 2751                                      | 65               | 2720                                      | 30               | 2697                                       | 17               | 99.9                           | <0.1             |
| SIS1_z1@1               | 18.86                                    | 15.62                                    | 38.34                                    | 2412                                      | 61               | 2572                                      | 27               | 2701                                       | 8                | 99.9                           | <0.1             |
| SIbc@5                  | 18.86                                    | 15.62                                    | 38.34                                    | 2793                                      | 74               | 2740                                      | 30               | 2701                                       | 9                | 99.9                           | <0.1             |
| SIsc@1                  | 18.86                                    | 15.62                                    | 38.34                                    | 2730                                      | 78               | 2718                                      | 32               | 2710                                       | 21               | 99.7                           | 0.1              |

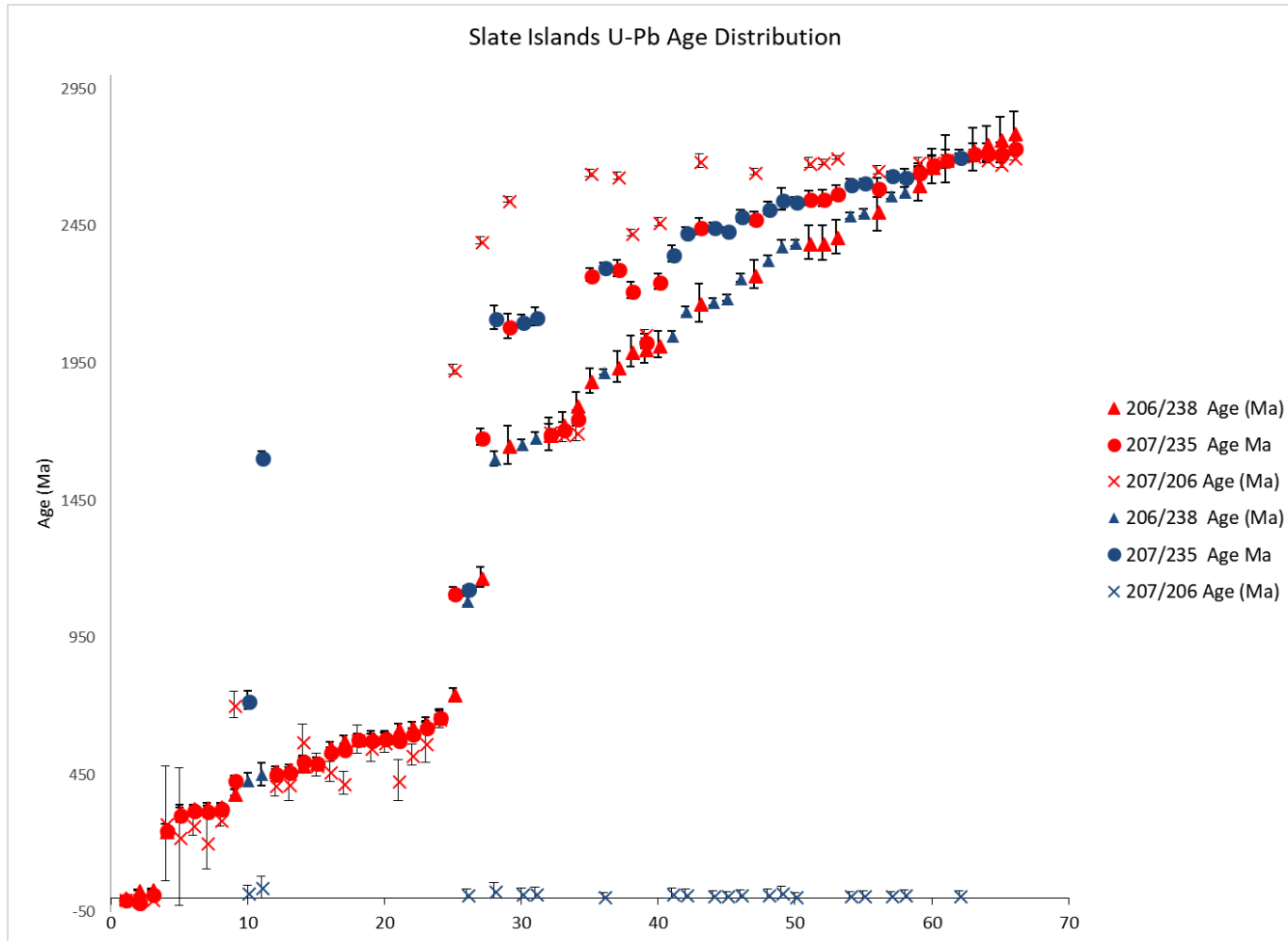


Figure 6.5 Age distribution plot of all measurements from Slate Islands zircons. Red data points indicate zircons analyzed via SIMS, blue data points indicate zircons analyzed via LA-ICP-MS. Error bars designate  $2\sigma$ .

## 6.5 Data from $^{40}\text{Ar}/^{39}\text{Ar}$ analysis via step heating performed at Oregon State University

Table 6.6: Data from step heating analysis of Sample S4 9022' from the Ames Astrobleme.

| Laser Output | $^{36}\text{Ar}$<br>[fA] | % 1s  | $^{37}\text{Ar}$<br>[fA] | % 1s    | $^{38}\text{Ar}$<br>[fA] | % 1s   | $^{39}\text{Ar}$<br>[fA] | % 1s  | $^{40}\text{Ar}$<br>[fA] | % 1s  | 40(r)/39(k) | $\pm 2s$      | Age<br>(Ma) | $\pm 2s$    |
|--------------|--------------------------|-------|--------------------------|---------|--------------------------|--------|--------------------------|-------|--------------------------|-------|-------------|---------------|-------------|-------------|
| 0.2 %        | 0.072537                 | 1.471 | 0.118234                 | 208.037 | 0.010735                 | 88.224 | 0.4059                   | 3.365 | 56.98                    | 0.515 | 87.53876    | $\pm 6.26179$ | 239.86      | $\pm 16.07$ |
| 0.4 %        | 1.381841                 | 0.299 | 0.867974                 | 26.324  | 0.969684                 | 0.999  | 56.6646                  | 0.070 | 5111.44                  | 0.006 | 83.00042    | $\pm 0.12504$ | 228.18      | $\pm 0.32$  |
| 0.5 %        | 0.750971                 | 0.337 | 0.522967                 | 43.310  | 0.550264                 | 1.759  | 32.9817                  | 0.079 | 3524.46                  | 0.009 | 100.13432   | $\pm 0.16627$ | 271.90      | $\pm 0.42$  |
| 0.6 %        | 0.404608                 | 0.427 | 0.624653                 | 38.347  | 0.341628                 | 2.947  | 21.0220                  | 0.094 | 2272.56                  | 0.013 | 102.42038   | $\pm 0.19991$ | 277.65      | $\pm 0.50$  |
| 0.7 %        | 0.570598                 | 0.379 | 0.877491                 | 27.633  | 0.521405                 | 1.902  | 32.9502                  | 0.079 | 3789.09                  | 0.008 | 109.88071   | $\pm 0.17844$ | 296.30      | $\pm 0.44$  |
| 0.8 %        | 0.178058                 | 0.724 | 0.750321                 | 30.086  | 0.147234                 | 6.296  | 9.1464                   | 0.167 | 1025.03                  | 0.029 | 106.32784   | $\pm 0.37036$ | 287.44      | $\pm 0.93$  |
| 0.9 %        | 0.165365                 | 0.733 | 0.272356                 | 88.599  | 0.145696                 | 7.284  | 9.3632                   | 0.163 | 1071.96                  | 0.028 | 109.27185   | $\pm 0.37006$ | 294.79      | $\pm 0.92$  |
| 1.0 %        | 0.144295                 | 0.802 | 0.061336                 | 377.022 | 0.141667                 | 6.835  | 8.5171                   | 0.170 | 971.23                   | 0.030 | 109.02793   | $\pm 0.38570$ | 294.18      | $\pm 0.96$  |
| 1.2 %        | 0.151725                 | 0.782 | 0.206611                 | 116.402 | 0.136153                 | 7.292  | 9.0497                   | 0.165 | 1044.61                  | 0.028 | 110.47881   | $\pm 0.37811$ | 297.79      | $\pm 0.94$  |
| 1.4 %        | 0.598830                 | 0.359 | 0.348253                 | 70.078  | 0.324185                 | 3.083  | 16.5708                  | 0.110 | 2085.91                  | 0.014 | 115.20257   | $\pm 0.26656$ | 309.49      | $\pm 0.66$  |
| 1.6 %        | 0.509379                 | 0.393 | 0.439626                 | 54.181  | 0.302238                 | 3.064  | 15.8926                  | 0.113 | 1994.62                  | 0.015 | 116.03921   | $\pm 0.27531$ | 311.55      | $\pm 0.68$  |
| 1.8 %        | 0.692789                 | 0.333 | 0.461310                 | 49.156  | 0.523056                 | 1.864  | 30.1174                  | 0.081 | 3782.57                  | 0.008 | 118.79851   | $\pm 0.19966$ | 318.35      | $\pm 0.49$  |
| 2.0 %        | 0.218446                 | 0.606 | 0.126748                 | 190.623 | 0.175346                 | 5.481  | 10.6258                  | 0.149 | 1306.93                  | 0.023 | 116.91875   | $\pm 0.36009$ | 313.72      | $\pm 0.89$  |
| 2.3 %        | 0.264188                 | 0.543 | 0.151300                 | 154.631 | 0.252126                 | 3.598  | 15.0327                  | 0.112 | 1865.63                  | 0.016 | 118.91263   | $\pm 0.27575$ | 318.63      | $\pm 0.68$  |
| 2.6 %        | 0.354303                 | 0.463 | 0.505079                 | 47.224  | 0.274438                 | 3.469  | 16.6822                  | 0.109 | 2093.72                  | 0.014 | 119.23420   | $\pm 0.26894$ | 319.42      | $\pm 0.66$  |
| 2.9 %        | 0.571683                 | 0.366 | 0.288944                 | 86.449  | 0.450348                 | 2.151  | 26.6826                  | 0.085 | 3363.25                  | 0.009 | 119.71657   | $\pm 0.20936$ | 320.60      | $\pm 0.51$  |
| 3.3 %        | 0.543453                 | 0.367 | 0.173986                 | 131.426 | 0.388988                 | 2.536  | 22.2897                  | 0.090 | 2821.74                  | 0.011 | 119.38961   | $\pm 0.22212$ | 319.80      | $\pm 0.55$  |
| 3.8 %        | 1.521674                 | 0.298 | 0.703592                 | 34.907  | 1.068317                 | 0.878  | 59.5382                  | 0.069 | 7418.22                  | 0.004 | 117.04487   | $\pm 0.16820$ | 314.03      | $\pm 0.41$  |
| 4.2 %        | 1.580397                 | 0.288 | 0.599378                 | 37.672  | 1.300953                 | 0.752  | 76.1310                  | 0.068 | 9410.09                  | 0.004 | 117.47039   | $\pm 0.16287$ | 315.08      | $\pm 0.40$  |
| 4.6 %        | 2.494610                 | 0.278 | 0.635933                 | 37.532  | 1.946280                 | 0.531  | 111.8892                 | 0.066 | 14006.25                 | 0.003 | 118.59179   | $\pm 0.16041$ | 317.84      | $\pm 0.39$  |
| 5.0 %        | 2.486399                 | 0.280 | 0.935112                 | 26.023  | 2.100580                 | 0.457  | 124.2168                 | 0.065 | 15333.81                 | 0.003 | 117.52968   | $\pm 0.15681$ | 315.23      | $\pm 0.39$  |
| 5.3 %        | 1.908620                 | 0.289 | 0.829882                 | 28.833  | 1.687593                 | 0.601  | 99.0916                  | 0.066 | 12070.95                 | 0.003 | 116.12512   | $\pm 0.15808$ | 311.77      | $\pm 0.39$  |
| 5.6 %        | 2.703088                 | 0.278 | 1.299277                 | 19.320  | 2.414901                 | 0.419  | 142.6312                 | 0.065 | 17403.20                 | 0.002 | 116.41614   | $\pm 0.15453$ | 312.48      | $\pm 0.38$  |
| 5.9 %        | 2.993777                 | 0.275 | 1.676551                 | 13.761  | 2.666376                 | 0.399  | 157.1840                 | 0.065 | 19177.63                 | 0.002 | 116.38047   | $\pm 0.15567$ | 312.40      | $\pm 0.38$  |
| 6.2 %        | 3.063785                 | 0.272 | 1.677917                 | 14.232  | 2.834407                 | 0.373  | 168.2208                 | 0.065 | 20298.39                 | 0.002 | 115.28432   | $\pm 0.15188$ | 309.69      | $\pm 0.37$  |
| 6.5 %        | 3.401016                 | 0.272 | 2.262739                 | 10.719  | 3.429887                 | 0.314  | 209.6373                 | 0.065 | 25503.37                 | 0.002 | 116.86188   | $\pm 0.15311$ | 313.58      | $\pm 0.38$  |
| 6.8 %        | 2.385446                 | 0.279 | 1.430953                 | 16.885  | 2.272050                 | 0.444  | 136.4878                 | 0.065 | 16624.02                 | 0.003 | 116.63516   | $\pm 0.15554$ | 313.02      | $\pm 0.38$  |

Table 6.6 Continued

|        |          |       |          |          |          |        |          |       |          |       |           |          |        |        |
|--------|----------|-------|----------|----------|----------|--------|----------|-------|----------|-------|-----------|----------|--------|--------|
| 7.1 %  | 5.327967 | 0.266 | 3.155965 | 7.483    | 4.965070 | 0.244  | 295.0787 | 0.064 | 35930.58 | 0.002 | 116.43166 | ±0.15202 | 312.52 | ±0.37  |
| 7.5 %  | 2.917403 | 0.273 | 1.746838 | 13.157   | 2.850219 | 0.372  | 170.8446 | 0.065 | 21086.01 | 0.002 | 118.37715 | ±0.15539 | 317.31 | ±0.38  |
| 8.0 %  | 1.069942 | 0.310 | 0.850515 | 29.341   | 1.068658 | 0.947  | 64.4823  | 0.070 | 7957.95  | 0.004 | 118.51125 | ±0.16785 | 317.64 | ±0.41  |
| 8.5 %  | 0.849490 | 0.319 | 0.510387 | 46.373   | 0.851235 | 1.065  | 52.3132  | 0.071 | 6448.68  | 0.005 | 118.47315 | ±0.17151 | 317.55 | ±0.42  |
| 9.0 %  | 0.030463 | 3.306 | 0.102267 | 230.083  | 0.027567 | 35.768 | 1.7576   | 0.758 | 219.69   | 0.134 | 119.87846 | ±1.87793 | 321.00 | ±4.61  |
| 9.5 %  | 0.237020 | 0.589 | 0.096006 | 238.090  | 0.252285 | 3.979  | 15.1486  | 0.115 | 1922.01  | 0.016 | 122.25449 | ±0.28898 | 326.82 | ±0.71  |
| 10.0 % | 0.124574 | 0.921 | 0.023305 | 1047.671 | 0.107813 | 8.668  | 6.8031   | 0.206 | 847.14   | 0.035 | 119.10987 | ±0.50826 | 319.11 | ±1.25  |
| 10.5 % | 0.018028 | 5.484 | 0.029778 | 821.495  | 0.010162 | 96.678 | 0.7847   | 1.666 | 102.34   | 0.287 | 123.62023 | ±4.25167 | 330.16 | ±10.38 |
| 11.3 % | 0.034060 | 2.946 | 0.104634 | 243.270  | 0.025615 | 37.440 | 1.8006   | 0.766 | 223.15   | 0.132 | 118.33015 | ±1.87104 | 317.20 | ±4.60  |
| 12.1 % | 0.069624 | 1.488 | 0.254308 | 97.361   | 0.062258 | 15.302 | 3.8637   | 0.361 | 479.14   | 0.061 | 118.69681 | ±0.88556 | 318.10 | ±2.18  |

Table 6.7: Data from step heating analysis of Sample S5 9026' from the Ames Astrobleme.

| Laser Output | <sup>36</sup> Ar [fA] | % 1s  | <sup>37</sup> Ar [fA] | % 1s     | <sup>38</sup> Ar [fA] | % 1s   | <sup>39</sup> Ar [fA] | % 1s  | <sup>40</sup> Ar [fA] | % 1s  | 40(r)/39(k) | ±2s      | Age (Ma) | ±2s   |
|--------------|-----------------------|-------|-----------------------|----------|-----------------------|--------|-----------------------|-------|-----------------------|-------|-------------|----------|----------|-------|
| 0.2 %        | 0.010518              | 6.312 | 0.0272423             | 878.406  | 0.015744              | 58.853 | 0.65335               | 1.790 | 42.602                | 0.314 | 60.44313    | ±2.28319 | 168.88   | ±6.09 |
| 0.4 %        | 0.702728              | 0.338 | 1.2359936             | 19.870   | 2.373303              | 0.442  | 180.76475             | 0.064 | 14987.794             | 0.002 | 81.76481    | ±0.10576 | 224.88   | ±0.27 |
| 0.5 %        | 0.102774              | 0.833 | 0.0435693             | 550.889  | 0.155282              | 6.071  | 9.91399               | 0.128 | 904.146               | 0.016 | 88.13573    | ±0.23284 | 241.29   | ±0.60 |
| 0.6 %        | 0.137940              | 0.625 | 0.4421702             | 54.046   | 0.235396              | 4.222  | 17.17917              | 0.090 | 1588.886              | 0.009 | 90.11936    | ±0.16521 | 246.36   | ±0.42 |
| 0.7 %        | 0.097317              | 0.873 | 0.2759657             | 91.939   | 0.165647              | 5.799  | 12.11621              | 0.111 | 1074.427              | 0.013 | 86.30585    | ±0.19811 | 236.59   | ±0.51 |
| 0.8 %        | 0.093725              | 0.846 | 0.0691837             | 358.491  | 0.157401              | 5.969  | 11.07298              | 0.124 | 1027.215              | 0.014 | 90.26688    | ±0.22851 | 246.74   | ±0.58 |
| 0.9 %        | 0.198839              | 0.531 | 0.2028990             | 118.378  | 0.434037              | 2.195  | 31.71934              | 0.076 | 3053.288              | 0.005 | 94.40745    | ±0.14475 | 257.29   | ±0.37 |
| 1.0 %        | 0.092117              | 0.898 | 0.1619539             | 152.071  | 0.152359              | 6.529  | 10.71721              | 0.128 | 1040.824              | 0.014 | 94.57878    | ±0.24749 | 257.72   | ±0.63 |
| 1.2 %        | 0.164034              | 0.598 | 0.2652485             | 86.817   | 0.305922              | 3.112  | 21.96939              | 0.083 | 2191.814              | 0.007 | 97.56149    | ±0.16512 | 265.28   | ±0.42 |
| 1.4 %        | 0.161287              | 0.600 | 0.5272018             | 44.114   | 0.286001              | 3.214  | 20.87947              | 0.085 | 2073.526              | 0.007 | 97.02968    | ±0.16859 | 263.94   | ±0.43 |
| 1.6 %        | 0.087686              | 0.896 | 0.1072402             | 218.049  | 0.137647              | 6.820  | 9.43227               | 0.141 | 941.307               | 0.015 | 97.05038    | ±0.27911 | 263.99   | ±0.71 |
| 1.8 %        | 0.072988              | 1.016 | 0.0118721             | 2068.358 | 0.107211              | 8.486  | 7.84544               | 0.163 | 779.460               | 0.018 | 96.60205    | ±0.32265 | 262.86   | ±0.82 |
| 2.0 %        | 0.128463              | 0.697 | 0.0658105             | 361.230  | 0.200013              | 4.819  | 13.83152              | 0.109 | 1410.226              | 0.010 | 99.21306    | ±0.22084 | 269.46   | ±0.56 |
| 2.3 %        | 0.080197              | 0.951 | 0.2152327             | 114.790  | 0.123330              | 7.594  | 8.46246               | 0.153 | 852.972               | 0.016 | 97.99740    | ±0.30693 | 266.39   | ±0.78 |
| 2.6 %        | 0.095158              | 0.869 | 0.1955704             | 121.792  | 0.135488              | 7.028  | 10.04365              | 0.130 | 1021.792              | 0.014 | 98.93199    | ±0.26279 | 268.75   | ±0.66 |
| 2.9 %        | 0.330039              | 0.400 | 0.2893697             | 81.289   | 0.412114              | 2.341  | 27.11492              | 0.080 | 2795.837              | 0.006 | 99.51485    | ±0.16202 | 270.22   | ±0.41 |
| 3.3 %        | 0.130365              | 0.688 | 0.1901955             | 122.380  | 0.164597              | 5.645  | 10.74450              | 0.120 | 1101.284              | 0.013 | 98.90904    | ±0.24427 | 268.69   | ±0.62 |
| 3.8 %        | 0.142473              | 0.633 | 0.0396260             | 577.452  | 0.182246              | 5.195  | 12.44539              | 0.114 | 1284.484              | 0.011 | 99.82575    | ±0.23204 | 271.00   | ±0.58 |
| 4.2 %        | 0.237333              | 0.462 | 0.0377744             | 589.743  | 0.275882              | 3.406  | 17.84958              | 0.090 | 1800.229              | 0.008 | 96.92567    | ±0.17972 | 263.68   | ±0.45 |
| 4.6 %        | 0.860485              | 0.313 | 0.0370666             | 675.604  | 0.773111              | 1.235  | 44.53341              | 0.070 | 4527.218              | 0.004 | 95.94858    | ±0.13977 | 261.20   | ±0.35 |
| 5.0 %        | 0.729461              | 0.328 | 0.1154212             | 213.083  | 0.673549              | 1.457  | 39.31464              | 0.072 | 3971.305              | 0.004 | 95.53048    | ±0.14205 | 260.14   | ±0.36 |
| 5.3 %        | 0.877666              | 0.306 | 0.1912767             | 122.568  | 0.767804              | 1.267  | 44.64971              | 0.070 | 4455.346              | 0.004 | 93.97599    | ±0.13699 | 256.19   | ±0.35 |
| 5.6 %        | 0.319699              | 0.414 | 0.0693844             | 344.653  | 0.275007              | 3.721  | 16.23097              | 0.097 | 1563.598              | 0.009 | 90.51270    | ±0.18236 | 247.37   | ±0.47 |
| 5.9 %        | 0.503069              | 0.365 | 0.1154477             | 198.643  | 0.473508              | 2.041  | 27.39132              | 0.080 | 2691.843              | 0.006 | 92.84655    | ±0.15418 | 253.32   | ±0.39 |
| 6.2 %        | 0.521581              | 0.362 | 0.0215396             | 1119.433 | 0.446918              | 2.057  | 24.79077              | 0.080 | 2392.055              | 0.007 | 90.27228    | ±0.15180 | 246.75   | ±0.39 |
| 6.5 %        | 0.358692              | 0.402 | 0.1868216             | 130.006  | 0.310496              | 3.153  | 18.01220              | 0.090 | 1779.080              | 0.009 | 92.88435    | ±0.17520 | 253.42   | ±0.45 |
| 6.8 %        | 0.819972              | 0.327 | 0.3304313             | 73.864   | 0.756492              | 1.223  | 42.74356              | 0.071 | 4128.401              | 0.004 | 90.91721    | ±0.13391 | 248.40   | ±0.34 |
| 7.1 %        | 0.343640              | 0.406 | 0.2697050             | 88.910   | 0.286659              | 3.279  | 15.76183              | 0.100 | 1542.171              | 0.010 | 91.39680    | ±0.19177 | 249.63   | ±0.49 |
| 7.5 %        | 0.767906              | 0.325 | 0.2913558             | 82.541   | 0.769503              | 1.201  | 44.34321              | 0.070 | 4385.928              | 0.004 | 93.79186    | ±0.13519 | 255.73   | ±0.34 |

Table 6.7 Continued

|        |          |       |           |          |          |        |          |       |          |       |           |          |        |       |
|--------|----------|-------|-----------|----------|----------|--------|----------|-------|----------|-------|-----------|----------|--------|-------|
| 8.0 %  | 0.482612 | 0.357 | 0.1477623 | 156.145  | 0.454972 | 2.108  | 25.95031 | 0.079 | 2603.690 | 0.006 | 94.83845  | ±0.15485 | 258.38 | ±0.39 |
| 8.5 %  | 0.330947 | 0.421 | 0.1126982 | 206.205  | 0.308806 | 3.101  | 16.61357 | 0.098 | 1665.591 | 0.009 | 94.36705  | ±0.19201 | 257.19 | ±0.49 |
| 9.0 %  | 0.171204 | 0.584 | 0.0038873 | 6504.333 | 0.163059 | 6.276  | 9.06724  | 0.146 | 909.248  | 0.016 | 94.69837  | ±0.28558 | 258.03 | ±0.73 |
| 9.5 %  | 0.100453 | 0.798 | 0.0749776 | 304.897  | 0.104778 | 9.286  | 6.33927  | 0.189 | 638.769  | 0.022 | 96.07913  | ±0.37281 | 261.53 | ±0.94 |
| 10.0 % | 0.129030 | 0.694 | 0.2947937 | 78.282   | 0.145056 | 6.442  | 8.19234  | 0.151 | 837.279  | 0.017 | 97.55317  | ±0.30296 | 265.26 | ±0.77 |
| 10.5 % | 0.132460 | 0.728 | 0.1406812 | 159.674  | 0.120081 | 7.871  | 6.90329  | 0.164 | 709.420  | 0.019 | 97.09784  | ±0.33207 | 264.11 | ±0.84 |
| 11.0 % | 0.101829 | 0.818 | 0.1113227 | 209.927  | 0.106389 | 9.188  | 6.27145  | 0.182 | 676.109  | 0.020 | 103.01149 | ±0.38603 | 279.02 | ±0.97 |
| 11.5 % | 0.009927 | 6.272 | 0.0048672 | 5215.643 | 0.019502 | 51.450 | 0.58364  | 1.781 | 57.763   | 0.232 | 93.94659  | ±3.43639 | 256.12 | ±8.74 |
| 12.0 % | 0.050487 | 1.363 | 0.2224308 | 117.829  | 0.053113 | 17.854 | 2.69668  | 0.420 | 272.342  | 0.050 | 95.47078  | ±0.82226 | 259.99 | ±2.09 |
| 12.5 % | 0.029961 | 2.181 | 0.1710856 | 143.142  | 0.035677 | 26.053 | 1.57669  | 0.701 | 156.097  | 0.087 | 93.40263  | ±1.34429 | 254.74 | ±3.42 |
| 13.0 % | 0.010550 | 5.889 | 0.2150531 | 118.302  | 0.032743 | 28.658 | 0.96513  | 1.126 | 93.129   | 0.144 | 93.29531  | ±2.15441 | 254.46 | ±5.48 |

Table 6.8: Data from step heating analysis of Sample S6 9027' from the Ames Astrobleme.

| Laser Output | <sup>36</sup> Ar [fA] | % 1s  | <sup>37</sup> Ar [fA] | % 1s    | <sup>38</sup> Ar [fA] | % 1s  | <sup>39</sup> Ar [fA] | % 1s  | <sup>40</sup> Ar [fA] | % 1s  | 40(r)/39(k) | ±2s      | Age (Ma) | ±2s   |
|--------------|-----------------------|-------|-----------------------|---------|-----------------------|-------|-----------------------|-------|-----------------------|-------|-------------|----------|----------|-------|
| 0.4 %        | 4.840339              | 0.281 | 17.956092             | 3.250   | 7.643576              | 0.367 | 512.8796              | 0.064 | 38430.24              | 0.002 | 72.14541    | ±0.09320 | 199.75   | ±0.24 |
| 0.5 %        | 0.396856              | 0.527 | 2.812824              | 9.122   | 1.233281              | 0.862 | 96.5158               | 0.069 | 9932.62               | 0.002 | 101.70038   | ±0.14070 | 275.60   | ±0.35 |
| 0.6 %        | 0.207292              | 0.836 | 1.237017              | 19.068  | 0.618656              | 1.614 | 51.1522               | 0.080 | 5383.99               | 0.003 | 104.05970   | ±0.16878 | 281.52   | ±0.42 |
| 0.7 %        | 0.172085              | 0.968 | 0.398446              | 58.239  | 0.541763              | 1.876 | 44.8335               | 0.084 | 4776.97               | 0.003 | 105.41543   | ±0.17937 | 284.92   | ±0.45 |
| 0.8 %        | 0.098182              | 1.533 | 0.065752              | 349.413 | 0.277942              | 3.753 | 22.5872               | 0.126 | 2398.02               | 0.004 | 104.88263   | ±0.26770 | 283.58   | ±0.67 |
| 0.9 %        | 0.069223              | 2.177 | 0.185689              | 125.421 | 0.179823              | 5.711 | 14.8115               | 0.178 | 1566.96               | 0.006 | 104.41384   | ±0.37669 | 282.41   | ±0.94 |
| 1.0 %        | 0.073189              | 2.023 | 0.061676              | 380.622 | 0.208414              | 4.849 | 16.3515               | 0.163 | 1734.68               | 0.006 | 104.76287   | ±0.34578 | 283.28   | ±0.87 |
| 1.2 %        | 0.152104              | 1.064 | 0.612354              | 36.908  | 0.453507              | 2.204 | 34.9137               | 0.096 | 3773.27               | 0.003 | 106.78882   | ±0.20745 | 288.35   | ±0.52 |
| 1.4 %        | 0.148477              | 1.087 | 0.443655              | 49.869  | 0.467812              | 2.147 | 34.9492               | 0.096 | 3774.34               | 0.003 | 106.74082   | ±0.20587 | 288.23   | ±0.51 |
| 1.6 %        | 0.061558              | 2.369 | 0.070070              | 320.466 | 0.173757              | 6.032 | 12.0693               | 0.210 | 1278.44               | 0.007 | 104.41859   | ±0.44535 | 282.42   | ±1.12 |
| 1.8 %        | 0.059390              | 2.464 | 0.563472              | 39.128  | 0.175531              | 5.882 | 12.8574               | 0.199 | 1361.01               | 0.006 | 104.49552   | ±0.42246 | 282.61   | ±1.06 |
| 2.0 %        | 0.076217              | 1.966 | 0.024828              | 949.756 | 0.232297              | 4.392 | 16.9867               | 0.158 | 1814.04               | 0.005 | 105.46487   | ±0.33744 | 285.04   | ±0.84 |
| 2.3 %        | 0.075269              | 1.942 | 0.130423              | 171.949 | 0.240957              | 3.973 | 17.5174               | 0.154 | 1865.17               | 0.005 | 105.20606   | ±0.32865 | 284.39   | ±0.82 |
| 2.6 %        | 0.145877              | 1.069 | 0.451589              | 49.707  | 0.324117              | 3.078 | 23.0381               | 0.124 | 2475.61               | 0.004 | 105.58863   | ±0.26524 | 285.35   | ±0.66 |

Table 6.8 Continued

|        |          |        |          |          |          |         |          |       |          |       |           |          |        |       |
|--------|----------|--------|----------|----------|----------|---------|----------|-------|----------|-------|-----------|----------|--------|-------|
| 2.9 %  | 0.091895 | 1.618  | 0.384303 | 61.094   | 0.265601 | 3.579   | 19.7665  | 0.141 | 2111.98  | 0.005 | 105.47491 | ±0.30015 | 285.06 | ±0.75 |
| 3.3 %  | 0.167288 | 0.985  | 0.128868 | 171.627  | 0.361358 | 2.647   | 26.2599  | 0.114 | 2829.41  | 0.004 | 105.86395 | ±0.24337 | 286.04 | ±0.61 |
| 3.8 %  | 0.139385 | 1.121  | 0.115981 | 206.396  | 0.382509 | 2.772   | 27.9400  | 0.108 | 2986.10  | 0.004 | 105.40135 | ±0.23020 | 284.88 | ±0.58 |
| 4.2 %  | 0.216274 | 0.767  | 0.270568 | 84.055   | 0.504630 | 1.916   | 34.9751  | 0.095 | 3718.04  | 0.003 | 104.47871 | ±0.20109 | 282.57 | ±0.50 |
| 4.6 %  | 0.645020 | 0.387  | 0.849299 | 27.248   | 1.091741 | 1.007   | 78.4738  | 0.071 | 8272.07  | 0.002 | 102.98396 | ±0.14745 | 278.83 | ±0.37 |
| 5.0 %  | 0.334055 | 0.552  | 0.083911 | 279.483  | 0.604410 | 1.632   | 42.9060  | 0.086 | 4449.94  | 0.003 | 101.41268 | ±0.17684 | 274.88 | ±0.44 |
| 5.5 %  | 0.927701 | 0.337  | 0.402589 | 56.505   | 1.650340 | 0.641   | 114.8337 | 0.067 | 11764.50 | 0.002 | 100.06085 | ±0.13539 | 271.48 | ±0.34 |
| 6.0 %  | 0.864508 | 0.353  | 0.416625 | 56.642   | 1.442485 | 0.695   | 99.1485  | 0.069 | 10301.22 | 0.002 | 101.32034 | ±0.14102 | 274.65 | ±0.35 |
| 6.5 %  | 4.264146 | 0.269  | 2.248157 | 10.497   | 6.693846 | 0.197   | 457.6240 | 0.063 | 47424.58 | 0.001 | 100.87888 | ±0.12892 | 273.54 | ±0.32 |
| 6.8 %  | 0.996639 | 0.335  | 0.451349 | 48.345   | 1.429974 | 0.713   | 95.2965  | 0.069 | 9774.98  | 0.002 | 99.48419  | ±0.13877 | 270.02 | ±0.35 |
| 7.1 %  | 2.800362 | 0.274  | 1.577011 | 14.114   | 4.368172 | 0.274   | 296.2946 | 0.064 | 30551.00 | 0.002 | 100.31759 | ±0.12945 | 272.12 | ±0.33 |
| 7.3 %  | 0.749196 | 0.365  | 0.287474 | 83.038   | 1.114610 | 0.892   | 75.9590  | 0.072 | 7918.90  | 0.002 | 101.33776 | ±0.14771 | 274.69 | ±0.37 |
| 7.6 %  | 0.358288 | 0.544  | 0.010761 | 2112.643 | 0.572977 | 1.756   | 39.2100  | 0.090 | 4050.28  | 0.003 | 100.59635 | ±0.18412 | 272.82 | ±0.46 |
| 7.9 %  | 0.695746 | 0.387  | 0.419434 | 56.737   | 1.161902 | 0.876   | 80.2248  | 0.072 | 8251.92  | 0.002 | 100.29740 | ±0.14549 | 272.07 | ±0.37 |
| 8.2 %  | 0.327640 | 0.569  | 0.245746 | 94.653   | 0.562389 | 1.815   | 39.4500  | 0.090 | 4087.97  | 0.003 | 101.17041 | ±0.18485 | 274.27 | ±0.46 |
| 8.5 %  | 0.650444 | 0.395  | 0.304399 | 73.078   | 1.120384 | 0.942   | 77.2169  | 0.072 | 8039.08  | 0.002 | 101.62119 | ±0.14705 | 275.40 | ±0.37 |
| 9.0 %  | 0.569906 | 0.419  | 0.227049 | 102.473  | 0.884282 | 1.121   | 59.9435  | 0.076 | 6157.73  | 0.003 | 99.91625  | ±0.15402 | 271.11 | ±0.39 |
| 9.5 %  | 0.288621 | 0.631  | 0.155375 | 152.969  | 0.444883 | 2.363   | 30.1074  | 0.104 | 3149.82  | 0.004 | 101.78679 | ±0.21445 | 275.82 | ±0.54 |
| 10.0 % | 0.226252 | 0.744  | 0.203945 | 117.116  | 0.359788 | 2.849   | 24.7700  | 0.117 | 2615.94  | 0.004 | 102.91061 | ±0.24342 | 278.64 | ±0.61 |
| 10.5 % | 0.416118 | 0.487  | 0.337394 | 70.134   | 0.728613 | 1.384   | 50.0429  | 0.081 | 5409.33  | 0.003 | 105.63726 | ±0.17228 | 285.47 | ±0.43 |
| 11.0 % | 0.152402 | 1.027  | 0.094159 | 237.189  | 0.268874 | 3.794   | 18.5049  | 0.145 | 1970.92  | 0.005 | 104.07443 | ±0.30624 | 281.56 | ±0.77 |
| 11.5 % | 0.336682 | 0.544  | 0.207563 | 110.659  | 0.537962 | 1.805   | 36.9039  | 0.093 | 3951.84  | 0.003 | 104.38908 | ±0.19575 | 282.35 | ±0.49 |
| 12.0 % | 0.042640 | 3.388  | 0.046861 | 474.567  | 0.051189 | 19.325  | 2.7973   | 0.857 | 296.59   | 0.024 | 101.52300 | ±1.76744 | 275.16 | ±4.44 |
| 12.5 % | 0.039906 | 3.614  | 0.161432 | 143.356  | 0.047008 | 21.249  | 4.4221   | 0.545 | 458.91   | 0.016 | 101.10400 | ±1.12018 | 274.10 | ±2.82 |
| 13.0 % | 0.013611 | 10.286 | 0.197815 | 116.539  | 0.007624 | 129.497 | 1.4982   | 1.601 | 157.09   | 0.045 | 102.14916 | ±3.31857 | 276.73 | ±8.34 |

Table 6.9: Data from step heating analysis of Sample S7 9031' from the Ames Astrobleme.

| Laser Output | 36Ar [fA] | % 1s  | 37Ar [fA] | % 1s     | 38Ar [fA] | % 1s  | 39Ar [fA] | % 1s  | 40Ar [fA] | % 1s  | 40(r)/39(k) | ±2s      | Age (Ma) | ±2s   |
|--------------|-----------|-------|-----------|----------|-----------|-------|-----------|-------|-----------|-------|-------------|----------|----------|-------|
| 0.4 %        | 0.790222  | 0.328 | 0.841731  | 27.113   | 1.149156  | 0.918 | 79.6456   | 0.066 | 6270.89   | 0.008 | 75.80379    | ±0.10238 | 209.08   | ±0.27 |
| 0.5 %        | 0.261846  | 0.540 | 0.100669  | 224.139  | 0.292375  | 3.397 | 19.4814   | 0.086 | 1845.78   | 0.024 | 90.77426    | ±0.16753 | 247.66   | ±0.43 |
| 0.6 %        | 0.215975  | 0.571 | 0.122374  | 189.387  | 0.257476  | 3.741 | 16.5278   | 0.097 | 1596.23   | 0.028 | 92.71497    | ±0.19285 | 252.60   | ±0.49 |
| 0.7 %        | 0.197435  | 0.624 | 0.292946  | 79.983   | 0.257396  | 3.567 | 16.2538   | 0.096 | 1602.21   | 0.028 | 94.98693    | ±0.19513 | 258.37   | ±0.49 |
| 0.8 %        | 0.187725  | 0.638 | 0.177473  | 130.543  | 0.236025  | 4.140 | 15.4660   | 0.103 | 1544.35   | 0.029 | 96.26844    | ±0.21130 | 261.61   | ±0.53 |
| 0.9 %        | 0.173632  | 0.670 | 0.006262  | 3606.963 | 0.223750  | 4.267 | 14.3850   | 0.103 | 1467.96   | 0.030 | 98.48058    | ±0.21782 | 267.20   | ±0.55 |
| 1.0 %        | 0.153203  | 0.731 | 0.098113  | 213.671  | 0.197180  | 4.821 | 13.5749   | 0.103 | 1399.80   | 0.032 | 99.78029    | ±0.22129 | 270.47   | ±0.56 |
| 1.2 %        | 0.196814  | 0.609 | 0.061964  | 352.057  | 0.239294  | 3.920 | 16.4686   | 0.093 | 1728.18   | 0.026 | 101.40536   | ±0.20026 | 274.56   | ±0.50 |
| 1.4 %        | 0.225406  | 0.579 | 0.065774  | 318.135  | 0.236738  | 3.940 | 15.9171   | 0.097 | 1709.94   | 0.026 | 103.24348   | ±0.21428 | 279.17   | ±0.54 |
| 1.6 %        | 0.173486  | 0.651 | 0.014229  | 1538.179 | 0.214709  | 4.596 | 14.9715   | 0.100 | 1608.14   | 0.028 | 103.98849   | ±0.22100 | 281.04   | ±0.55 |
| 1.8 %        | 0.140860  | 0.790 | 0.005291  | 4542.800 | 0.151607  | 6.756 | 11.4501   | 0.117 | 1232.23   | 0.036 | 103.98154   | ±0.26096 | 281.02   | ±0.65 |
| 2.0 %        | 0.264310  | 0.538 | 0.108092  | 203.923  | 0.235372  | 3.927 | 15.2657   | 0.098 | 1682.32   | 0.026 | 105.08672   | ±0.22193 | 283.79   | ±0.55 |
| 2.3 %        | 0.167159  | 0.676 | 0.323783  | 73.328   | 0.166338  | 5.621 | 11.6827   | 0.118 | 1270.44   | 0.035 | 104.52119   | ±0.26494 | 282.37   | ±0.66 |
| 2.6 %        | 0.424774  | 0.392 | 0.173572  | 128.856  | 0.306969  | 3.163 | 18.5247   | 0.088 | 2074.24   | 0.021 | 105.19692   | ±0.19785 | 284.06   | ±0.49 |
| 2.9 %        | 0.293956  | 0.474 | 0.333723  | 68.425   | 0.243455  | 3.902 | 16.1785   | 0.097 | 1765.13   | 0.025 | 103.73625   | ±0.21394 | 280.41   | ±0.54 |
| 3.3 %        | 0.364507  | 0.432 | 0.278669  | 80.554   | 0.306347  | 3.139 | 18.8479   | 0.089 | 2025.19   | 0.022 | 101.73614   | ±0.19403 | 275.39   | ±0.49 |
| 3.8 %        | 0.947575  | 0.304 | 0.315036  | 69.423   | 0.682583  | 1.417 | 39.4000   | 0.071 | 4248.66   | 0.011 | 100.72787   | ±0.15059 | 272.86   | ±0.38 |
| 4.2 %        | 1.367448  | 0.286 | 0.414174  | 51.215   | 0.969911  | 1.024 | 55.5400   | 0.068 | 5880.12   | 0.008 | 98.59695    | ±0.14053 | 267.49   | ±0.35 |
| 4.6 %        | 2.284170  | 0.276 | 0.714173  | 33.648   | 1.835530  | 0.565 | 105.6748  | 0.065 | 10930.70  | 0.004 | 97.05036    | ±0.13112 | 263.59   | ±0.33 |
| 5.0 %        | 1.913707  | 0.283 | 0.508951  | 44.095   | 1.567916  | 0.651 | 91.8714   | 0.065 | 9576.05   | 0.005 | 98.07812    | ±0.13304 | 266.18   | ±0.34 |
| 5.5 %        | 2.344005  | 0.271 | 0.980430  | 22.617   | 1.962442  | 0.508 | 114.0354  | 0.064 | 12016.34  | 0.004 | 99.30049    | ±0.13164 | 269.27   | ±0.33 |
| 6.0 %        | 2.478824  | 0.275 | 0.974683  | 23.593   | 2.055596  | 0.496 | 117.8241  | 0.065 | 12258.06  | 0.004 | 97.82075    | ±0.13111 | 265.53   | ±0.33 |
| 6.5 %        | 2.681605  | 0.275 | 0.827147  | 27.353   | 2.378092  | 0.469 | 140.0218  | 0.064 | 14536.14  | 0.004 | 98.15454    | ±0.12934 | 266.38   | ±0.33 |
| 7.0 %        | 4.026771  | 0.266 | 1.307936  | 16.761   | 3.620666  | 0.296 | 211.5487  | 0.063 | 21835.30  | 0.003 | 97.59204    | ±0.12732 | 264.96   | ±0.32 |
| 7.7 %        | 4.352896  | 0.265 | 1.491156  | 15.664   | 3.909554  | 0.290 | 229.3144  | 0.063 | 23975.14  | 0.002 | 98.94255    | ±0.12849 | 268.36   | ±0.32 |
| 8.4 %        | 2.072212  | 0.274 | 0.784575  | 27.518   | 1.924513  | 0.502 | 113.1384  | 0.064 | 11968.07  | 0.002 | 100.37071   | ±0.13200 | 271.96   | ±0.33 |
| 8.9 %        | 1.373975  | 0.293 | 0.460758  | 50.330   | 1.207245  | 0.864 | 71.1994   | 0.066 | 7474.08   | 0.002 | 99.27186    | ±0.13515 | 269.19   | ±0.34 |
| 9.5 %        | 0.204661  | 0.482 | 0.023146  | 1024.658 | 0.151795  | 6.392 | 8.7619    | 0.143 | 933.59    | 0.006 | 99.64842    | ±0.29289 | 270.14   | ±0.74 |

Table 6.9 Continued

|        |          |       |          |         |          |        |         |       |         |       |           |          |        |       |
|--------|----------|-------|----------|---------|----------|--------|---------|-------|---------|-------|-----------|----------|--------|-------|
| 10.0 % | 0.237368 | 0.451 | 0.069923 | 308.725 | 0.193003 | 4.900  | 10.2268 | 0.122 | 1115.77 | 0.005 | 102.24459 | ±0.25767 | 276.67 | ±0.65 |
| 10.5 % | 0.064526 | 0.901 | 0.049321 | 457.097 | 0.050296 | 19.261 | 3.1183  | 0.341 | 344.15  | 0.011 | 104.25062 | ±0.72105 | 281.69 | ±1.80 |
| 11.0 % | 0.128750 | 0.600 | 0.112095 | 204.730 | 0.107311 | 9.149  | 5.7621  | 0.192 | 619.63  | 0.007 | 100.93002 | ±0.39508 | 273.37 | ±0.99 |
| 11.5 % | 0.125462 | 0.627 | 0.082187 | 269.872 | 0.086143 | 11.072 | 5.4118  | 0.208 | 583.94  | 0.007 | 101.04872 | ±0.43002 | 273.66 | ±1.08 |

Table 6.10: Data from step heating analysis of Sample S9 9034' from the Ames Astrobleme.

| Laser Output | <sup>36</sup> Ar [fA] | % 1s  | <sup>37</sup> Ar [fA] | % 1s    | <sup>38</sup> Ar [fA] | % 1s  | <sup>39</sup> Ar [fA] | % 1s | <sup>40</sup> Ar [fA] | % 1s | 40(r)/39(k) | ±2s  | Age (Ma) | ±2s   |
|--------------|-----------------------|-------|-----------------------|---------|-----------------------|-------|-----------------------|------|-----------------------|------|-------------|------|----------|-------|
| 1.0 %        | 1.78                  | 0.31  | 1.61                  | 18.32   | 2.70                  | 0.37  | 188.27                | 0.06 | 17262.83              | 0.00 | 88.90       | 0.12 | 242.71   | 0.29  |
| 1.8 %        | 1.05                  | 0.38  | 0.35                  | 84.21   | 1.47                  | 0.68  | 102.62                | 0.07 | 11886.23              | 0.01 | 112.82      | 0.15 | 302.82   | 0.38  |
| 2.0 %        | 0.56                  | 0.57  | 0.21                  | 139.39  | 0.73                  | 1.37  | 50.43                 | 0.07 | 6032.67               | 0.01 | 116.35      | 0.18 | 311.54   | 0.44  |
| 3.0 %        | 0.42                  | 0.70  | 0.03                  | 898.42  | 0.51                  | 1.91  | 34.52                 | 0.09 | 4150.03               | 0.02 | 116.64      | 0.21 | 312.24   | 0.52  |
| 4.0 %        | 0.43                  | 0.68  | 0.02                  | 1477.62 | 0.51                  | 1.95  | 33.54                 | 0.09 | 4057.13               | 0.02 | 117.14      | 0.21 | 313.46   | 0.52  |
| 2.9 %        | 0.39                  | 0.73  | 0.05                  | 557.98  | 0.43                  | 2.28  | 28.15                 | 0.09 | 3401.68               | 0.02 | 116.71      | 0.23 | 312.41   | 0.58  |
| 3.3 %        | 0.42                  | 0.70  | 0.07                  | 416.98  | 0.42                  | 2.35  | 26.83                 | 0.10 | 3234.34               | 0.02 | 115.95      | 0.24 | 310.54   | 0.59  |
| 3.8 %        | 0.68                  | 0.50  | 0.01                  | 3492.06 | 0.58                  | 1.73  | 34.49                 | 0.08 | 4095.02               | 0.02 | 112.90      | 0.20 | 303.01   | 0.50  |
| 4.2 %        | 0.71                  | 0.48  | 0.06                  | 468.78  | 0.52                  | 1.83  | 30.92                 | 0.09 | 3706.12               | 0.02 | 113.04      | 0.22 | 303.38   | 0.54  |
| 4.6 %        | 0.69                  | 0.48  | 0.02                  | 1466.92 | 0.47                  | 2.13  | 26.63                 | 0.10 | 3159.59               | 0.02 | 110.99      | 0.24 | 298.30   | 0.58  |
| 5.0 %        | 0.95                  | 0.39  | 0.22                  | 134.90  | 0.58                  | 1.69  | 30.78                 | 0.09 | 3627.88               | 0.02 | 108.77      | 0.22 | 292.79   | 0.54  |
| 5.5 %        | 1.24                  | 0.35  | 0.14                  | 201.65  | 0.68                  | 1.45  | 33.92                 | 0.09 | 3967.47               | 0.02 | 106.17      | 0.21 | 286.31   | 0.52  |
| 6.0 %        | 1.70                  | 0.32  | 0.23                  | 128.99  | 0.91                  | 1.05  | 44.18                 | 0.08 | 5124.60               | 0.01 | 104.64      | 0.19 | 282.49   | 0.47  |
| 6.5 %        | 2.18                  | 0.30  | 0.27                  | 110.45  | 1.11                  | 0.92  | 53.66                 | 0.07 | 6207.14               | 0.01 | 103.69      | 0.18 | 280.11   | 0.45  |
| 7.0 %        | 2.70                  | 0.29  | 0.59                  | 50.94   | 1.48                  | 0.70  | 70.73                 | 0.07 | 8224.06               | 0.01 | 105.00      | 0.17 | 283.38   | 0.42  |
| 7.7 %        | 3.50                  | 0.28  | 0.85                  | 34.65   | 1.86                  | 0.55  | 87.05                 | 0.07 | 10096.85              | 0.01 | 104.10      | 0.17 | 281.15   | 0.41  |
| 8.4 %        | 3.48                  | 0.27  | 0.65                  | 45.23   | 1.77                  | 0.60  | 81.52                 | 0.07 | 9548.05               | 0.01 | 104.53      | 0.17 | 282.21   | 0.42  |
| 9.2 %        | 3.42                  | 0.28  | 0.89                  | 32.29   | 1.67                  | 0.60  | 74.61                 | 0.07 | 8792.88               | 0.01 | 104.30      | 0.17 | 281.66   | 0.44  |
| 10.0 %       | 1.65                  | 0.32  | 0.43                  | 66.08   | 0.88                  | 1.06  | 41.86                 | 0.08 | 5038.05               | 0.01 | 108.69      | 0.20 | 292.58   | 0.50  |
| 11.0 %       | 0.95                  | 0.40  | 0.32                  | 92.64   | 0.56                  | 1.71  | 26.46                 | 0.10 | 3246.60               | 0.02 | 112.08      | 0.25 | 301.00   | 0.61  |
| 12.0 %       | 0.60                  | 0.53  | 0.25                  | 118.14  | 0.30                  | 3.30  | 12.98                 | 0.16 | 1575.80               | 0.04 | 107.77      | 0.40 | 290.29   | 0.99  |
| 13.0 %       | 0.88                  | 0.42  | 0.11                  | 276.43  | 0.44                  | 2.15  | 20.07                 | 0.12 | 2438.88               | 0.03 | 108.62      | 0.29 | 292.42   | 0.72  |
| 14.0 %       | 0.23                  | 1.14  | 0.07                  | 454.85  | 0.13                  | 7.49  | 5.35                  | 0.36 | 640.63                | 0.10 | 106.70      | 0.87 | 287.63   | 2.16  |
| 15.0 %       | 0.41                  | 0.70  | 0.12                  | 242.86  | 0.22                  | 4.37  | 10.05                 | 0.20 | 1249.35               | 0.05 | 112.19      | 0.51 | 301.28   | 1.25  |
| 16.0 %       | 0.33                  | 0.85  | 0.10                  | 292.58  | 0.16                  | 6.07  | 6.96                  | 0.28 | 886.26                | 0.08 | 113.21      | 0.71 | 303.79   | 1.75  |
| 17.0 %       | 0.06                  | 4.47  | 0.01                  | 1981.91 | 0.03                  | 35.85 | 1.55                  | 1.22 | 196.80                | 0.34 | 116.12      | 3.12 | 310.95   | 7.66  |
| 18.0 %       | 0.10                  | 2.54  | 0.04                  | 659.84  | 0.06                  | 15.80 | 2.54                  | 0.76 | 315.26                | 0.21 | 112.10      | 1.89 | 301.04   | 4.68  |
| 19.0 %       | 0.09                  | 2.78  | 0.02                  | 1772.24 | 0.07                  | 14.67 | 3.38                  | 0.55 | 423.36                | 0.16 | 117.10      | 1.43 | 313.36   | 3.52  |
| 20.0 %       | 0.02                  | 12.04 | 0.33                  | 90.33   | 0.01                  | 91.31 | 0.59                  | 3.21 | 76.65                 | 0.87 | 119.53      | 8.39 | 319.33   | 20.54 |

## 6.6 Data from step heating analysis of samples from Slate Islands

Table 6.11: Data from step heating analysis of Sample S2 (metasyenite) from the Slate Islands.

| Laser Output | <sup>36</sup> Ar<br>[fA] | %1σ   | <sup>37</sup> Ar<br>[fA] | %1σ    | <sup>38</sup> Ar<br>[fA] | %1σ     | <sup>39</sup> Ar<br>[fA] | %1σ  | <sup>40</sup> Ar<br>[fA] | %1σ  | 40(r)/39(k) | ± 2σ  | Age<br>(Ma) | ± 2σ  |
|--------------|--------------------------|-------|--------------------------|--------|--------------------------|---------|--------------------------|------|--------------------------|------|-------------|-------|-------------|-------|
| 0.3 %        | 0.12                     | 0.59  | 0.67                     | 32.55  | 0.04                     | 21.63   | 1.01                     | 1.15 | 1304.24                  | 0.01 | 1257.06     | 28.87 | 2004.69     | 27.83 |
| 0.4 %        | 0.04                     | 1.34  | 0.59                     | 38.34  | 0.04                     | 27.16   | 1.89                     | 0.56 | 2356.71                  | 0.01 | 1239.71     | 14.01 | 1987.89     | 13.63 |
| 0.5 %        | 0.01                     | 4.62  | 0.13                     | 173.39 | 0.01                     | 80.22   | 0.90                     | 1.21 | 1231.40                  | 0.01 | 1358.86     | 32.98 | 2100.24     | 30.15 |
| 0.6 %        | 0.01                     | 6.64  | 0.10                     | 217.72 | 0.01                     | 160.69  | 0.77                     | 1.45 | 1092.21                  | 0.02 | 1416.59     | 40.97 | 2152.26     | 36.40 |
| 0.7 %        | 0.01                     | 9.05  | 0.03                     | 764.25 | 0.01                     | 155.99  | 0.49                     | 2.29 | 758.65                   | 0.02 | 1557.46     | 71.32 | 2273.25     | 59.25 |
| 0.8 %        | 0.01                     | 6.22  | 0.14                     | 159.78 | 0.00                     | 1025.87 | 0.90                     | 1.19 | 1177.94                  | 0.01 | 1300.85     | 31.02 | 2046.42     | 29.21 |
| 0.9 %        | 0.01                     | 7.94  | 0.09                     | 234.00 | 0.00                     | 341.26  | 0.66                     | 1.60 | 962.23                   | 0.02 | 1455.96     | 46.64 | 2186.90     | 40.64 |
| 1.0 %        | 0.01                     | 8.71  | 0.03                     | 835.52 | 0.00                     | 737.90  | 0.60                     | 1.81 | 866.51                   | 0.02 | 1446.32     | 52.29 | 2178.48     | 45.78 |
| 1.1 %        | 0.01                     | 7.18  | 0.08                     | 260.16 | 0.00                     | 365.93  | 0.67                     | 1.60 | 1056.64                  | 0.02 | 1569.65     | 50.30 | 2283.35     | 41.56 |
| 1.2 %        | 0.01                     | 3.57  | 0.03                     | 683.44 | 0.02                     | 54.48   | 1.05                     | 1.03 | 1470.08                  | 0.01 | 1401.69     | 29.02 | 2138.97     | 25.96 |
| 1.3 %        | 0.01                     | 6.98  | 0.12                     | 186.34 | 0.00                     | 1075.39 | 0.84                     | 1.35 | 1207.25                  | 0.01 | 1437.48     | 38.96 | 2170.72     | 34.26 |
| 1.4 %        | 0.01                     | 4.83  | 0.02                     | 999.57 | 0.02                     | 62.40   | 0.97                     | 1.08 | 1465.16                  | 0.01 | 1513.38     | 32.77 | 2236.26     | 27.79 |
| 1.5 %        | 0.00                     | 10.00 | 0.05                     | 436.35 | 0.01                     | 72.94   | 0.67                     | 1.51 | 1063.50                  | 0.02 | 1594.26     | 48.15 | 2303.56     | 39.34 |
| 1.6 %        | 0.02                     | 2.65  | 0.11                     | 195.05 | 0.02                     | 52.86   | 1.18                     | 0.89 | 1792.35                  | 0.01 | 1509.61     | 27.00 | 2233.05     | 22.93 |
| 1.7 %        | 0.01                     | 5.15  | 0.05                     | 475.60 | 0.01                     | 78.64   | 0.92                     | 1.18 | 1463.31                  | 0.01 | 1583.19     | 37.41 | 2294.50     | 30.72 |
| 1.8 %        | 0.01                     | 5.62  | 0.08                     | 303.94 | 0.00                     | 270.79  | 0.87                     | 1.24 | 1445.28                  | 0.01 | 1654.77     | 40.90 | 2352.34     | 32.52 |
| 1.9 %        | 0.01                     | 4.71  | 0.19                     | 119.43 | 0.02                     | 50.16   | 0.90                     | 1.21 | 1470.90                  | 0.01 | 1639.11     | 39.55 | 2339.84     | 31.67 |
| 2.0 %        | 0.01                     | 5.46  | 0.14                     | 158.63 | 0.01                     | 63.02   | 0.81                     | 1.39 | 1393.62                  | 0.01 | 1710.17     | 47.69 | 2395.86     | 37.02 |
| 2.1 %        | 0.01                     | 3.75  | 0.34                     | 66.86  | 0.01                     | 69.88   | 0.82                     | 1.35 | 1425.66                  | 0.01 | 1734.19     | 46.93 | 2414.42     | 36.06 |
| 2.2 %        | 0.02                     | 3.02  | 0.08                     | 263.04 | 0.01                     | 66.17   | 0.87                     | 1.25 | 1410.05                  | 0.01 | 1608.06     | 40.07 | 2314.81     | 32.53 |
| 2.3 %        | 0.01                     | 3.81  | 0.04                     | 619.02 | 0.01                     | 134.12  | 0.79                     | 1.34 | 1251.90                  | 0.01 | 1585.97     | 42.50 | 2296.78     | 34.85 |
| 2.5 %        | 0.02                     | 3.19  | 0.07                     | 297.73 | 0.01                     | 74.73   | 0.77                     | 1.32 | 1196.50                  | 0.01 | 1556.40     | 41.25 | 2272.37     | 34.28 |
| 2.8 %        | 0.17                     | 0.52  | 0.44                     | 51.38  | 0.09                     | 11.37   | 4.77                     | 0.24 | 4860.21                  | 0.00 | 1009.10     | 4.92  | 1748.38     | 5.46  |
| 3.1 %        | 0.13                     | 0.63  | 0.30                     | 73.62  | 0.06                     | 15.44   | 2.62                     | 0.40 | 2681.10                  | 0.01 | 1008.87     | 7.99  | 1748.13     | 8.87  |
| 3.4 %        | 0.19                     | 0.49  | 0.19                     | 117.52 | 0.08                     | 12.21   | 3.74                     | 0.30 | 3309.11                  | 0.01 | 870.63      | 5.19  | 1587.66     | 6.30  |
| 3.7 %        | 0.29                     | 0.44  | 0.30                     | 70.43  | 0.10                     | 9.89    | 3.60                     | 0.31 | 3804.05                  | 0.00 | 1031.86     | 6.45  | 1773.48     | 7.06  |

Table 6.11 Continued

|        |      |      |      |         |      |        |      |       |         |      |         |         |         |        |
|--------|------|------|------|---------|------|--------|------|-------|---------|------|---------|---------|---------|--------|
| 4.0 %  | 0.16 | 0.54 | 0.16 | 139.77  | 0.06 | 17.18  | 1.52 | 0.70  | 2207.79 | 0.01 | 1420.65 | 19.88   | 2155.86 | 17.62  |
| 4.3 %  | 0.10 | 0.71 | 0.05 | 455.95  | 0.04 | 25.48  | 0.76 | 1.40  | 1018.12 | 0.02 | 1295.26 | 36.20   | 2041.15 | 34.19  |
| 4.6 %  | 0.19 | 0.49 | 0.35 | 63.14   | 0.04 | 22.28  | 0.81 | 1.33  | 1446.21 | 0.01 | 1707.88 | 45.41   | 2394.08 | 35.29  |
| 5.0 %  | 0.19 | 0.51 | 0.28 | 77.85   | 0.05 | 20.92  | 0.71 | 1.48  | 1284.25 | 0.01 | 1730.44 | 51.38   | 2411.53 | 39.54  |
| 5.4 %  | 0.26 | 0.43 | 0.07 | 293.63  | 0.06 | 15.73  | 0.75 | 1.49  | 1455.61 | 0.01 | 1833.99 | 54.71   | 2489.52 | 40.33  |
| 5.8 %  | 0.28 | 0.42 | 0.01 | 2229.21 | 0.06 | 15.90  | 0.75 | 1.38  | 1504.50 | 0.01 | 1889.24 | 52.26   | 2529.79 | 37.68  |
| 6.2 %  | 0.11 | 0.74 | 0.03 | 690.04  | 0.02 | 52.39  | 0.32 | 3.33  | 658.88  | 0.03 | 1930.54 | 128.79  | 2559.32 | 91.34  |
| 6.6 %  | 0.10 | 0.73 | 0.23 | 93.44   | 0.02 | 62.35  | 0.25 | 4.24  | 469.31  | 0.04 | 1793.42 | 152.13  | 2459.37 | 114.02 |
| 7.0 %  | 0.04 | 1.42 | 0.05 | 425.30  | 0.00 | 269.11 | 0.12 | 9.29  | 212.78  | 0.08 | 1745.98 | 324.44  | 2423.45 | 248.05 |
| 7.4 %  | 0.06 | 1.03 | 0.05 | 467.61  | 0.01 | 73.33  | 0.43 | 2.48  | 349.50  | 0.05 | 774.20  | 38.42   | 1466.67 | 49.86  |
| 7.8 %  | 0.04 | 1.38 | 0.02 | 1234.97 | 0.01 | 77.43  | 0.12 | 9.20  | 172.51  | 0.10 | 1320.53 | 242.94  | 2064.85 | 226.48 |
| 8.2 %  | 0.02 | 2.46 | 0.23 | 102.18  | 0.01 | 159.88 | 0.09 | 12.42 | 78.66   | 0.21 | 818.99  | 203.18  | 1523.88 | 255.46 |
| 8.6 %  | 0.08 | 0.81 | 0.06 | 381.02  | 0.03 | 34.44  | 1.18 | 0.96  | 347.16  | 0.05 | 276.04  | 5.34    | 666.65  | 10.79  |
| 9.0 %  | 0.03 | 1.96 | 0.16 | 131.14  | 0.01 | 117.83 | 0.03 | 33.34 | 69.10   | 0.24 | 1902.59 | 1264.87 | 2539.39 | 907.00 |
| 9.5 %  | 0.03 | 1.96 | 0.23 | 94.76   | 0.01 | 72.72  | 0.05 | 20.28 | 89.05   | 0.19 | 1580.75 | 639.44  | 2292.50 | 525.60 |
| 10.0 % | 0.03 | 1.80 | 0.07 | 330.63  | 0.01 | 78.41  | 0.10 | 10.48 | 207.08  | 0.08 | 1945.06 | 407.83  | 2569.59 | 287.60 |
| 10.7 % | 0.02 | 2.39 | 0.09 | 239.86  | 0.00 | 634.37 | 0.04 | 27.46 | 83.63   | 0.20 | 2059.28 | 1133.08 | 2648.40 | 764.97 |
| 11.5 % | 0.12 | 0.63 | 0.17 | 126.92  | 0.03 | 37.21  | 0.27 | 4.06  | 575.75  | 0.03 | 2000.17 | 162.63  | 2608.04 | 112.27 |

## VII: REFERENCES

- Alvarez, L., Alvarez, W., Asaro, F., & Michel, H. (1980). Extraterrestrial cause for the Cretaceous-Tertiary extinction. *Science*.  
<https://doi.org/10.1126/science.208.4448.1095>
- Alwmark, C., & Schmitz, B., (2009), Relict silicate inclusions in extraterrestrial chromite and their use in the classification of fossil chondritic material: *Geochimica et Cosmochimica Acta*, v. 73, p. 1472–1486, doi: 10.1016/j.gca.2008.12.006
- Ambers, C., Brändlein, P., Golbert., M; (1997). Petrology of Enigmatic Rocks from 2.75 Km Depth in the Ames Structural Anomaly, Major Country, Oklahoma, and Their Relationship to Suevite from the Ries Crater, Nördlingen, Bavaria. in *Ames Structure in Northwest Oklahoma and Similar Features: Origin and Petroleum Production (1995 Symposium)*, K. S. Johnson and J. A. Campbell, Oklahoma Geological Survey, Norman, Oklahoma, Circular 100, 302-309.
- Barringer, D. (1905). Coon Mountain and its crater. *Proceedings Academy of Natural Sciences of Philadelphia*, v. 57, pp. 861-886
- Barringer, D. (1915). Further notes on Meteor crater, Arizona. *American Journal of Science*, v. 39, pp. 482-483.
- Barringer, D. (1924). Further notes on Meteor crater in northern central Arizona. *Proceedings Academy of Natural Sciences of Philadelphia*, v. 76, pp. 275-278.
- Bevan, A. W. R., Bland, P. A., & Jull, A. J. T. (1998). Meteorite flux on the Nullarbor region, Australia. *Meteorites; Flux with Time and Impact Effects.*, 140, 59–73.  
<https://doi.org/10.1144/gsl.sp.1998.140.01.07>
- Bickford, M. E., & Lewis, R. D. (1979). U-Pb geochronology of exposed basement rocks in Oklahoma. *Bulletin of the Geological Society of America*, 90(6), 540–544.  
[https://doi.org/10.1130/0016-7606\(1979\)90<540:UGOEBR>2.0.CO;2](https://doi.org/10.1130/0016-7606(1979)90<540:UGOEBR>2.0.CO;2)
- Bland, P. (2001). Quantification of Meteorite Infall Rates from Accumulations in Deserts, and Meteorite Accumulations on Mars. *Accretion of Extraterrestrial Matter Throughout Earth's History*, 267–303. [https://doi.org/10.1007/978-1-4419-8694-8\\_15](https://doi.org/10.1007/978-1-4419-8694-8_15)
- Bogard D. D. & Hirsch W. C. (1980).  $^{40}\text{Ar}/^{39}\text{Ar}$  dating, Ar diffusion properties, and cooling rate determinations of severely shocked chondrites. *Geochimica et Cosmochimica Acta* 44, 1667–1682.
- Bogard D. D., Husain L., & Wright R. J. (1976).  $^{40}\text{Ar}$ - $^{39}\text{Ar}$  dating of collisional events in chondrite parent bodies. *Journal of Geophysical Research*. 32, 5664–5678.
- Bogard D. D., Garrison D. H., Norman M., Scott E. R. D., & Keil K. (1995).  $^{39}\text{Ar}$ - $^{40}\text{Ar}$  age and petrology of Chico: Large-scale impact melting on the L-chondrite parent body. *Geochimica et Cosmochimica Acta*, 59, 1383–1399.
- Bottomley, R., York, D., & Grieve, R. (1990). Argon-40-argon-39 dating of impact craters. *Lunar and Planetary Science Conference Proceedings*, 20, 421–431.

- Brenan R. L., Petersen B. L. & Smith H. J. (1975). The Origin of Red Wing Creek Structure, McKenzie County, North Dakota. Wyoming Geological Association, *Earth Science Bulletin*, 8 (3), 1-41.
- Bridges, D.L.W., 1997, Ames depression, Oklahoma: Domal collapse and later subsurface solution: Oklahoma Geological Survey Circular 100, pp. 153-168.
- Bridges, J.C., Schmitz, B., Hutchison, R., Greenwood, R.C., Tassinari, M., Franchi, I.A., (2007). Petrographic classification of mid-Ordovician fossil meteorites from Sweden. *Meteorit. Planet. Sci.* 42, 1781–1789.
- Card, K.D., Sanford, B., and Davidson, A., (1994). Bedrock geology, Lake Superior, Ontario, USA. Natural Resources Canada, Map NL-16/17-G.
- Carpenter, B., & Carlson, R., (1992). The Ames Impact Crater: Oklahoma Geology Notes, V. 52, p 208-223
- Carpenter B. N. & Carlson R. (1997) The Ames meteorite-impact crater, in K.S. Johnson and J.A. Campbell, editors, Ames structure in northwest Oklahoma and similar features; origin and petroleum production (1995 symposium): Oklahoma Geological Survey Circular 100, p. 104-119.
- Chen, J., & Lindström, M., (1991). Cephalopod septal strength indices (SSI) and depositional depth of Swedish Orthoceratite limestone. *Geol. Palaeontol.* 25, 5–18.
- Cocks, L., & Torsvik, T. (2005). Baltica from the late Precambrian to mid-Palaeozoic times: The gain and loss of a terrane's identity. *Earth-Science Reviews*, 72(1–2), 39–66. <https://doi.org/10.1016/j.earscirev.2005.04.001>
- Cohen, K.M., Harper, D.A.T., & Gibbard, P.L. 2017. ICS International Chronostratigraphic Chart 2018/06. International Commission on Stratigraphy, IUGS. [www.stratigraphy.org](http://www.stratigraphy.org)
- Coleman, A.P., 1901. The Slate Islands in Iron Ranges of Northwestern Ontario, Ontario Bureau of Mines, v. 11, 552-555
- Coughlon, J., & Denney, P. (1993). The Ames structural depression; an endogenic cryptoexplosion feature along a transverse shear. *Shale Shaker*, 43(4), 44–58. Retrieved from <https://www.lib.uwo.ca/cgi-bin/ezpauthn.cgi/docview/50316912?accountid=15115>
- Coughlon, J. P. & Denney, P. P. (1997), The Ames structure and other North American cryptoexplosion features: Evidence for endogenic emplacement. *Ames Structure in Northwest Oklahoma and Similar Features: Origin and Petroleum Production (1995 Symposium)*, K. S. Johnson and J. A. Campbell, Oklahoma Geological Survey, Norman, Oklahoma, v. Circular 100, 133-152.
- Crabb, J., & Schultz, L. (1981). Cosmic-ray exposure ages of the ordinary chondrites and their significance for parent body stratigraphy. *Geochimica et Cosmochimica Acta*, 45(11), 2151–2160. [https://doi.org/10.1016/0016-7037\(81\)90067-3](https://doi.org/10.1016/0016-7037(81)90067-3)
- Cronholm, A., & Schmitz, B. (2010). Extraterrestrial chromite distribution across the mid-Ordovician Puxi River section, central China: Evidence for a global major spike in flux of L-chondritic matter. *Icarus*, 208(1), 36–48. <https://doi.org/10.1016/j.icarus.2010.02.004>

- Deane, B., Lee, P., Milam, K., Evenick, J., & Zawislak, R. (2004). The Howell Structure, Lincoln County, Tennessee: A Review of Past and Current Research. *Lunar and Planetary Science XXXV*, (1692), 4–5.
- Denison, R. E. (1966). Basement Rocks in Adjoining Parts of Oklahoma, Kansas, Missouri, and Arkansas, 1–300.
- Dietz, R., & McHone, J., Astroblemes recently confirmed with shatter cones (abstract). *Meteoritics*, v. 26, p. 332. 1991.
- Dressler, B. O., & Sharpton, V. L. (1997). Breccia formation at a complex impact crater: Slate Islands, Lake Superior, Ontario, Canada, 275, 275–285.
- Dressler, B.O., Sharpton, V.L., Schnieders, B. and Scott, J., (1995). New observations at the Slate Islands impact structure, Lake Superior. Ontario Geological Survey, Miscellaneous Publication 164: 53-61.
- Dressler, B.O., Sharpton, V.L. and Schuraytz, B.C., (1998). Shock metamorphism and shock barometry at a complex impact structure: Slate Islands, Canada. *Contributions to Mineralogy and Petrology*, 130, 275-287.
- Dressler, B.O., Sharpton, V.L. and Copeland, P., (1999). Slate Islands, Lake Superior, Canada: A mid-size, complex impact structure. Geological Society of America, Special Paper 339, 109-124.
- Evans, J. (1997), Historical development and production of the Arbuckle and exotic lithologies in *Ames structure, Oklahoma. Ames Structure in Northwest Oklahoma and Similar Features: Origin and Petroleum Production (1995 Symposium)*, ) (eds. K. S. Johnson and J. A. Campbell), pp. 207-213. Oklahoma Geological Survey, Norman, Oklahoma, v. Circular 100,
- Fay, R. (1989). Geology of the Arbuckle Mountains Along Interstate 35, Carter and Murray Counties, Oklahoma, 59. Retrieved from <http://www.ogs.ou.edu/pubsscanned/guidebooks/GB26wm.pdf>
- Fischer, J. F. (1997) The Nicor No. 18-4 Chestnut core, Ames Structure, Oklahoma: Description and petrography. In *Ames Structure in Northwest Oklahoma and Similar Features: Origin and Petroleum Production (1995 Symposium)* (eds. K. S. Johnson and J. A. Campbell), pp. 223-239. Oklahoma Geological Survey Circular 100, Norman, Oklahoma, USA.
- French, B., & Cordua, W. (1999). Intense fracturing of quartz at the Rock Elm (Wisconsin) “cryptoexplosion” structure; evidence for meteorite impact. *Abstracts of Papers Submitted to the Lunar and Planetary Science Conference*, 30(1992), abstr. no. 1123.
- Glass, B., & Simonson, B., (2013) Distal Impact Ejecta Layers: A Record of Large Impacts in Sedimentary Deposits. Impact Studies Series Springer-Verlag, Berlin, Heidelberg (2013) 716 pp.
- Haack, H., Farinella, P., Scott, E. R. D., & Keil, K. (1996). Meteoritic, Asteroidal, and Theoretical Constraints on the 500 Ma Disruption of the L-Chondrite Parent Body. *Icarus*, 119(1), 182–191. <https://doi.org/10.1006/icar.1996.0010>

- Hägström, T., & Schmitz, B. (2007). Distribution of extraterrestrial chromite in Middle Ordovician Komstad Limestone in the Killeröd quarry, Scania, Sweden. *Bulletin of the Geological Society of Denmark*, 55, 37–58.
- Halliday, I., Blackwell, A., & Griffin, A. (1989). The flux of meteorites on the earth's surface. *Meteoritics*, 24, 173–178. <https://doi.org/10.1111/maps.12478>
- Halls, H.C., (1975). Shock-induced remanent magnetization in Late Precambrian rocks from Lake Superior. *Nature*, 255, 692-695.
- Halls, H.C., (1976). The Slate Islands: The Central Uplift of a meteorite impact crater. Institute on Lake Superior Geology, 22nd Annual Meeting, St Paul, Minnesota, p. 27
- Halls, H. C., and Grieve, R. A. F., (1976), The Slate Islands: A probable complex meteorite impact structure in Lake Superior: *Canadian Journal of Earth Sciences*, v. 13, 1301–1309.
- Halls, H. C., and Stesky, R.M., (1978). Paleomagnetic and shatter cone measurements from the Slate Islands, Northern Lake Superior. Canadian Geophysical Union, 5th Annual Meeting, London, Ontario, 34.
- Harper, D. A. (2006). The Ordovician biodiversification: Setting an agenda for marine life. *Palaeogeography, Palaeoclimatology, Palaeoecology*, 232(2), 148-166.
- Heck, P. R., Schmitz, B., Baur, H., & Wieler, R. (2008). Noble gases in fossil micrometeorites and meteorites from 470 Myr old sediments from southern Sweden, and new evidence for the L-chondrite parent body breakup event. *Meteoritics & Planetary Science*, 43(3), 517–528. <https://doi.org/10.1111/j.1945-5100.2008.tb00669.x>
- Heck, P. R., Schmitz, B., Baur, H., Halliday, A. N., & Wieler, R. (2004). Fast delivery of meteorites to Earth after a major asteroid collision. *Nature*, 430(6997), 323–325. <https://doi.org/10.1038/nature02736>
- Heck, P. R., Ushikubo, T., Schmitz, B., Kita, N. T., Spicuzza, M. J., & Valley, J. W. (2010). A single asteroidal source for extraterrestrial Ordovician chromite grains from Sweden and China: High-precision oxygen three-isotope SIMS analysis. *Geochimica et Cosmochimica Acta*, 74(2), 497–509. <https://doi.org/10.1016/j.gca.2009.10.027>
- Higley, D., Gaswirth, S. B., Abbott, M. M., Charpentier, R. R., Hatch, J. R., Klett, T. R., Nelson, P., Pawlewicz, M., Pearson, O., Pollastro, R., & Schenk, C. J. (2014). Assessment of undiscovered oil and gas resources of the Anadarko Basin Province of Oklahoma, Kansas, Texas, and Colorado, 2010. Retrieved from <http://pubs.usgs.gov/fs/2011/3003/pdf/FS11-3003.pdf>
- Hinze, W.J., O'Hara, W.N., Trow, J.W. & Secor, G.B., (1966). Aeromagnetic studies of eastern Lake Superior, in Steinhart, J.S., ed., *The earth beneath the continents*. American Geophysical Union, Geophysical Monograph, 10, 95-110.
- Hollings, P; Smyk, M; Addison, B; & Fralick, P. (2006). Field Trip Guidebook for the Slate Islands, Ontario. *Institute on Lake Superior Geology, Special Publication*.
- Huffman, A., (1997). Shock-Induced Microstructures and Experimental Constraints on the Formation of the Ames Impact Structure. in *Ames Structure in Northwest*

- Oklahoma and Similar Features: Origin and Petroleum Production (1995 Symposium)*, K. S. Johnson and J. A. Campbell, Oklahoma Geological Survey, Norman, Oklahoma, Circular 100, 302-309.
- Huss, G. (1991). Meteorite mass distributions and differences between Antarctic and non-Antarctic meteorites. *GCA*, 55, 105–111.
- Jaanusson, V. (1972). Constituent analysis of an Ordovician limestone from Sweden. *Lethaia*, 5(2), 217–237. <https://doi.org/10.1111/j.1502-3931.1972.tb00853.x>
- Jaanusson, V. (1973). Aspects of carbonate sedimentation in the Ordovician of Baltoscandia. *Lethaia*, 6(1), 11–34. <https://doi.org/10.1111/j.1502-3931.1973.tb00871.x>
- Jackson, S. E., Pearson, N. J., Griffin, W. L., and Belousova, E. A. (2004). The application of laser ablation-inductively coupled plasma-mass spectrometry to in situ U-Pb zircon geochronology. *Chemical Geology*, 211(1–2), 47–69. <https://doi.org/10.1016/j.chemgeo.2004.06.017>
- Johnson, K. S., (2008), Geologic history of Oklahoma, in Johnson, K. S., and Luza, K. V., eds., Earth sciences and mineral resources of Oklahoma: Oklahoma Geological Survey Educational Publication 9, 3–5.
- Johnson, K., & Campbell, J.; (1997) Ames Structure in Northwest Oklahoma and Similar Features: Origin and Petroleum Production. Oklahoma Geological Survey, Norman, Oklahoma, v. Circular 100, pp. 169-198. 1995 Symposium.
- Johnson, K., and Smith, D. (1997) Ames structure of northwestern Oklahoma is reflected in overlying Permian strata. in *Ames Structure in Northwest Oklahoma and Similar Features: Origin and Petroleum Production (1995 Symposium)*, K. S. Johnson and J. A. Campbell, Oklahoma Geological Survey, Norman, Oklahoma, Circular 100, 357-362.
- Kallesen, E., Corfu, F., & Dypvik, H. (2009). U-Pb systematics of zircon and titanite from the Gardnos impact structure, Norway: Evidence for impact at 546 Ma? *Geochimica et Cosmochimica Acta*, 73(10), 3077–3092. <https://doi.org/10.1016/j.gca.2009.02.020>
- Kamo, S. L., Reimold, W. U., Krogh, T. E., & Colliston, W. P. (1996). A 2.023 Ga age for the Vredefort impact event and a first report of shock metamorphosed zircons in pseudotachylitic breccias and Granophyre. *Earth and Planetary Science Letters*, 144(3), 369–387. [https://doi.org/http://dx.doi.org/10.1016/S0012-821X\(96\)00180-X](https://doi.org/http://dx.doi.org/10.1016/S0012-821X(96)00180-X)
- Kirschner, C. E., Grantz, A. & Mullen, M.W., (1992). Impact origin of the Avak Structure, Arctic Alaska, and genesis of the Barrow gas fields. *The American Association of Petroleum Geologists Bulletin*, 76, 651-679.
- Kisvarsanyi, E. B. (1990). General features of the St. Francis and Spavinaw granite-rhyolite terranes and the Precambrian metallogenic region of southeast Missouri. *US Geological Survey Bulletin*, 1932, 48-57.
- Koerberl, C. & Reimold, W. U. (1995) Shock metamorphism at the Red Wing Creek structure, North Dakota: Confirmation of impact origin (abstract). Abstracts of the 26th Lunar and Planetary Science Conference, 769-770.

- Koerberl, C., & Anderson, R. R., (1996). Manson and company: Impact structures in the United States. Geological Society of America Special Paper 302, 1-29.
- Koerberl, C., Reimold, W. U. & Brandt, D. (1996). Red Wing Creek structure, North Dakota: Petrographical and geochemical studies, and confirmation of impact origin. *Meteoritics & Planetary Science*, 31(3), 335-342.
- Koerberl, C., Reimold, W. U., Brandt, D., Dallmeyer, R., & Powell, R. (1997). Target Rocks and Breccias at Ames: Petrology, Minerology, Geochemistry and Age. Oklahoma Geological Survey Circular #100, 169– 198
- Koerberl, C., Reimold, W., & Kelley, S. (2001). Petrography, geochemistry, and argon-40/argon-39 ages of impact-melt rocks and breccias from the Ames impact structure, Oklahoma: The Nicor Chesnut 18-4 drill core. *Meteoritics and Planetary Science*, 36(5), 651–669. <https://doi.org/10.1111/j.1945-5100.2001.tb01907.x>
- Korochantseva, E, Trieloff, M., Lorenz, C. a, Buykin, A, Ivanova, M, Schwarz, W., Hopp, J., Jessberger, E. (2007). L-chondrite asteroid breakup tied to Ordovician meteorite shower by multiple isochron 40Ar-39Ar dating. *Meteoritics & Planetary Science*, 42(1), 113–130. <https://doi.org/10.1111/j.1945-5100.2007.tb00221.x>
- Krogh, T. E., Kamo, S. L., Sharpton, V. L., Marin, L. E., & Hildebrands, A. R. (1993). U–Pb ages of single shocked zircons linking distal K/T ejecta to the Chicxulub crater. *Nature*, 366(6457), 731–734. <https://doi.org/10.1038/366731a0>
- Kunz, J., Falter, M., & Jessberger, E. K. (1997). Shocked meteorites: Argon-40-argon-39 evidence for multiple impacts. *Meteoritics and Planetary Science*, 32(5), 647–670. <https://doi.org/10.1111/j.1945-5100.1997.tb01550.x>
- Levin, V., Long, M. D., Skryzalin, P., Li, Y., & López, I. (2018). Seismic evidence for a recently formed mantle upwelling beneath New England. *Geology*, 46(1), 87–90. <https://doi.org/10.1130/G39641.1>
- Li, Z. X., Bogdanova, S. V., Collins, A. S., Davidson, A., De Waele, B., Ernst, R. E., Fitzsimons, I. C.W., Fuck, R. A., Gladkochub, D. P., Jacobs, J., Karlstrom, K. E., Lu, S., Natapov, L. M., Pease, V., Pisarevsky, S. A., Thrane, K. & Vernikovskiy, V. (2008). Assembly, configuration, and break-up history of Rodinia: A synthesis. *Precambrian Research*, 160(1–2), 179–210. <https://doi.org/10.1016/j.precamres.2007.04.021>
- Lindskog, A., Schmitz, B., Cronholm, A., & Dronov, A. (2012). A Russian record of a Middle Ordovician meteorite shower: Extraterrestrial chromite at Lynna River, St. Petersburg region. *Meteoritics and Planetary Science*, 47(8), 1274–1290. <https://doi.org/10.1111/j.1945-5100.2012.01383.x>
- Lindström, M., (1962). Sedimentary folds and the development of limestone in an early Ordovician sea. *Sedimentology* 2, 243–293.
- Lindström, M., (1971). Vom Anfang. Hochstand und Ende eines Epikontinentalmeeres. *Geology Rundschau* 60, 419–43.
- Lundquist, R. (2006). Provenance Analysis of the Marquette Range Supergroup Sedimentary Rocks Using U-Pb Isotope Geochemistry on Detrital Zircons By La-Icp-Ms. *Group*, 147–151.

- Mariano, J., and Hinze, W. J., (1994), Structural interpretation of the Midcontinental rift in eastern Lake Superior from seismic reflection and potential-field studies: *Canadian Journal of Earth Sciences*, v. 31, 619– 628.
- McConville P., Kelley S., & Turner G. (1988). Laser probe  $^{40}\text{Ar}$ - $^{39}\text{Ar}$  studies of the Peace River shocked L6 chondrite. *Geochimica et Cosmochimica Acta* 52, 2487–2499.
- Milstein, R. L., (1994). The Calvin impact crater, Cass County, Michigan: Identification and analysis of a subsurface Ordovician astrobleme. Ph. D. Thesis, Oregon State University, 86..
- Muehlberger, W. R., Denison, R. E., & Lidiak, E. G. (1967). Basement rocks in continental interior of United States. *AAPG Bulletin*, 51(12), 2351–2380. Retrieved from <http://archives.datapages.com/data/bulletns/1965-67/images/pg/00510012/2350/23510.pdf>
- Nesvorný, D., Morbidelli, A., Vokrouhlicky, D., Bottke, W., & Broz, M. (2002). The Flora Family: A Case of the Dynamically Dispersed Collisional Swarm? *Icarus*, 157(1), 155–172. <https://doi.org/10.1006/icar.2002.6830>
- Norris, A.W. & Sanford, B.V., (1969). Paleozoic and Mesozoic geology of the Hudson Bay lowlands. In Hood, P.J., ed., Earth science symposium on the Hudson Bay. Geological Survey of Canada, Paper 68-53, 169-205.
- Nystrom, J., & Wickman, F. (1991). The Ordovician chondrite from Brunflo, central Sweden, II. Secondary minerals. *Lithos*, 27(3), 167–185. [https://doi.org/10.1016/0024-4937\(91\)90011-9](https://doi.org/10.1016/0024-4937(91)90011-9)
- Ojakangas, R. W., Morey, G. B., & Green, J. C. (2001). The mesoproterozoic midcontinent rift system, Lake Superior region, USA. *Sedimentary Geology*, 141–142, 421–442. [https://doi.org/10.1016/S0037-0738\(01\)00085-9](https://doi.org/10.1016/S0037-0738(01)00085-9)
- Parnell, J. (2009). Global mass wasting at continental margins during Ordovician high meteorite influx. *Nature Geoscience*, 2(1), 57–61. <https://doi.org/10.1038/ngeo386>
- Parsons, A.L. (1918). Slate Islands, Lake Superior; Ontario Bureau of Mines, Annual Report, vol.27, pt.1, p.155-167.
- Pearson, B. O. N., Miller, J. J., & Jewell, S. (2014). Tectonic and Structural Evolution of the Anadarko Basin and Structural Interpretation and Modeling of a Composite Regional 2D Seismic Line.
- Peplowski, P. N., Bazell, D., Evans, L. G., Goldsten, J. O., Lawrence, D. J., & Nittler, L. R. (2015). Hydrogen and major element concentrations on 433 Eros: Evidence for an L- or LL-chondrite-like surface composition. *Meteoritics and Planetary Science*, 50(3), 353–367. <https://doi.org/10.1111/maps.12434>
- Peters, C., Middleton, M., & Cordua, W. (2002). "Paleontology of the Rock Elm Disturbance". Abstracts with Programs - Geological Society of America. 34 (2): 95.
- Renard, G. (2011). Ejecta strata of recent origin have been identified in central Wisconsin at glover bluff impact site. GSA Annual Meeting in Minneapolis (9–12 October 2011). Abstract.
- Renne, P. R., Swisher, C. C., Deino, A. L., Karner, D. B., Owens, T. L., & DePaolo, D. J. (1998). Intercalibration of standards, absolute ages and uncertainties in  $^{40}\text{Ar}/^{39}\text{Ar}$

- dating. *Chemical Geology*, (3–4), 117–152. [https://doi.org/10.1016/S0009-2541\(98\)00047-3](https://doi.org/10.1016/S0009-2541(98)00047-3)
- Repetski, J., (1997). Conodont age constraints on the Middle Ordovician black shale within the Ames structure, Major County, Oklahoma. Ames Structure in Northwest Oklahoma and Similar Features: Origin and Petroleum Production (1995 Symposium), K. S. Johnson and J. A. Campbell, Oklahoma Geological Survey, Norman, Oklahoma, v. Circular 100, pp. 363-369.
- Roberts, C., & Sandridge, B. (1992). The Ames “hole.” *Shale Shaker*, 42(5), 118–121. Retrieved from <https://www.lib.uwo.ca/cgi-bin/ezpauthn.cgi/docview/50420026?accountid=15115>
- Roberston, P.B. & Grieve, R.A.E., (1976). Comparison of the distribution of shock metamorphism at Charlevoix, P.Q., and Slate Islands, Ontario. Geological Association of Canada – Mineralogical Association of Canada, Annual Meeting, Program with Abstracts, 1, p.42.
- Rubin, A. E. (1994). Metallic copper in ordinary chondrites. *Meteoritics*, 29(1), 93–98. <https://doi.org/10.1111/j.1945-5100.1994.tb00659.x>
- Sage, R.P. (1974). Geology of the Slate Islands, District of Thunder Bay; p.80-86 in Summary of Field Work, Milne, V.G. et al., editors, Ontario Division of Mines, Miscellaneous Paper 59.
- Sage, R. P. (1991). *Precambrian Geology, Slate Islands*.
- Sage, R.P., (1999). The Slate Islands: A uniquely sited cryptoexplosion structure. In Summary of Field work and other activities 1999, Ontario Geological Survey, Open File Report 6000, 28-1 to 28-13.
- Schmieder, M., Tohver, E., Denyszyn, S., Jourdan, F., & Haines, P. W. (2013). Shock-Metamorphosed Zircons From the Acraman Impact Structure (South Australia) - Tracers of Multi-Stage Impact Crater Evolution. *44th Lunar and Planetary Science Conference*, (March), 2–4. Retrieved from <http://adsabs.harvard.edu/abs/2013LPICo1719.1991S>
- Schmieder, M., Tohver, E., Jourdan, F., Denyszyn, S. W., & Haines, P. W. (2015). Zircons from the Acraman impact melt rock (South Australia): Shock metamorphism, U-Pb and  $^{40}\text{Ar}/^{39}\text{Ar}$  systematics, and implications for the isotopic dating of impact events. *Geochimica et Cosmochimica Acta*, 161, 71–100. <https://doi.org/10.1016/j.gca.2015.04.021>
- Schmitz, B. (2013). Extraterrestrial spinels and the astronomical perspective on Earth’s geological record and evolution of life. *Chemie Der Erde - Geochemistry*, 73(2), 117–145. <https://doi.org/10.1016/j.chemer.2013.04.002>
- Schmitz, B., & Häggström, T. (2006). Extraterrestrial chromite in Middle Ordovician marine limestone at Kinnekulle, southern Sweden-Traces of a major asteroid breakup event. *Meteoritics & Planetary Science*, 41(3), 455–466. <https://doi.org/10.1111/j.1945-5100.2006.tb00473.x>
- Schmitz, B., Boschi, S., Cronholm, A., Heck, P., Monechi, S., Montanari, A., & Terfelt, F. (2015). Fragments of Late Eocene Earth-impacting asteroids linked to disturbance

- of asteroid belt. *Earth and Planetary Science Letters*, 425.  
<https://doi.org/10.1016/j.epsl.2015.05.041>
- Schmitz, B., Harper, D., Peucker-Ehrenbrink, B., Stouge, S., Alwmark, C., Cronholm, A., Bergström, S., Tassinari, M., Wang, X., (2008). Asteroid breakup linked to mid-Ordovician biodiversification event. *Nat. Geosci.* 1, 49–53.
- Schmitz, B., Lindström, M., Asaro, F., & Tassinari, M. (1996). Geochemistry of meteorite-rich marine limestone strata and fossil meteorites from the lower Ordovician at Kinnekulle, Sweden. *Earth and Planetary Science Letters*, 145(1–4), 31–48. [https://doi.org/10.1016/S0012-821X\(96\)00205-1](https://doi.org/10.1016/S0012-821X(96)00205-1)
- Schmitz, B., Peucker-ehrenbrink, B., Lindstrm, M., & Tassinari, M. (1997). Accretion Rates of Meteorites and Cosmic Dust in the Early Ordovician, 278(5335), 88–90.
- Schmitz, B., Tassinari, M., & Peucker-Ehrenbrink, B. (2001). A rain of ordinary chondritic meteorites in the early Ordovician. *Earth and Planetary Science Letters*, 194(1), 1–15. [https://doi.org/10.1016/s0012-821x\(01\)00559-3](https://doi.org/10.1016/s0012-821x(01)00559-3)
- Schmitz, B., Yin, Q.-Z., Sanborn, M. E., Tassinari, M., Caplan, C. E., & Huss, G. R. (2016). A new type of solar-system material recovered from Ordovician marine limestone. *Nature Communications*, 7(May). <https://doi.org/10.1038/ncomms11851>
- Schmitz, M. D., Bowring, S. A., & Ireland, T. R. (2003). Evaluation of Duluth Complex anorthositic series (AS3) zircon as a U-Pb geochronological standard: New high-precision isotope dilution thermal ionization mass spectrometry results. *Geochimica et Cosmochimica Acta*, 67(19), 3665–3672. [https://doi.org/10.1016/S0016-7037\(03\)00200-X](https://doi.org/10.1016/S0016-7037(03)00200-X)
- Schmitz, B., Yin, Q.-Z., Sanborn, M. E., Tassinari, M., Caplan, C. E., & Huss, G. R. (2016). A new type of solar-system material recovered from Ordovician marine limestone. *Nature Communications*, 7(May), ncomms11851. <https://doi.org/10.1038/ncomms11851>
- Schneider, D. A., Bickford, M. E., Cannon, W. F., Schulz, K. J., & Hamilton, M. A. (2002). Age of volcanic rocks and syndeositional iron formations, Marquette Range Supergroup: implications for the tectonic setting of Paleoproterozoic iron formations of the Lake Superior region. *Canadian Journal of Earth Sciences*, 39(6), 999–1012. <https://doi.org/10.1139/e02-016>
- Schulz, K. J., & Cannon, W. F. (2007). The Penokean orogeny in the Lake Superior region. *Precambrian Research*, 157(1–4), 4–25. <https://doi.org/10.1016/j.precamres.2007.02.022>
- Servais, T., Owen, A., Harper, D., Kröger, B., & Munnecke, A. (2010). The Great Ordovician Biodiversification Event (GOBE): The palaeoecological dimension. *Palaeogeography, Palaeoclimatology, Palaeoecology*, 294(3–4), 99–119. <https://doi.org/10.1016/j.palaeo.2010.05.031>
- Sharpton, L., Dressler, B., Herrick, R., Schnieders, B., & Scott, J. (1996). New constraints on the Slate Islands Impact structure, Ontario, Canada, (9).
- Sharpton, V.L., Copeland, P., Dressler, B.O. & Spell, T.L., (1997). New age constraints on the Slate Islands impact structure, Lake Superior, Canada. Lunar and Planetary Science Conference XXVIII, pg. 1287-1288.

- Sims, P. K., Schmus, W. R. Van, Schulz, K. J., & Peterman, Z. E. (1989). Tectono-stratigraphic evolution of the Early Proterozoic Wisconsin magmatic terranes of the Penokean Orogen. *Canadian Journal of Earth Sciences*, 26(10), 2145–2158. <https://doi.org/10.1139/e89-180>
- Sláma, J., Košler, J., Condon, D. J., Crowley, J. L., Gerdes, A., Hanchar, J. M., & Whitehouse, M. J. (2008). Plešovice zircon - A new natural reference material for U-Pb and Hf isotopic microanalysis. *Chemical Geology*, 249(1–2), 1–35. <https://doi.org/10.1016/j.chemgeo.2007.11.005>
- Stacey, J. S., & Kramers, J. D. (1975). Approximation of terrestrial lead isotope evolution by a two-stage model. *Earth and Planetary Science Letters*, 26(2), 207–221. [https://doi.org/10.1016/0012-821X\(75\)90088-6](https://doi.org/10.1016/0012-821X(75)90088-6)
- Stöffler, D., Keil, K., & Edward R.D, S. (1991). Shock metamorphism of ordinary chondrites. *Geochimica et Cosmochimica Acta*, 55(12), 3845–3867. [https://doi.org/10.1016/0016-7037\(91\)90078-J](https://doi.org/10.1016/0016-7037(91)90078-J)
- Stöffler, D., & Grieve, R. A. F. (2007). Impactites. *Metamorphic Rocks: A Classification and Glossary of Terms, Recommendations of the International Union of Geological Sciences*, 82–92, 111–125 and 126–242.
- Strong, T.R., & Driscoll, R. L. (2016). *A Process for Reducing Rocks and Concentrating Heavy Minerals*. Retrieved from <https://pubs.er.usgs.gov/publication/ofr20161022>
- Swindle, T. D., Kring, D. A., & Weirich, J. R. (2014).  $^{40}\text{Ar}/^{39}\text{Ar}$  ages of impacts involving ordinary chondrite meteorites. *Geological Society, London, Special Publications*, 378(1), 333–347. <https://doi.org/10.1144/SP378.6>
- Tassinari, M., Schmitz, B., & Löfgren, A. (2004). The first fossil meteorite from the mid-Ordovician of the Gullhögen quarry, Billingen, southern Sweden. *Gff*, 126(4), 321–324. <https://doi.org/10.1080/11035890401264321>
- Taylor, J. G., Maggiore, P., Scott, E. R. D., Rubin, A. E., & Keil, K. (1987). Original structures, and fragmentation and reassembly histories of asteroids: Evidence from meteorites. *Icarus*, 69(1), 1–13. [https://doi.org/10.1016/0019-1035\(87\)90002-9](https://doi.org/10.1016/0019-1035(87)90002-9)
- Thorslund, P., & Wickman, F. (1981). Middle Ordovician Chondrite in Fossiliferous Limestone from Brunflo, Central Sweden. *Nature*, 289(5795), 285–286. <https://doi.org/10.1038/289285a0>
- Thorslund, P., Nystrom, J., & Wickman, F. (1984). The Ordovician chondrite from Brunflo, central Sweden, I. Secondary minerals. *Lithos*, 17, 87–100. [https://doi.org/10.1016/0024-4937\(84\)90008-2](https://doi.org/10.1016/0024-4937(84)90008-2)
- Tohver, E., Holm, D. K., van der Pluijm, B. A., Essene, E. J., & Cambray, F. W. (2007). Late Paleoproterozoic (geon 18 and 17) reactivation of the Neoproterozoic Great Lakes Tectonic Zone, northern Michigan, USA: Evidence from kinematic analysis, thermobarometry and  $^{40}\text{Ar}/^{39}\text{Ar}$  geochronology. *Precambrian Research*, 157(1–4), 144–168. <https://doi.org/10.1016/j.precamres.2007.02.014>
- Turner G. (1969). Thermal histories of meteorites by the  $^{39}\text{Ar}$ - $^{40}\text{Ar}$  method. In *Meteorite research: Reidel*. 407–417.
- Turner, G., Miller, J.A. & Grasty, R. L. (1966). The thermal history of the Bruderheim meteorite. *Earth & Planetary Science Letters*, 1, 155–157.

- Vernazza P., Binzel R. P., Thomas C. A., DeMeo F. E., Bus S. J., Rivkin A. S., & Tokunaga A. T. (2008). Compositional differences between meteorites and near-Earth asteroids. *Nature* 454, 858–860.
- Vokrouhlicky, D., & Farinella, P. (2000). Efficient delivery of meteorites to the Earth from a wide range of asteroid parent bodies. *Nature*, 407(6804), 606–8.  
<https://doi.org/10.1038/35036528>
- Whitmeyer, S. J., & Karlstrom, K. E. (2007). Tectonic model for the Proterozoic growth of North America. *Geosphere*, 3(4), 220–259. <https://doi.org/10.1130/GES00055.1>
- Wood, J. A. (1979). Review of the metallographic cooling rates of meteorites and a new model for the planetesimals in which they formed. In *Asteroids* (T. Gehrels, Ed.), 849–891. Univ. of Arizona Press, Tucson.
- Zawacki, E., and Bjørnerud, M., (2015). A previously unrecognized impact structure at Brussels Hill, Door County, Wisconsin: Brecciation and shock-metamorphic features. *Geological Society of America Abstracts with Programs*, vol. 47, no. 5, p.82. Poster